AZARM ALI

NEUTRAL DISSOCIATION OF SUPEREXCITED MOLECULES IN A STRONG LASER FIELD

Thèse présentée
à la Faculté des études supérieures et postdoctorales de l'Université Laval
dans le cadre du programme de doctorat en physique
pour l'obtention du grade de Philosophiae Doctor (Ph.D.)

DÉPARTMENT DE PHYSIQUE, DE GÉNIE PHYSIQUE ET D'OPTIQUE
FACULTÉ DES SCIENCES ET DE GÉNIE
UNIVERSITÉ LAVAL
QUÉBEC

2012

Résumé

L'objectif principal de cette thèse est de rendre compte d'une étude expérimentale sur la dissociation neutre de molécules simples dans un champ laser intense créé par un cristal titane saphir. Nous souhaitons montrer que, dans un champ laser intense, les molécules peuvent être très excitées par l'effet de l'absorption multiphotonique. Ces excitations fortement non linéaires impliquent que les molécules peuvent être peuplées dans les états superexcités.

L'importance des caractéristiques des états hyperexcités d'une molécule en fragmentation neutre a été soulignée pour la première fois par Platzman en 1962. Des états hypererexcités sont des états dans une molécule possédant une énergie au−dessus du potentiel d'ionisation. Dans un champ laser intense l'énergie totale absorbée est suffisante pour stimuler la molécule à la plupart des états hypererexcités. C'est ce qui explique que l'effet de l'excitation multiphotonique est plus ou moins équivalent à l'excitation par un photon unique à la région des ultraviolets extrêmes par le rayonnement synchrotron.

Dans ce travail, un laser titane saphir femtoseconde est utilisé pour amener les molécules de $H_2, O_2, NO, CH_4, C_2H_4, C_3H_6, 1-C_4H_8$ et $cis-2-C_4H_8$ dans les états hypererexcités. En utilisant une méthode de.spectroscopie, on arrive à détecter des signaux de fluorescence. Le diagramme d'énergie des fragments excités et molécules neutres supporte l'excitation des états hypererexcités dans les molécules que nous avons étudiées. La dépendance hautement non linéaire du rendement produit selon la puissance du laser a été observée. En utilisant la technique de pompe (800 nm) et sonde (1338 nm) et aussi de la technique de spectroscopie par fluorescence, nous confirmons le mécanisme de hyperexcitation multiphotonique des molécules en présence d'un champ laser intense. Nous arrivons à déterminer la durée de vie des états hyperexcités en regardant l'atténuation des signaux de fluorescence observée à l'aide du faisceau sonde. Nos observations expérimentales ont été également vérifiées à l'aide des calculs semi−empiriques.

Finalment, nous constatons que si l'intensité du laser est de l'ordre de 3×10^{14}

W/cm^2, certaines impulsions laser provoquent la dissociation neutre de nombreuses molécules.

Résumé court

L'objectif principal de cette thèse est de rendre compte d'une étude expérimentale sur la dissociation neutre de molécules simples dans un champ laser intense créé par un cristal titane saphir. Ces excitations fortement non linéaires nous indiquent que les molécules peuvent être peuplées dans les états hyperexcités. Dans ce travail, un laser titane saphir femtoseconde est utilisé pour amener les molécules de $H_2, O_2, NO, CH_4, C_2H_4, C_3H_6, 1-C_4H_8$ et $cis-2-C_4H_8$ dans les états très excités. En utilisant une méthode de spectroscopie, on arrive à détecter des signaux de fluorescence. Le diagramme d'énergie des fragments excités et molécules neutres supporte l'excitation des états hyperexcités dans les molécules que nous avons étudiées. La dépendance hautement non linéaire du rendement produit selon la puissance du laser a été observée. En outre, les résultats soutiennent le mécanisme d'hyperexcitation multiphotonique. En utilisant la technique de pompe (800 nm) et sonde (1338 nm) et aussi de la technique de spectroscopie par fluorescence, nous confirmons le mécanisme de hyperexcitation multiphotonique des molécules en présence d'un champ laser intense. Nous arrivons à déterminer la durée de vie des états hyperexcités en regardant l'atténuation des signaux de fluorescence observée à l'aide du faisceau sonde. Nos observations expérimentales ont été également vérifiées à l'aide des calculs semi−empiriques. Nous constatons que certaines impulsions laser provoquent la dissociation neutre de nombreuses molécules.

Abstract

The primary objective of this thesis is to report on an experimental study of neutral dissociation of simple molecules in a strong Ti−Sapphire laser field. We will show that in an intense laser field, molecules can be highly excited owing to multiphoton absorption. Such highly nonlinear excitation means that the superexcited states (SESs) of molecules can be populated.

The important features of SESs that they lead to fragmentation of molecule was first proposed by Platzman in 1962. A SES of a molecule is an energy state possessing the energy above the ionization potential. In a strong laser field the total energy absorbed is sufficient to stimulate molecules to many of the SESs and obeying the selection rules. This implies that the effect of multiphoton excitation is more or less equivalent to single photon excitation in the extreme-ultraviolet(XUV) region by synchrotron radiation (SR).

In this work, an intense femtosecond Ti−Sapphire laser is used to excite many molecules ($H_2, O_2, NO, CH_4, C_2H_4, C_3H_6, 1-C_4H_8$ and $cis-2-C_4H_8$) into highly excited states. We detect all of the fluorescence signal from excited fragments by a spectroscopies method. The energy diagram of excited fragments and neutral molecules supports excitation of SESs in the molecules we have investigated. The highly nonlinear laser power dependence of product yield was obtained. Also, it supports the multiphoton super excitation mechanism. Using a pump (800 nm) and probe (1338 nm) technique and fluorescence spectroscopy, we confirm multiphoton superexcitation of the molecules in a strong laser field. We detect the depletion of the fluorescence signals by the probe pulse and determine the lifetime of the SESs. Our experimental evidence was strengthened with semiempirical calculations as well.

To sum up, we find that at the laser intensity of the order of 3×10^{14} W/cm^2, ultrashort laser pulse causes neutral dissociation of many molecules by way of SESs. It could be a general pathway in strong laser field interaction with molecules.

Acknowledgement

First, I would like to acknowledge my thesis advisor, Professor See Leang Chin. I appreciate very much that Prof. Chin has provided me the great opportunity to join his research group, which is always working at the forefront of the field in laser science. I want to express to him my sincere thankfulness for his direction and patience during all these years of my study. I have been impressed by his meticulous thinking, availability and creativity. I profited from his rich experience. Through him, I have learned a lot about the scientific world.

Moreover, during my studies I have received generous help from Prof. S. H. Lin from National Chiao Tung University and Academia Sinica, as well as, Prof. F. Kong from Chinese Academy of Science. Prof. S. H. Lin is an excellent scientist and through him, I have been introduced to the theoretical aspect of the work. It is my greatest pleasure to get to know him and collaborate with him closely. In addition, I would appreciate the help of Prof. S. H. Lin group's member, Dr. H. Mineo and Dr Y. Teranishi. They warmly welcomed me twice in Taiwan.

In addition, I would also like to express my appreciation to Prof. A. Bandrauk, Prof. T. Seideman and Prof. K. Yamanouchi and their group members for their valuable helps and discussions.

I would like to express my deep gratitude to Mr. Mario Martin for his technical support in the Lab. His kind assistance helped me a lot in performing the experiments.

I would also thank Dr. Y. Kamali, Dr. J.–F. Daigle, Dr. F. Theberge, Dr. A. Talebpour, Mrs. S. Lessard, Dr S. M. Sharifi, Dr. J. Berndhardt, Mr. C. Marceau, Dr. H. Xu and Dr. Zhendong Sun, for their suggestions and fruitful discussions and helping me to do some of the experiment. I would like to acknowledge those whom I have been fortunate to know and work in proximity with in the laboratory but I forget to name them. It is my greatest pleasure to get to know them and work with them closely. Also, I express my sincere gratitude to all the staffs of the Physics Department and COPL.

Last, but not the least, I thank my beloved wife Mrs. Sima Hosseini. Apart from being an ideal wife for me, she is an helpful colleague who has fruitful discussions and suggestions. Without my wife's patience and constant support, it was definitely impossible for me to pursue this long and difficult journey. I owe her all of my success.

Finally, I gratefully appreciate the financial support I received from Prof. Chin through all these years.

The thesis consists of the following papers:

- A. Azarm, D. Song, K. Liu, S. Hosseini, Y. Teranishi, S. H. Lin, A. Xia, F. Kong, and S. L. Chin. Neutral dissociation of hydrogen molecules in a strong laser field through superexcited states. Journal of Physics B: Atomic, Molecular and Optical Physics,44(8):085601, 2011.

- D. Song, A. Azarm, Y. Kamali, K. Liu, A. Xia, Y. Teranishi, S. H. Lin, F. Kong and S. L. Chin. Neutral dissociation of superexcited oxygen molecules in intense laser fields. The journal of Physical Chemistry A, 114(9):3087, 2010.

- K. Liu, D. Song, A. Azarm, S. L. Chin, and F. Kong. Neutral dissociation of superexcited nitric oxide induced by intense laser fields. Chinese Journal of Chemical Physics, 23(3):252, 2010.

- A. Azarm, H. L. Xu, Y. Kamali, J. Bernhardt, D. Song, A. Xia, Y. Teranishi, S. H. Lin, F. Kong, and S. L. Chin. Direct observation of super−excited states in methane created by a femtosecond intense laser field. Journal of Physics B: Atomic, Molecular and Optical Physics, 41(22):225601, 2008.

to my wife Sima

Contents

List of Tables

List of Figures

Chapter 1

Introduction

Over the past century, understanding the interaction of light with matter has been one of the central themes of research in physics and chemistry. With the birth of the laser in 1960 [3], a new coherent and monochromatic source was provided for scientists to explore materials. The laser became a new spectroscopic tool to discover atomic and molecular structure in more detail and, as a result, our knowledge of atoms and molecules is widely broadened. Moreover, the advent and continuous development of pulsed lasers with durations from the microsecond domain in free running regime to the nanosecond regime with Q−switching [4], then to the picosecond and few−femtosecond regime [5] with mode locking [6] and most recently to attosecond regime with high harmonic generation [7, 8] made it possible to investigate dynamical processes in different systems. Using the pump and probe technique with ultrashort laser pulses, one can monitor atomic and molecular behavior occurring on an ultrashort timescale. This concept in femtosecond regime has led to the birth of femtochemistry, for which the 1999 Nobel Prize in chemistry was awarded to Ahmed Zewail [9]. At the same time, soon after the advent of the laser in the 1960s the first nonlinear optical effects were demonstrated [10]. Intensity passed the perturbation regime, and then multiphoton [11, 12] and tunnelling regimes [13] were observed; nowadays relativistic intensity is available [14]. Investigation on highly nonlinear phenomena was revolutionized after the introduction of the Chirped Pulse Amplification (CPA) technique in 1985 [15]. With the help of intense laser fields, very interesting and new phenomena were observed. In fact, strong laser field is a very popular tool used in physics and chemistry. The community has now mushroomed to a size that was hard to imagine in the beginning days. However, the never ending search for shorter pulses and higher intensity laser is a very active field of research. These demands result in deepening our knowledge about atoms and molecules.

In this chapter we give a brief overview of the developments in the strong laser field interaction with materials with an emphasis on neutral dissociation of molecules through single to multiphoton processes. Finally a brief outline of the thesis will be given.

1.1 Strong laser field interaction with matter

The behavior of atoms and molecules submitted to intense electromagnetic fields has been a subject of wide interest and active research in recent years. Strong laser field theory was introduced since many order perturbation theory failed to explain experimental results. At an intensity of about 10^{16} W/cm^2, the laser electric field strength becomes as strong as the field binding the $1s$ electron in a hydrogen atom. In this regime the external electric field is very near the atomic Coulomb field (5×10^9 V/cm). At these and even at lower intensities, light−atom interaction is so strong that normal perturbative approaches break down, leading to the novel phenomena collectively termed as multiphoton processes.

The first most relevant empirical finding in the development of intense−field science was the observation of breakdown of atomic gases in air when a laser was shone on it [16]. This was because the laser photon energy was much lower than the ionization potentials of the gases. As a result of the interaction of a strong field with atoms, the products of interaction consist of ions, photons and electrons. Much of the knowledge in the beginning of this field was provided by studying ionization. And also most of the attention to strong field matter interaction has been concentrated on atoms. The first fruit of this new field by increasing the intensity of the laser field was multiphoton ionization (MPI). MPI is the process by which an atom is ionized by the simultaneous absorption of several photons [11, 12]. Tunneling ionization happens while the electron tunnels through the barrier formed by combination of internal (Coulomb) and laser electric fields. Intense field ionization can be divided into two regimes: multiphoton vs tunnel ionization. Keldysh [17] coined a parameter γ that separates the regimes of MPI and tunnel ionization where $\gamma = \frac{\omega}{\mathrm{E}}\sqrt{2\mathrm{I_B}}$(in atomic units), ω is the laser frequency, E the laser electric field strength and I_B the ionization potential of the atom. It was concluded that when $\gamma \ll 1$, tunnel ionization prevails while when $\gamma \gg 1$, it is a multiphoton effect.

New phenomena such as the so−called "above−threshold ionization" (ATI) [18] were observed by studying the ejected electrons. In ATI, electrons were found to be ejected from an atom not at a single energy but at a sequence of energies separated by

the photon energy. Another remarkable phenomenon that was observed later was high harmonic generation (HHG) [19, 20]. The HHG could be explained by a simple three step model [21]: (1) The laser field releases the least bound electron through tunneling ionization; (2) the free electron evolves in the laser field; and (3) under certain phase conditions, the electron can return to the vicinity of the ion core, and either collisionally ionize a second electron [18], scatter off the core and gain additional kinetic energy [22], or recombine with the core and produce a harmonic photon (HHG). Above a certain threshold electric field the electron is able to escape even classically from the atomic nucleus, i.e., without tunneling through the barrier formed by the Coulomb potential and the external electric field. This is called "barrier−suppression ionization" BSI [23].

In addition to the effects observed in atoms, molecules in a strong field exhibit new phenomena associated with additional vibrational and rotational degrees of freedom. The most well known and interesting phenomenon is unique to molecules molecular alignment upon strong field interaction and rotational revival under field free condition [24]. Actually much of the work on molecules in strong laser fields has focused on the dependence of strong field phenomena, such as ionization [25, 26] and high−harmonic generation [27], on angular orientation and internuclear separation. Also, the molecular bond is softened by strong laser fields, resulting in photodissociation of the molecules in strongly bound vibrational states (bound softening)[28].

Therefore, the interaction of even simple diatomic molecules with strong laser fields is considerably more complicated than the interaction with atoms. Hence we will focus in this thesis on one phenomenon called neutral dissociation and more specifically on neutral dissociation of molecules through superexcited states. The applications of neutral dissociation through superexcited molecules range from remote sensing to acting as a gain medium. From a physical point of view, it is also an important new strong field issue because we study the effect of highly excited states in strong laser field interaction.

1.2 Single ionizing photon interaction with molecules

In order to explore neutral dissociation in a strong laser field by multiphoton processes, we start by looking at neutral dissociation in a single photon process. The main knowledge of single photon neutral dissociation of molecules through super excited states is reviewed by Y. Hatano in ref. [29]. Also, Berkowitz [30] compiled the experimental data on photoabsorption, photoionization and photoelectron spectroscopy in the photon energy range much wider than that in photochemistry, i.e., from absorption thresholds to the vacuum ultraviolet(VUV), soft X−ray regions in some cases even

to hard X−ray region. He summarized theoretical backgrounds, then briefly introduced a general scheme of the dynamics of superexcited states.

The interactions of single photons with molecules are classified into absorption, scattering, and pair production. Our interest is in photons of moderate energies particularly in the vacuum ultraviolet (VUV) region, and therefore only the absorption process is considered. The absorption of a single photon by a molecule in the electronical ground state changes its electronic state from the ground state to a final excited or ionized state. Franck-Condon transition is assumed. Its transition probability could be expressed in terms of the optical oscillator strength. Oscillator−strength values have long been measured for various molecules in the wavelength regions at least longer than the near−ultraviolet (UV) region. Since there have been remarkable advances in synchrotron radiation (SR) research and related experimental techniques in the VUV region ($200 - 0.2\text{nm} \sim 6\text{eV} - 6\text{keV}$), many measurements in this region have recently become available [29, 30].

The pioneering scientist in this field, R. Platzman, first considered theoretically the interactions of ionizing radiation with atoms and molecules. He pointed out that atoms and molecules receive a large fraction of energy from ionizing radiation with a spectrum determined by their optical oscillator strength distribution [31]. He also pointed out the following important features, although very few experimental data were available at that time:

- The value of the oscillator strength distribution shows generally its maximum at the energy of 10 to 30 eV, which is larger than the first ionization potential of most molecules.
- Ionization efficiency (η[1]) values of molecules are much smaller than unity in the energy range just above the ionization potential.

By combining all available information at that time, R. Platzman indicated an important role of highly excited electronic states in the primary action of ionizing radiation as follows:

$$AB + h\nu \longrightarrow AB^+ + e^- \qquad \text{direct ionization} \qquad (1.1)$$

$$\longrightarrow AB^* \qquad \text{excitation} \qquad (1.2)$$

$$\longrightarrow AB^{**} \qquad \text{Superexcitation} \qquad (1.3)$$

[1] η is the quantum yield for ionization

Then superexcited molecules can decay to the following:

$$AB^{**} \longrightarrow AB^{+} + e^{-} \quad \text{autoionization} \tag{1.4}$$

$$\longrightarrow A^{*} + B \quad \text{neutral dissociation} \tag{1.5}$$

$$\longrightarrow \textit{other minor processes} \quad \text{like ion pair formation} \tag{1.6}$$

When a molecule AB absorbs an energy which is larger than its ionization potential, AB may be directly ionized (1.1) and may be excited to form AB^{**} (1.3) which was emphasized by R. Platzman as a superexcited molecule [31]. To prevent a misunderstanding, the term "superexcited states" was coined by G. S. Hurst, and not by Platzman, as Platzman stated [31]. Platzman then stressed the need for elucidating the properties of superexcited states, in which dissociation into neutral fragments and autoionization occur in competition [32]. Superexcited states of atoms and molecules are electronically excited states with energies higher than the first ionization potentials. They are hence degenerate with the ionization continua or, in other words, embedded in the ionization continua. Platzman's concept of the superexcited state has made a profound influence on the science of excited states and motivated researchers in a wide field to find new objectives of research. In order to study experimentally the superexcited states or to substantiate Platzman's ideas, scientists had to find the way to produce such superexcited states. From the first to even now the main source to superexcite a molecule was an electron beam, then after 1980s laser multiphoton absorption and synchrotron radiation have been used.

Based on Y. Hatano's reports [33], most of the observed molecular superexcited states are assigned to high Rydberg states which are vibrationally (or/and rotationally), doubly, or inner−core excited and converge to each of ion states. Non−Rydberg states are also observed. Dissociation into neutral fragments in competition with autoionization is of great importance in the observed decay of each of these state-assigned superexcited molecules. In fact we use above mentioned definition in the following chapters.

There are two distinct kinds of superexcited states depending on how they obtain an energy higher than the first ionization potential [34]. In Figure 1.1, we take a diatomic molecule AB. The solid curve is the potential energy curve of an ionic state of AB, and the space above the curve represents the continuum of $AB^{+}+e$, where e is a free electron and, thus, it has a continuous energy. As seen in Figure 1.1, the other potential energy curve, that is, the red dashed line, is embedded in the electronic continuum. Such states are called superexcited states of the first kind. On the other hand, the potential energy curves, that are, the red dashed lines, in Figure 1.2 are below the electronic continuum. Hence, some readers may think that such states are not superexcited states. However,

the vibrational−rotational level can be higher than the zero point energy associated with the potential energy of $AB^+ + e$ with zero kinetic energy of e, that is, the lower part of the continuum. Such states are called superexcited states of the second kind. Their energies exceed the lowest energy of $AB^+ + e$ by vibrational or rotational excitation, and thus they are embedded in the ionization continuum.

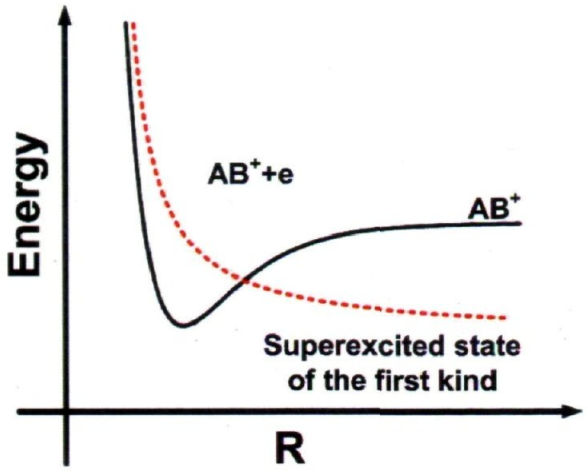

Figure 1.1: *Potential energy curve of a typical diatomic molecules AB. Solid black curve belongs to ionic AB^+ and the red dashed curve is a super excited state of first kind*

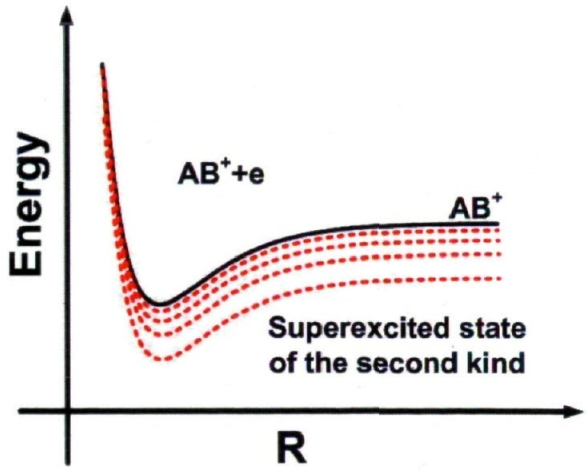

Figure 1.2: *Potential energy curve of a typical diatomic molecules AB, solid black curve belongs to ionic AB^+ and red dashed curve is super excited state of second kind*

The superexcited molecule can spontaneously ionize since it is degenerate with the ionization continuum. This process is called autoionization (1.4). Superexcited

molecules decay through not only by autoionization but also by neutral dissociation (1.5). In other words, neutral dissociation competes with autoionization. Figure 1.3 shows the total cross section of single photoabsorption from ref [35] for methane molecules. Figure 1.3 shows some general trends. Also, neutral dissociation and photoionization cross sections behave more or less in the same way for many molecules. The competition between dissociation and photo ionization cross sections well above the first ionization potential is shown clearly in figure 1.3. This implies that photo ionization prevents the superexcited states from being observed for incident high energy photons. Therefore for the energy just above the ionization potential, the cross section of dissociation is comparable to that of the photoionization, and the effect of SESs will be more important.

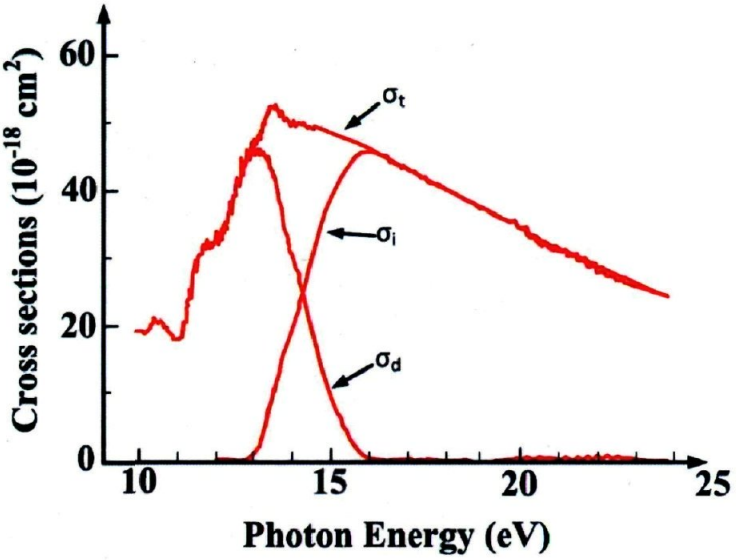

Figure 1.3: *Photoabsorption σ_t, photoionization σ_i, and neutral-dissociation σ_d cross sections of CH_4 as a function of incident photon energy measured with a wavelength resolution of 0.1 nm, which corresponds to the energy resolution of 32 meV at an incident photon energy of 20* eV. *The relation among σ_t, σ_i, and σ_d is $\sigma_t = \sigma_i + \sigma_d$ (taken from [35]).*

1.3 Multiphoton superexcitation

Pioneering work to excite a SES with a laser was described by resonance−enhanced multiphoton ionization (REMPI) technique, for example in NO [36]. The REMPI

technique typically involves a resonant single or multiple photon absorption to an electronically excited intermediate state followed by another photon which ionizes the atom or molecule. Actually, for weak electromagnetic fields, vibrational and electronic excitation of molecules generally occurs through resonant one−photon interactions or two−photon Raman−type transitions. Short pulse strong laser fields open up a variety of new excitation schemes, which are characterized by non−resonant or high−order resonant interactions. The first work including strong laser field excitation of SESs was done by Helm et al. [37] on hydrogen molecules. They have studied high resolution photoelectron spectra resulting from the response of molecular hydrogen to intense laser fields ($> 10^{13}$ W/cm^2) at wavelength between 310 and 330 nm. The result shows that multiphoton ionization of the molecules competes with photodissociation of the neutral. Although they did not mention SESs, they observed the photoelectrons from ionization of neutral fragments. They concluded that this fragmentation scheme should be generally applicable to molecules in strong laser fields.

In addition, Prof. Chin's research group started to study neutral dissociation of molecules in strong laser field through SESs. In recent years, they tentatively proved that SESs exist in a strong laser field interaction with hydrocarbons [38]. For the parent molecule of methane, ethylene, 1−butene and $cis-2-$butene fluorescence from $H(n=3\rightarrow 2)$, $CH(A^2\Delta \rightarrow X^2\Pi)$, $CH(B^2\Sigma^+ \rightarrow X^2\Pi)$, $CH(C^2\Sigma^+ \rightarrow X^2\Pi)$ and C_2 $(A^3\Pi_g \rightarrow X'^3\Pi_u)$ are observed. Also, they have shown that the laser power dependence of $CH(A^2\Delta \rightarrow X^2\Pi)$ emission of methane on a log−log scale has a slope of 10±1. As you will see this thesis is a continuation of this work and chapter four is a completion of this work.

In the recent theoretical investigation of C. J. G. J. Uiterwaal et al. [39], it has been shown that a multiphoton process is a kind of single photon process. They introduced a new approach to intense−field photoionization that is based on the ad hoc assumption that m photons of energy E_{ph} arriving within a typical electronic response time are effectively equivalent to a single photon of energy mE_{ph}. This method does not contain any adjustable parameters, its predictions are in satisfactory agreement with reported experiments on intense−field ionization of both atoms and molecules, over a wide range of parameters such as pulse duration, wavelength and ionization energy of the target particle. Although this technique is very successful, it does not get any popularity because it ignores many properties of strong laser fields mainly the changes of field free potential.

The existing models on photo−ionization or strong field ionization could not explain neutral dissociation of molecules in a strong laser field. For example the rescattering model of Corkum [21] is employed to explain HHG, etc. in atoms. In this scheme

for circular polarization there should not be any consequence during the rescattering of the electron. We have conducted an experiment to compare the fluorescence yield using both linearly and circularly polarized fs laser pulses. It was found that the same fluorescence spectra were observed in both polarization cases. According to the re−scattering theory, circular polarization should reduce the probabilities of colliding the rescattered electron to the parent ion to nearly zero. Hence, no fluorescence is expected as long as the re−scattering is the only process depositing the energy to molecules. This would imply that the physical process in exciting SESs is not tunneling but multiphoton in nature. Therefore we will use a semiempirical model to explain our results. This model is used in the third chapter.

1.4 Thesis outline

This thesis is organized as follows. The second chapter describes the experimental setup including mode locked Ti−Sapphire laser. In addition, an optical parametric amplifier (OPA) is described. The detection system is also described in detail and a brief survey on automatic data acquisition is given. In the third chapter experimental results and discussion on SESs of simple molecules (hydrogen, oxygen and nitric oxides) are presented. The results include the spectra observed for each molecules. Then the intensity dependence of some strong lines and finally a proof of the short life time of SESs are presented. Each section of this chapter ends by a theoretical investigation. In the fourth chapter, we repeat what is shown in the former chapter but for some hydrocarbons. At the end, in the fifth chapter, we conclude the universality of SESs in strong laser field interaction with molecules.

Chapter 2

Experimental setup

The experimental study of strong laser field interaction with molecules requires three different parts. The first and most important part is a strong laser field. Nowadays, Ti sapphire based mode−locked laser followed by a chirped pulse amplification (CPA) module is a common part of all laboratories studying strong laser field interaction with materials. The second part is the interaction chamber and its vacuum requirements. Last but not least is the detection system. The selection of detection system depends on what we want to measure. The knowledge in this field is provided by studying the ionization dynamics, the energy and momentum of photoelectrons and the spectrum of emitted photons. In this thesis we focus on the fluorescence signal emitted during the interaction. In this chapter we explain the three important parts in our experiment, mentioned above and the the final configuration of the experiments. Mainly they already were in the laboratory.

2.1 Laser system

Ultra short laser pulses used in our experiments are produced through a Kerr lens mode−locked Ti Sapphire laser. Then intense ultra short pulses are created by using a CPA technique invented in the 1980's [15]. CPA consists of three main stages: a stretcher, an amplifier and finally a compressor.

The oscillator module to seed a CPA part is necessary. The oscillator is the heart of our laser system. It is a commercial laser system called Tsunami from Spectra Physics (for details see Newport Company website [40]). Tsunami is a Kerr lens mode−locked

Ti−sapphire laser that provides a pulse train with a repetition rate of 74 MHz, energy per pulse of 5 nJ, pulse duration of around 30 fs and a bandwidth of around 40 nm. The gain medium in Tsunami is pumped by another commercial laser called Millennia (for details see Newport Company website [41]). Millennia is a continuous laser at 532 nm. The lithium triborate (LBO) crystal used to have the second harmonic of the fundamental from a Neodymium Yttrium Orthovanadate ($Nd : YVO_4$) gain medium. The average output power of Millenia is 4.2 W. The two above mentioned modules together with other parts of laser system together are shown in Figure 2.1.

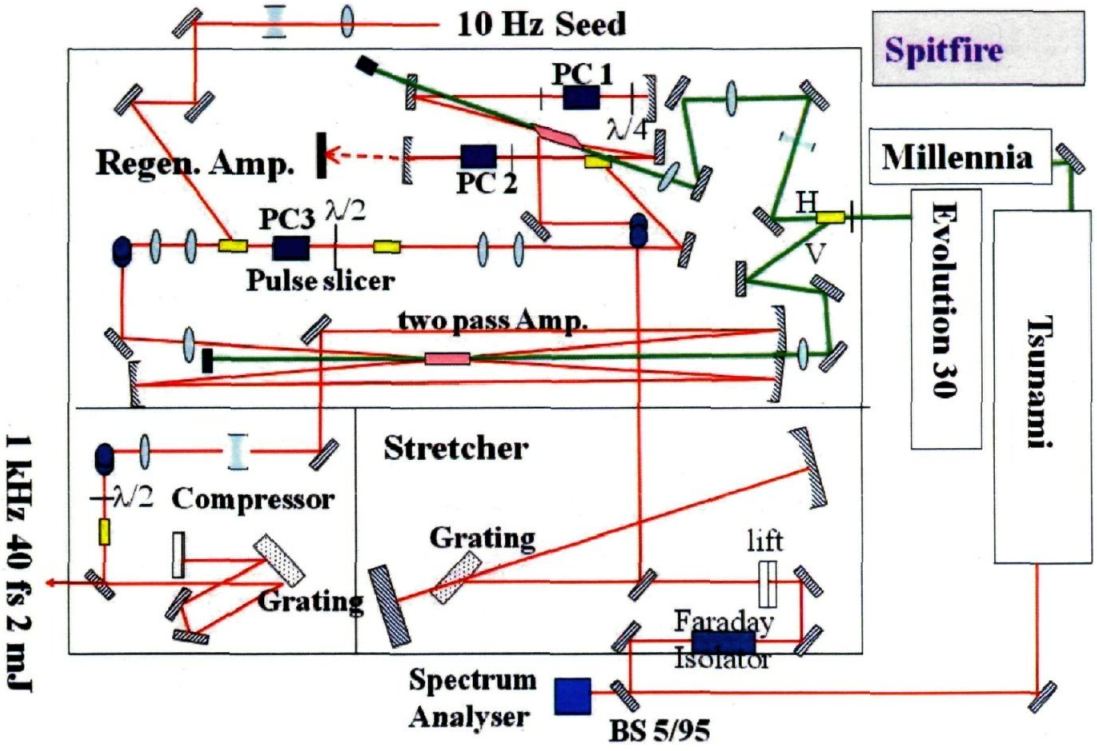

Figure 2.1: *The schematic diagram of ultra short intense laser pulse module. Yellow rectangles are polarizers*

The CPA module in the laboratory is a commercial amplification stage called Spitfire (for details see Newport Company website [42]), though it has a slight difference from the commercial version. As we mentioned earlier a typical CPA module consists of three main parts. These parts in the Spitfire are:

- A stretcher which preserves the bandwidth of the input pulse but lowers the peak power by the stretching factor.

- An amplification stage (regenerative and two−pass amplifier). Because of the peak power reduction associated with the stretcher, self-focusing and optical damage effects are completely suppressed.
- A compressor to achieve short amplified pulses by applying proper dispersion. Finally the amplified pulse is compressed to the bandwidth limit.

As it is shown in Figure 2.1, the pulse train from the oscillator (Tsunami) is directed to a stretcher by passing through a Faraday isolator. The Faraday isolator is used to protect the oscillator (Tsunami) against back−reflected pulses which could perturb the Kerr−lens mode−locking of the oscillator or even damage the optics inside the cavity. The pulse duration after the stretcher is about 200 ps (positively chirped) and the spectral width is still around 40 nm at FWHM. After the stretcher the pulse duration is larger, therefore the pulses with smaller peak power can safely propagate within a laser amplifier and they are not limited by nonlinear index effects. Optical damage issues also cannot occur. This is the key point of the CPA technique.

Then the pulses are ready to be amplified in Ti−Sapphire crystal. As shown in Figure 2.1, the amplification stage consists of two parts: a regenerative amplifier followed by a two−pass amplifier. Both of the Ti−Sapphire crystals are pumped by the second harmonic of a neodymium−doped yttrium−lithium−fluoride (Nd:YLF) laser generating pump pulses at a repetition rate of 1 kHz, pulse duration of 150 ns, energy of around 17 mJ per pulse and the central wavelength is 527 nm. This laser is called Evolution−30.

The injection of a seed pulse inside the regenerative cavity is done with a Pockels cell 1 (PC1) coupled with a quarter wave plate. When PC1 is activated at a proper delay time, only one seed pulse is trapped inside the regenerative cavity and all the other seed pulses from the oscillator will pass only once inside the regenerative cavity and will be eliminated by the thin plate polarizer (it is shown by yellow rectangle in the regenerative amplifier cavity). There is a synchronization between the pump pulse (repetition rate of 1 kHz) and the seed pulses (repetition rate of 74 MHz). The seed pulse trapped inside the cavity performs several round−trips to reach its maximum energy and, then, this amplified pulse will be extracted by the second Pockels cell (PC2). Before sending the 1.3 mJ amplified pulses with 1 kHz repetition rate to the two−pass amplifier, a 10 Hz slicer is used to select 10 out of 1000 pulses in a second to amplify more to reach the (0.2 or 2) TW power regime. However I did not use them for this thesis. After each pulse passes twice in the second amplifier the energy of each pulse reaches to around 3 mJ per pulse.

At last, a grating compressor is use to compensate the positive chirp that each pulse obtains from the stretcher or by propagating through the various optical media. However, because of gain narrowing, the original pulse duration cannot be fully achieved. Gain narrowing happens because the typical gain curve of an active medium has a finite bandwidth. Gain saturation in conjunction with chirp may also lead to spectral distortion. Hence, the amplification is accompanied by a narrowing of the pulse spectrum. Therefore the final pulse duration is not less than 40 fs with energy up to 2 mJ. As it is shown in Figure 2.1, before the grating compressor there is a polarizer and a half wave plate to control the output energy of laser pulses. The output of Spitfire could be used directly in an experiment or used to pump an Optical Parametric Amplifier (OPA) to have tunable wavelength ultra short laser pulses in the infrared domain.

The schematic diagram of the OPA 800C is depicted in Figure 2.2. The optical parametric amplification (OPA) is a nonlinear phenomena consisting of splitting the pump photon into two infrared photons: the signal photon and the idler photon where the pumps photon frequency is equal to the sum of the signal and idler photon frequencies. The OPA 800C creates a tunable fs pulse in infrared domain (1.1 μm to 2.2 μm). The pump pulses used for the parametric amplification are the output of Spitfire with energy of 1 mJ per pulse with roughly 60 fs pulse duration (negatively chirped). The other 1 mJ part could be used for other purposes, as we will discuss about it later in this chapter. The 1 mJ beam which enters the OPA is divided into three parts. The first part, a small portion 1% (see Figure 2.2 in the beginning) of the pump pulse was focused into a thin sapphire plate to generate white−light continuum by self−phase modulation. It includes signal and idler. In the OPA 800C a two−stage amplifier is used. The second part 30% (see Figure 2.2) of the pump beam was used as pump for the pre−amplification of the infrared pulses. The third part about 69% (see Figure 2.2) of the pump beam was used as pump to amplify infrared pulses in the beta barium borate (BBO) crystal for the second time. The temporal and spatial superposition of the pump beams with the white−light continuum seed was achieved by using the delay lines (brown double sides arrow in Figure 2.2). The amplified wavelengths of the signal and idler pulses are selected from the white-light continuum seed by adjusting the angle between the optical axis of the BBO crystal and the propagation axis of the laser beams. The BBO crystal is installed in a rotational stage that we can change the angle. The ordinary index of refraction of the BBO crystal is larger than its extraordinary index of refraction, thus quasi−perfect phase matching over narrow bandwidth was possible if the polarization of the pump and infrared pulses were perpendicular [43]. The output pulse central wavelength that we used was 1338 nm with the maximum energy of 120 μJ per pulse.

For detail discussion about ultrafast intense laser sources, amplifier, OPA etc., I

refer to three interesting books [44, 45, 46].

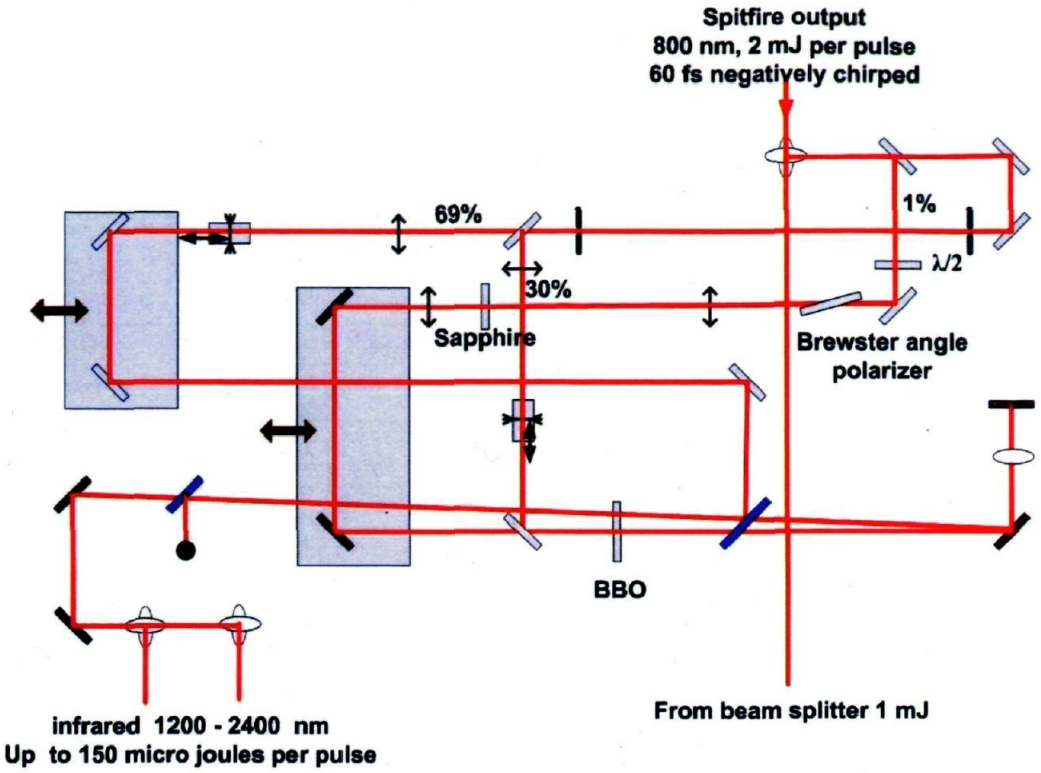

Figure 2.2: *Schematic diagram of OPA, gray components are metallic mirror, blue components are dichroic mirror, double side arrow in beam path are lenses to focus beam in BBO crystal, other double side arrows show translation stages and the rest are 800 nm mirrors*

2.2 Vacuum chamber and detection system

In the experiments, a vacuum chamber was used. It is evacuated by a TriScroll pump to about 10^{-2} torr. Pure gas was introduced. In each experiment a fixed amount of gas inside the chamber was used. In the beginning stage of the experiment, a continuous flow of gas inside the chamber was used during the experiment. As a results we did not find any differences between the two different cases (1.closed chamber with defined pressure of gas or 2.flowing gas chamber with defined pressure) of introducing sample gas in the chamber. This could be explained by the size of the interaction volume. It is very tiny and the chamber volume is very large (in comparison with each other). Therefore for each laser pulse fresh sample gas interact with the laser. The pressure was measured with proper vacuum gauges. A capacitance gauge was used to measure

pressures above 1 torr and a Pirani gauge was used for lower pressures (see chamber in Figures 2.3 and 2.4). Throughout this thesis we have used 100 or 30 cm lenses to focus the beam inside the chamber. The fluorescence signal was detected from the side through a fused silica window which was transparent for UV photons as well as visible photons (see chamber in Figures 2.3 and 2.4). Although we used the gated detector in the experiments to get rid of unwanted signals, we also used a proper pipe design inside the chamber to avoid scattered signal to enter the detector head. The pipe design is in front of opening window inside the chamber. Also there is a small hole for laser beam to pass through it.

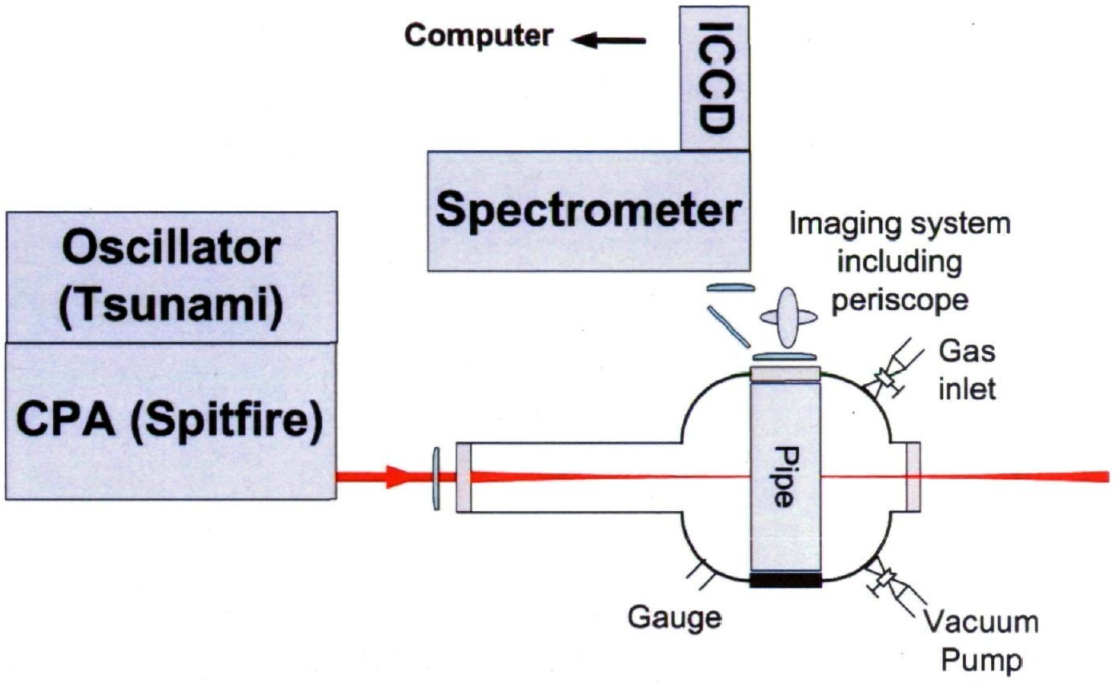

Figure 2.3: *Schematic diagram of experimental setup to observe fluorescence spectra and intensity dependent curves*

We have used two different detectors in our experiments. Each of them had a high speed electrical gating system (ns precision). The gating system was very useful to get rid of unwanted signals or white light generated in the interaction zone. For example if the fluorescence signal was around 800 nm, scattering of the strong fundamental beam (800 nm) would overlap with fluorescence and hide it totally. By opening the gate after a proper time from the arrival of the scattering light, we can easily detect the fluorescence signal because we get rid of the scattering by proper gating. In the case of unwanted light propagating with the laser pulses, we could set the gate delay few ns after laser pulse arrival into the interaction zone. In those cases, the lifetime of the fluorescing species should be larger than the selected gate delay. Then we could open

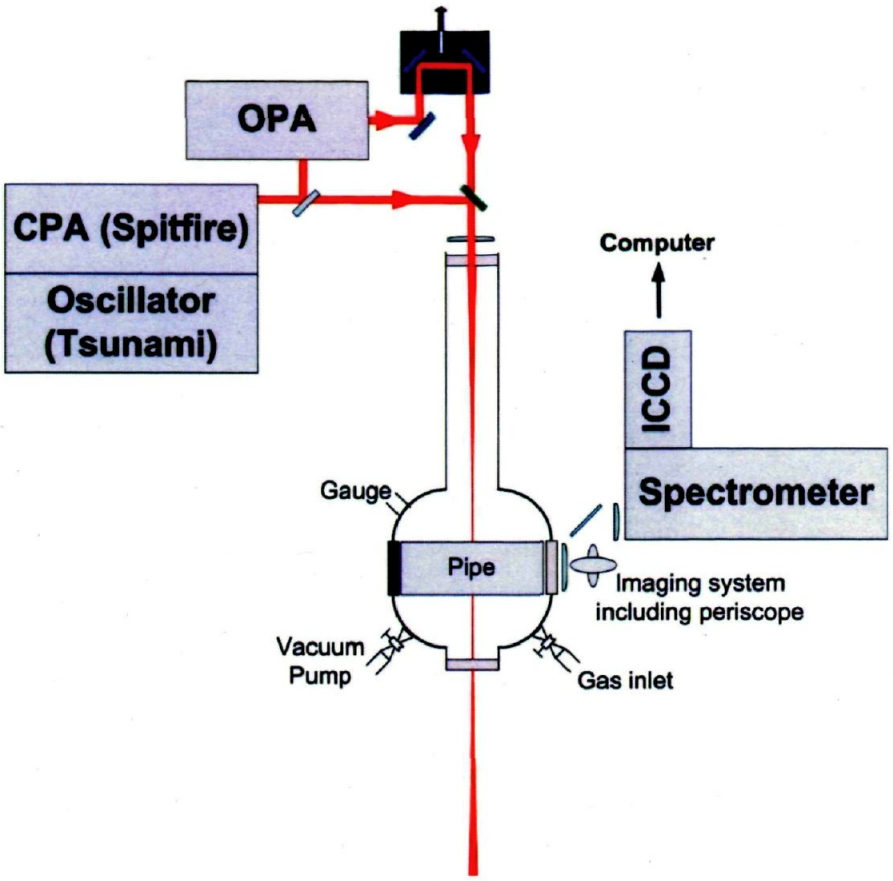

Figure 2.4: *Schematic diagram of pump and probe experiment*

the gate width as much as the lifetime of the fluorescing species. Also with the gating system we could measure the lifetime of each fluorescing line. Furthermore the gating system improved the signal to noise ratio. One of detectors was a gated microchannel plate photomultiplier tube (MCP−PMT, Hamamatsu R5916U − 52) [47]. Another one which we used more frequently in this thesis was an intensified charged coupled device (ICCD) camera (Princeton Instrument ICCD PIMAX 512) [48].

To resolve the detected photon coming from the interaction zone we used an interference filter in front of the gated MCP−PMT with a proper central wavelength (it is centered at studied florescence line for example for CH_4 it is centered at 430 nm) and 2.5 nm (FWHM) bandwidth in the transmission spectrum. In all of the cases we used a spectrometer (Acton Research Corporation, Spectra Pro 500i) before the ICCD. A schematic diagram of spectrometer is shown in Figure 2.5. The entrance slit width was 100 μm. The available gratings have the characteristics of 300, 1200 and 2400 grooves per millimeter. In the case of grating with 1200 g/mm, maximum error in reading photon wavelength is 0.3 nm in the range of 300 to 900 nm.

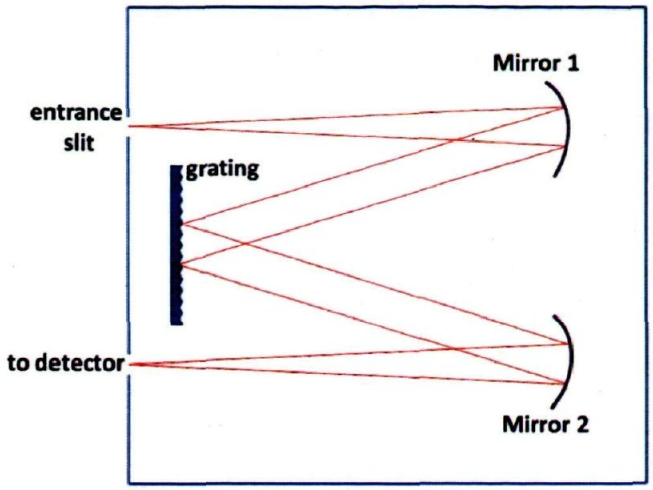

Figure 2.5: *Schematic diagram of spectrometer*

2.3 Experimental configuration

A schematic diagram of the experimental setup to obtain the fluorescence spectra is shown in Figure 2.3. The transform−limited pulse with pulse duration of about 40 fs at FWHM was sent into the chamber. The pulse duration was measured using a second−order single−shot autocorrelator (SSA, Positive Light). As we mentioned, the output beam has a 1 kHz repetition rate, maximum energy of 2 mJ/pulse with a diameter of about 5 mm ($1/e^2$ level of the fluence). This resulted in maximum intensity of 2.9×10^{14} W/cm^2 with a 1 meter focusing lens assuming a Gaussian beam. The Rayleigh range is 9.8 mm. A halfwaveplate and cubic polarizer were used before the compressor (see Figure 2.1 for detail) to change the output energy of the linearly polarized pulses. Therefore we obtained fluorescence signal versus intensity of the laser pulses with the experimental setup shown in Figure 2.3.

The pump and probe experimental setup sketch is illustrated in Figure 2.4. The laser beam after the Spitfire was separated into two arms by a 50/50 beam splitter. One was used as the pump beam (~900 μJ pulse). The other was sent to the OPA to generate the infrared probe pulses at 1338 nm with pulse duration of about 50 fs (FWHM) and pulse energy of around 65 μJ. All of the energies were measured in front of the entrance of the chamber. In fact the probe central wavelength is an important issue. Different wavelength could results in various yields of distinctive products [49]. In addition, depletion process of SESs is a nonlinear phenomenon. Therefore intensity of the probe is an important issue. The maximum energy of OPA is obtained for the central wavelength equal to 1338 nm. In the probe arm a high−resolution delay line

(40 nm) was used. The probe beam had a horizontal polarization parallel to that of the pump beam. Spatial superposition of the two pulses was checked with a far field measurement, while temporal superposition of these two pulses in air was checked by a four wave mixing (4WM) process, where two photons of 800 nm are mixed with one infrared photon ($2\omega_{800} - \omega_{ir}$), leading to a yellowish emission [50].

Finally, in all the experiments, the laser pulses were focused into a vacuum chamber by a plano–convex lens (f = 100 cm or 30 cm). From here on, if we do not mention the lens focal distance it is 1 m. We used an imaging system, including a periscope using metallic mirrors and fused silica lenses, to image the narrow and linear fluorescence column onto the spectrometer entrance slit. The image and the slit were parallel to each other.

In each experiment, proper softwares were written to acquire data automatically. For example to obtain the fluorescence signal versus delay time, we used a computer control translation stage to change the delay time. The spectrum was then read from the detector. In most of the experiments, we monitored the energy of the laser beam to be sure that change in the measurements are not because of energy fluctuations of laser pulses.

Chapter 3

Neutral dissociation of simple molecules through super−excited states

In this chapter, we present and discuss the results of neutral dissociation of simple molecules in a strong laser field. For brief reviews see ref. [51, 52, 53][1].All the experiments were carried out by the candidate and numerical calculations were done by our collaborators. We start with the hydrogen molecule, the simplest and the most abundant molecule in the universe. Fragmentation of hydrogen molecules in a strong laser field is studied experimentally and theoretically. In addition, oxygen and nitric oxide molecules were added to the investigation list. For all of the three molecules (H_2, O_2, NO), fluorescence spectra from neutral excited species were obtained. The emission intensity of some of the strongest lines versus laser intensity on log−log scale was obtained and interpreted. The large slopes of these plots indicate that some high−lying states in the continuum are excited resulting in neutral dissociation. Also, the upper limit of the lifetime of the superexcited states is obtained by an

[1]This chapter is based upon the following papers:

- A. Azarm, D. Song, K. Liu, S. Hosseini, Y. Teranishi, S. H. Lin, A. Xia, F. Kong, and S. L. Chin. Neutral dissociation of hydrogen molecules in a strong laser field through superexcited states. Journal of Physics B: Atomic, Molecular and Optical Physics,44(8):085601, 2011.
- D. Song, A. Azarm, Y. Kamali, K. Liu, A. Xia, Y. Teranishi, S. H. Lin, F. Kong and S. L. Chin. Neutral dissociation of superexcited oxygen molecules in intense laser fields. The journal of Physical Chemistry A, 114(9):3087, 2010.
- K. Liu, D. Song, A. Azarm, S. L. Chin, and F. Kong. Neutral dissociation of superexcited nitric oxide induced by intense laser fields. Chinese Journal of Chemical Physics, 23(3):252, 2010.

ultrafast pump and probe experiment by monitoring one of the fluorescence lines. Finally, semiempirical calculations clarify the possible mechanisms of neutral dissociation through superexcited states.

3.1 Hydrogen H_2

As we mentioned above, Hydrogen is the simplest and most abundant molecule in the universe. It shows rich and fundamental physical behavior while interacting with ionizing radiation [54]. Recently the dissociation behaviour of hydrogen molecules in a strong laser field has attracted considerable attention from scientists [55, 56, 57]. Neutral hydrogen atoms after strong field dissociation have already been observed using biased mass spectrometry. The interpretation of the dissociation mechanism is based upon a photoionization channel, where hydrogen molecules undergo ionization to H_2^+ ions [57]. Lyman−α radiation has also been detected after H_2 molecules are irradiated by a strong 800 nm laser pulse. It was attributed to the re−excitation of a neutral fragment, rather than direct dissociation from the excited state [56]. In this section, many spectral lines in the Balmer series are recorded. These series of radiations provide a window to further explore the dissociation mechanism. Also it will be shown that in an intense laser field, hydrogen molecules could be highly excited owing to multiphoton absorption. The highly nonlinear laser power dependence of product yield tends to support the multiphoton excitation mechanism. Such highly nonlinear excitation means that molecules can be populated in the superexcited states (SESs). Besides, using a pump−probe technique and fluorescence spectroscopy, we confirmed multiphoton superexcitation of hydrogen molecules in a strong laser field. We detect the depletion of the fluorescence signals by the probe pulse and determine the lifetime of the SESs. At the same time, coupled to potential energy curve (PEC) simulation, we found that repulsive PECs could explain the dissociation process.

Figure 3.1 shows the fluorescence spectra obtained in the range of 300−700 nm. The spectral lines are attributed to the Balmer series of the hydrogen atom ($n_f \rightarrow 2$), from $n_f = 3$ up to $n_f = 14$. Figure 3.2 shows the energy levels of fluorescing hydrogen atoms according to [2]. It is tabulated in table 3.1. The observation of so many excited hydrogen atoms as the dissociation products is indeed significant. On the one hand, the observation of the excited species implies that the parent molecule has been excited to some highly excited states. We note that the dissociation energy of a hydrogen molecule is 4.47 eV, while in the experiment the $H(3l)$ state is populated which needs an energy of 12.08 eV (see Figure 3.2). It means that the excitation energy in the dissociation process $H_2 + n\hbar\omega \rightarrow H(3l) + H(1s)$ needs to be at least 16.56 eV. All the

n_f	Observed wavelength(nm)	$\frac{1}{\lambda(nm)} = R_H{}^a(\frac{1}{(n_i=2)^2} - \frac{1}{n_f^2})$	Dissociation limit (eV) [1]	name
3	656.73	656.14	16.56	H_α
4	486.49	486.03	17.22	H_β
5	434.41	433.95	17.53	H_γ
6	410.45	410.09	17.69	H_δ
7	397.21	396.92	17.79	H_ε
8	389.10	388.82	17.86	H_ζ
9	383.84	383.46	17.90	H_η
10	380.06	379.71	17.93	H_θ
11	377.44	376.97	17.96	H_τ
12	375.33	374.94	17.98	H_κ
13	373.72	373.46	17.99	H_λ
14	372.46	372.12	18.00	H_μ

[a] $R_H = 1.0973731568539 \times 10^{-2} nm^{-1}$ [58].

Table 3.1: *Details of the observed atomic hydrogen lines [1].*

other dissociation limits energy (see table 3.1) are beyond the first ionization potential of the hydrogen molecule (15.42 eV) [1]. In other words, hydrogen molecules are excited to some highly excited states, i.e. SESs, in the intense laser field.

Taking the advantages of the gating system, we can extend the range of wavelength to 900 nm. The gating system can get rid of scattered 800 nm. The gate is opened for 10 ns after the laser pulse arrived at the interaction zone. In addition we have tried to use 30 cm lens to see the effect of higher intensity (2.7×10^{15} W/cm^2). We expected to see some lines from Paschen series which converge to the wavelength of 820 nm. Figure 3.3 shows molecular hydrogen spectra in an intense laser field with an extended x axis from 100 to 900 nm in comparison to Figure 3.1. The detector is not very sensitive to short wavelengths. The lines with the wavelength higher than the first Balmer line (H_α) are second order diffraction of other Balmer series line (H_γ and H_δ) from grating of spectrometer at 868.33 and 820.46 nm respectively. Generally, the data from Figure 3.3 do not give us any more information than those in Figure 3.1, except that we can conclude that SESs are populated at higher intensities (2.7×10^{15} W/cm^2) as well.

We have investigated the pressure dependence of the fluorescence signal to provide a proof that excited hydrogen fragments are the result of direct laser excitation rather than other processes (see for example [59]). Figure 3.4 shows the integrated fluorescence signal of the first Balmer line versus pressure in a log−log scale. It is obtained in more than three orders of magnitude in pressure. We have fitted a red line with a slope 1.08

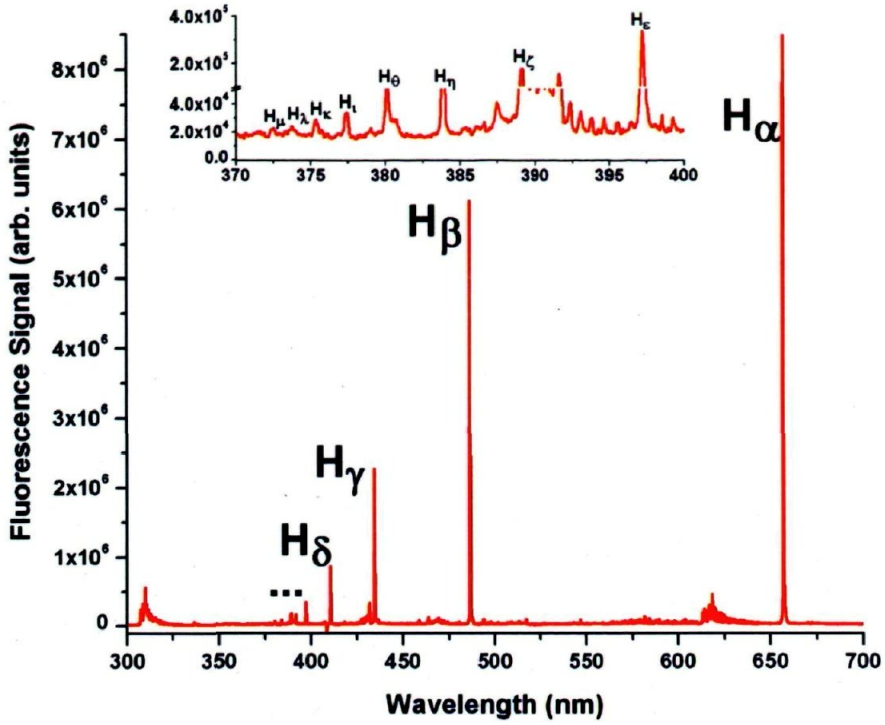

Figure 3.1: *The fluorescence spectra of H_2 in a strong laser field at around 8 Torr. The inset shows the lines of H atoms from 370 to 400 nm*

in the low−pressure region. Clearly, in the low−pressure region, the fluorescence signal increases linearly with pressure. At higher pressures, collisional quenching can decrease the fluorescence signal. Therefore, there is no other process that can create neutral excited atomic hydrogen. The abrupt increase starting from around 10 torr could be due to self−focusing and filamentation resulting in a sudden increase in intensity in the interaction zone. We have recorded the full spectra for various pressures. The observed Balmer series in all the pressures are identical except that the signal to noise ratio is different at different pressures. Moreover, based on lifetime measurement of SESs in hydrogen molecules we can exclude other processes such as collisions as a reason to create atomic excited hydrogen. We will discuss this latter problem in more detail at the end of this section. In addition, laser excitation to molecular Rydberg states resulting in neutral dissociation to atomic fragments and its competition with ionization was already shown by recording photoelectron spectra at different wavelengths (310−330 nm) in [37]. Moreover, we have studied the full spectrum versus pressure (see Figure 3.5). Generally, the fluorescence signal is very weak therefore it is necessary to find the pressure with the strongest florescence signal. The other benefit of pressure dependent study of fluorescence signal could be finding the proper pressure with the strongest signal. Therefore all of the data presented in this section were obtained in hydrogen

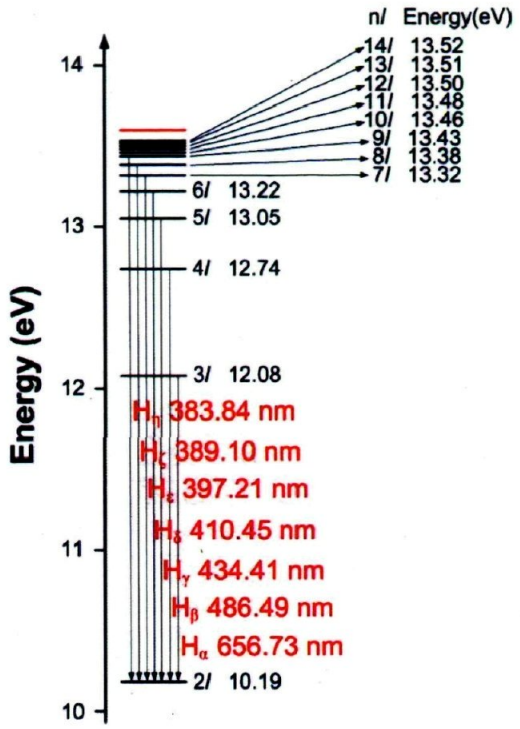

Figure 3.2: *The observed hydrogen atomic lines in Figure 3.1 attributed to excited atomic hydrogen, 12 Ballmer series (ground state energy is zero and the first ionization potential is 13.59 eV) [2]*

molecules at 8 torr. The data presented in this thesis were accumulated over several thousand laser shots for each point.

The highly nonlinear laser power dependence of product yield (fluorescence) provides an experimental evidence of the formation of SESs. Indeed, we measured the fluorescence intensity of two strong Balmer lines as a function of the laser energy. The laser energy is proportional to the intensity of the laser shots. Based on Gaussian beam propagation, one could estimate the intensity from the energy of the pulse (1−2 mJ corresponding to $1.4 \times 10^{14} - 2.9 \times 10^{14}$ Wcm^{-2}). We measured the slope of each line in the energy scale. The slopes are 11.7 and 11.5 in a log−log plot for the wavelengths of around 656 nm and 486 nm, respectively (Figure 3.6). These slopes indicate that the H_2 molecule can be excited to a highly excited state through the absorption of at least about 11 to 12 effective photons (one photon energy ∼1.55 eV) whose energy (17.05 − 18.6 eV) is beyond the first ionization potential (15.42 eV). The highly excited states, i.e. SESs, undergo dissociation leading to the production of H atoms which we observed. On the other hand, having observed different products suggests that a variety of dissociation channels exist simultaneously.

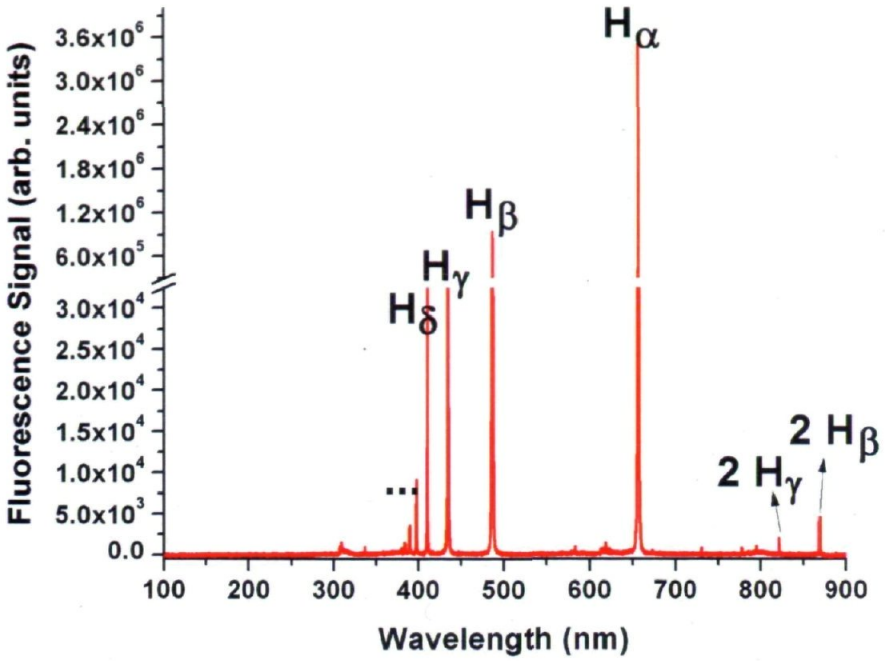

Figure 3.3: *The fluorescence spectra of H_2 in a strong laser field at around 8 Torr using 30-cm lens with extended x axis. The peak intenisty is $2.7 \times 10^{15}\,\mathrm{W/cm^2}$ approximately.*

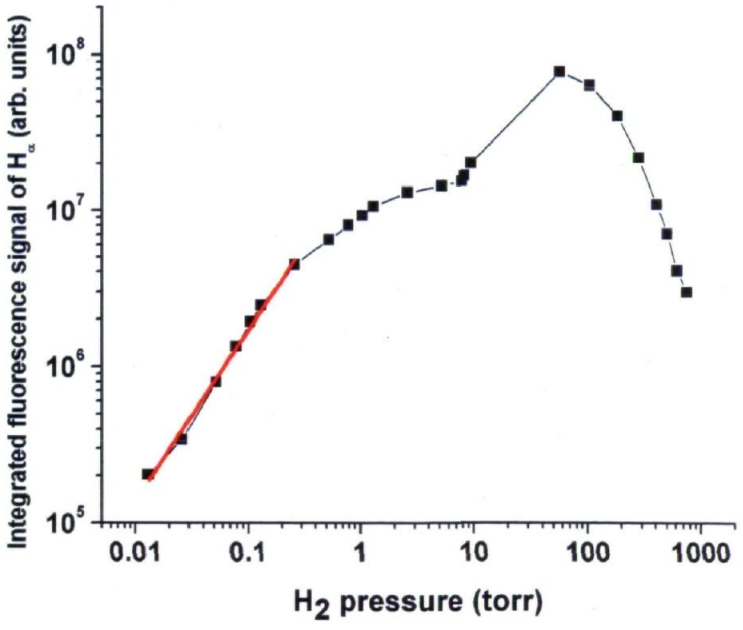

Figure 3.4: *Integrated fluorescence signal (around 656 nm) versus pressure of hydrogen molecules.*

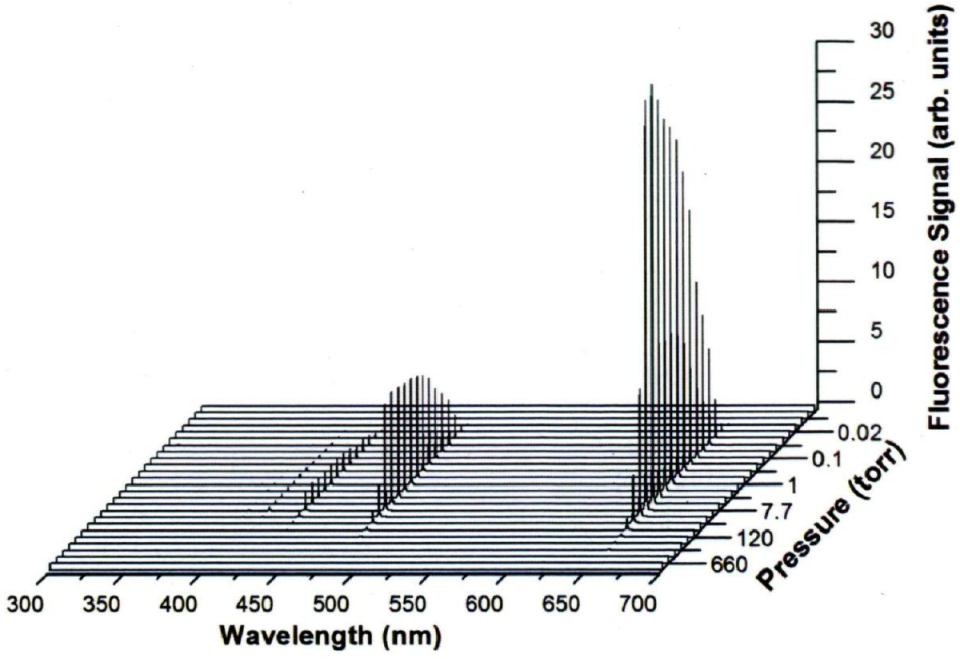

Figure 3.5: *Hydrogen full spectra versus pressure of hydrogen molecules.*

For the dissociation of molecules in intense laser fields, there are two classes of pathways. The first considers the dissociation of the molecules whose levels are affected under external laser fields. For example, our colleague proposed the field assisted dissociation (FAD) model which can successfully treat the dissociation of the molecular ions of acetone, methane, and acetyl aldehyde [60, 61]. FAD considers that the laser field distorts the potential surface straightforwardly, weakening the chemical bond, and leading to the bond rupture. Other theoretical models such as re−scattering, bond softening, or above threshold dissociation belong to this class of pathways. The second considers that the intense laser field causes an extremely high excitation of the molecule, equivalent to absorbing as many as 12 laser photons and leading to highly excited states with almost 18 eV. A spontaneous dissociation without laser fields thus takes place. Laser field free PECs (potential energy curves) can be applied in the subsequent dissociation process. This section of thesis treats the dissociation of a hydrogen molecule theoretically through the second pathway. However, there is no quantum mechanically calculated PEC for SESs, since the accurate calculation of the high−lying excited states of molecules is extremely difficult, even for a hydrogen molecule.

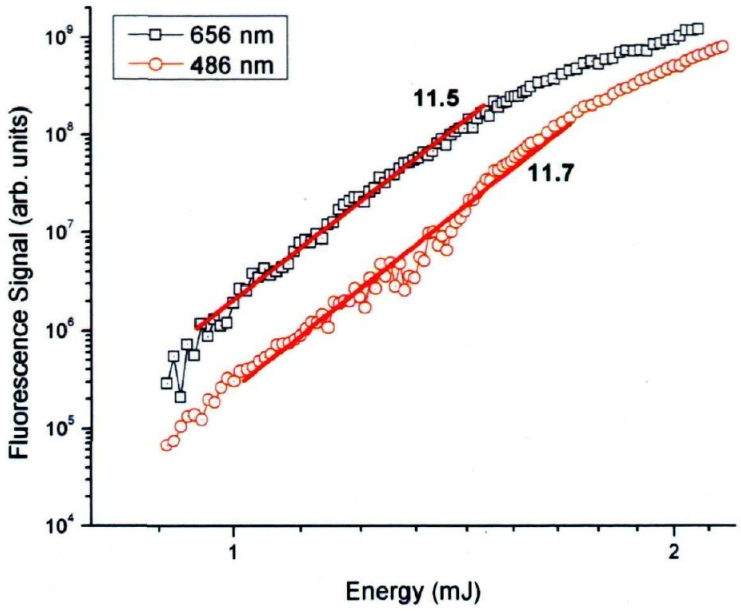

Figure 3.6: *Fluorescence signal versus the laser energy which is proportional to intensity. The fluorescence is collected and integrated around 656 nm and 486 nm from the first two Balmer series.*

Recently, our theoretician colleagues proposed a Rydberg molecule model to estimate the dissociation process. In the Rydberg model, the SES is considered as the Rydberg state which consists of an excited ion core and a Rydberg electron. The Rydberg electron can be treated as a spectator, not participating in the dissociation directly. The dissociation products are two neutral fragments. One of them is a Rydberg atom or molecule with the same principle quantum number n and angular momentum quantum number l of the superexcited parent molecule. To obtain the PECs of high−lying Rydberg states, our colleagues first calculate the PECs of the corresponding H_2^+ ion cores (Figure 3.7). The calculations are performed with the MOLPRO software package [62] at CASSCF/av5z level. Then, we shift down the curve (PEC) of the state $^2\Sigma_u^+$ until the energy limit on the long−distance side fits the experimental data. In this way, PECs of some superexcited H_2 states are obtained (Figure 3.7). With these Rydberg PECs, we are able to trace the dissociation pathway of the superexcited H_2 molecules. In a strong laser field, the ground state of H_2 molecules absorb many photons simultaneously accompanying a vertical excitation in the energy plot. Various SESs of hydrogen molecule, $H_2^{**}[(H_2^+, 1^2\Sigma_u^+)nl, 1\Lambda_{g/u}]$ and $H_2^{**}[(H_2^+, 1^2\Sigma_g^+)nl, 1\Lambda_{g/u}]$, with different quantum numbers are reached, where $(H_2^+, 1^2\Sigma_u^+)$ and $(H_2^+, 1^2\Sigma_g^+)$ stand for the ion core, nl stands for the spectator electron with a principle quantum number n and an angular quantum number l and $1\Lambda_{g/u}$ stands for the term of the superexcited H_2^{**}. Rydberg states, $H_2^{**}[(H_2^+, 1^2\Sigma_u^+)nl, 1\Lambda_{g/u}]$,

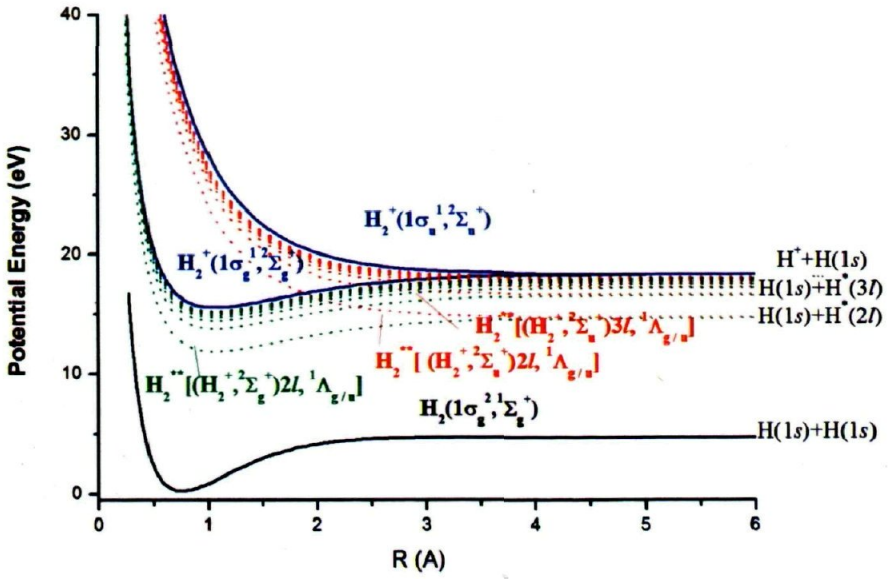

Figure 3.7: *Potential energy curves of H_2. H_2 in the ground state (black solid curve), H_2^+ ions (blue solid curves), Rydberg states (green dotted curves) and superexcited states (red dotted curves).*

dissociate spontaneously along the repulsive ion−state−shape PECs or transit to Rydberg states of $H_2^{**}[(H_2^+, 1^2\Sigma_g^+)nl, 1\Lambda_{g/u}]$ via avoided crossing, producing a ground state H atom and an excited H atom. The latter species emit lights at wavelengths of 656.73, 486.49, 434.41, 410.45 nm ... etc. which are observed in our experiment. But another Rydberg states series, $H_2^{**}[(H_2^+, 1^2\Sigma_g^+)nl, 1\Lambda_{g/u}]$, is not responsible for the observation of H excited atoms, because their vertical excitation energies are smaller than dissociation limits, and corresponding dissociation processes do not occur.

To know the dissociation dynamics and properties of SESs, we measured the fluorescence signals of some of the spectral lines as a function of the delay time between ultrashort pump (800 nm) and probe (1338 nm) pulses. Figure 3.8 shows the integrated 656 nm fluorescence intensity versus the delay time between pump and probe pulses. We can clearly see an obvious decrease of the fluorescence signal taking place when the delay time is around zero. The dip width of the fluorescence signal is about 180 fs (FWHM). Coupled to the PEC simulation, we can imagine that the population of the SESs will be decreased by the probe pulse when dissociation is underway. This results in the depletion of the florescence signals. Therefore, the dip width means the lifetime of the SESs. This experiment was performed for the other lines, namely 486 nm (see

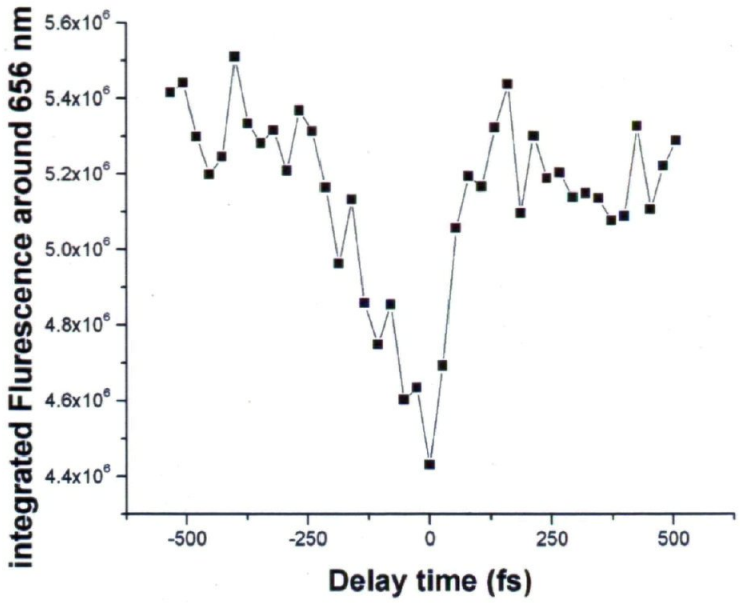

Figure 3.8: *Integrated fluorescence signal at around 656 nm versus the delay time between the pump and probe pulses, a negative delay time means the probe pulses are behind the pump pulses.*

figure 3.9). The result is roughly the same with a lifetime of 180 fs. We emphasize here

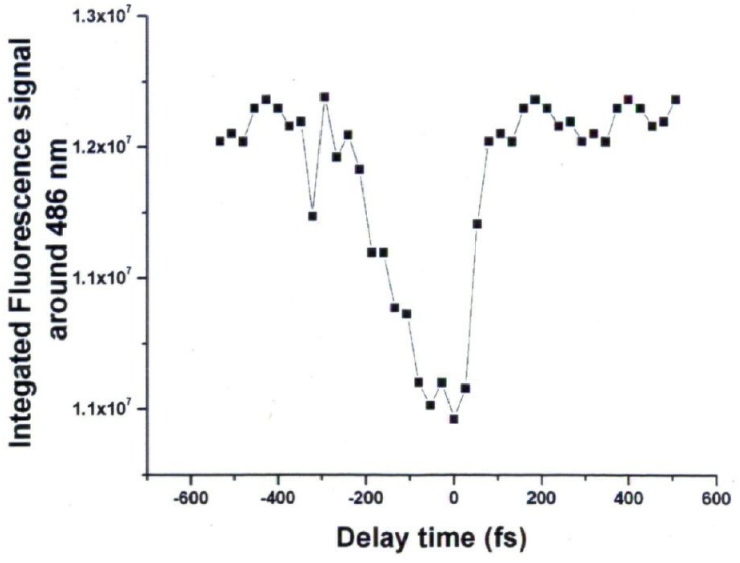

Figure 3.9: *Integrated fluorescence signal at around 486 nm versus the delay time between the pump and probe pulses, a negative delay time means the probe pulses are behind the pump pulses.*

that the fluorescence depletion could not be explained by other reasons. We exclude the simple ionization scheme where the neutral hydrogen atoms are generated by disintegration of the H_2^+ ion or electron−ion recombination since the lifetime of these two processes is very long.

Now we can discuss the fact that SESs are the result of direct laser excitation in more detail. As we showed above, the 42 fs laser pulse (800 nm) excites the molecule into the SESs. Within this pulse duration, there is no collision between molecules at 8 torr because the mean collision time is of the order of 50 ns. The dissociation of the molecule from the SESs into the two H neutrals takes about 180 fs according to our current measurement. This is the lifetime of the SES. During this time together with the pumping time of 42 fs, there is still no collision with any neighboring molecule while H^* is already formed and will fluoresce. During the fluorescence time of H^*, there is collision. But this will only reduce the fluorescence intensity. It would not contribute to the excitation of H atoms. And this is what the experimental data show: a decrease in the fluorescence signal at 8 torr. Electron collision can be neglected during the pumping and dissociation time of about 222 fs (pump duration + SES lifetime) because the mean free time of an electron at 8 torr is about 95 ps. Electron collisional excitation of the neutral ground state H atom could be neglected because the free electron energy through ATI (above threshold ionization) at the intensity level we are using is at best a few eV and the probability is very small. By the same argument, electron excitation of the SES can be neglected. Finally, we would claim that without any ambiguity, the excited hydrogen fragment is a result of direct laser excitation of a hydrogen molecule.

3.2 Oxygen O_2

In this section, we study the dissociation processes of the superexcited states of O_2 molecule induced by femtosecond intense laser pulses both theoretically and experimentally. The study of SESs of O_2 molecules can be treated as a typical example for a more complex molecule as compared to hydrogen. Ukai et al. [63] and Karawajczyk et al.[64] investigated neutral dissociation of SES in the energy region of $14-21$ eV by using synchrotron radiation (SR) as a conventional excitation method. They roughly assigned several excited O atoms observed in their excitation spectra to dissociation products in Rydberg states converging to the $B(^2\Sigma_g^-), b(^4\Sigma_g^-)$, or $A(^2\Pi_u)$ states of the O_2^+ ion, respectively, but they did not supply enough theoretical explanation of the dissociation mechanism. Odagiri et al. focused on experimentally identifying the inner valence excited states and multiply excited states of O_2 as SESs in the higher energy range of $23-47$ eV using the photon−photon coincidence method [65]. Therefore we

can compare single photon and multiphoton process resulting SESs in O_2 molecules.

In this section four issues will be described similar to H_2 molecule. First of all, we report that the thirty−three spectral lines from excited oxygen atoms are the dissociation products of the superexcited oxygen molecules produced in the intense laser field. It indicates that more dissociation channels occur in the intense laser field than those observed in synchrotron radiation excitation. Second, the product yield is strongly dependent on the laser intensity. The strong laser power dependence of the intensities of various fluorescence lines with slopes between 9 and 11 in a log−log plot provides the experimental evidence that the precursor states of excited O atoms should be some SESs of O_2 molecules. The above two issues prove that using a femtosecond intense laser to excite SES is complementary to synchrotron excitation. The third issue is that we have constructed empirical (Morse) potential energy curves (PECs) for the SESs of O_2. On the basis of the Morse PECs, we propose a predissociation mechanism to interpret the dissociation processes of SESs. The emissions of products thus could be well explained. These theoretical results can provide a better insight into the essence of SESs than before. Finally, we measured directly the lifetime of the SES and compared it with the quasiclassical trajectory (QCT) calculations. It showed that the neutral dissociation of a SES is indeed a fast predissociation process. Through the above studies, the concept of the SES of O_2 molecule and the mechanisms of the dissociation are better clarified. Considering that we proved multiphoton superexcitation in the case of H_2 the observation in O_2 starts to indicate that this process in molecules is a general process during intense femtosecond laser interaction with molecules.

3.2.1 Spectra of O_2

The SESs are produced by the intense Ti:sapphire laser pulses. Products of the neutral dissociation are detected by fluorescence spectroscopy. Figure 3.10 shows the fluorescence spectrum recorded between the wavelengths of 200 and 900 nm. It reveals that the SESs can also be created by intense laser excitation. It is an alternative method to produce the SESs of molecules, in addition to synchrotron radiation excitation. The emission bands between 306 and 320 nm are assigned to the rovibronic transitions of $O_2^+(A^2\Pi \rightarrow X^2\Pi)$ [66] which are not dealt with in the present thesis. The artifacts between 612 and 640 nm are attributed to the second−order diffraction of the same transitions of $O_2^+(A^2\Pi \rightarrow X^2\Pi)$. Similarly, the emissions at 789.7 and 873.8 nm are the second−order diffraction of the spectral lines at 394.8 and 436.8 nm, respectively. The rest of the spectral lines in the spectrum are attributed to the transitions in the oxygen atoms, which are the dissociation products of O_2. The assignment of spectral lines was done as well. Thirty−three spectral lines have been recorded in the fluorescence

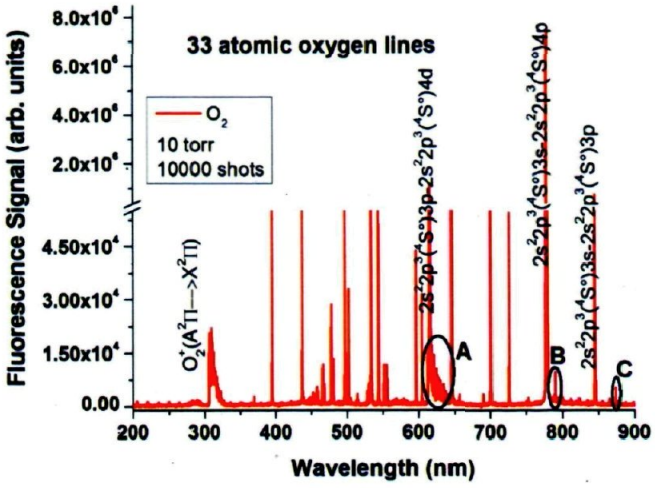

Figure 3.10: *Fluorescence spectrum of the photodissociation products of O_2 molecules. The artifacts between 612 and 640 nm are attributed to the second order diffraction of the transitions of $O_2^+(A^2\Pi \rightarrow X^2\Pi)$ (this is marked by an ellipse A). The emissions at 789.7 (this is marked by an ellipse B) and 873.8 nm (this is marked by an ellipse C) are the second order diffraction of the spectral lines at 394.8 and 436.8 nm, respectively. For details about these thirty three atomic oxygen lines see table 3.2 at the end of this chapter.*

spectrum (see Table 3.2 at the end of this chapter). Most observed lines actually contain a few lines. See for example the oxygen transitions around 777 nm on Figure 3.11. If we use the grating with higher number of grooves per millimeter in the spectrometer, we can easily resolve three lines. These lines could include a lot of information, but the goal of this thesis is to prove the universality of neutral dissociation in a strong laser field through SESs. In the last column of Table 3.2 at the end of this chapter, the observed wavelengths and the wavelengths reported in the literatures are listed. Ten of them are new observations. The remaining twenty three transitions can be found in the NIST database [2]. They are assigned to the transitions of six Rydberg series of O atoms. The observed transitions and their assignments are listed in columns 4 and 5 of table 3.2 at the end of this chapter. According to ref. [2], the transitions are:

- $2s^2 2p^3(^4S^o)3p\ ^5P$, $2s^2 2p^3(^4S^o)4p\ ^5P$ and $2s^2 2p^3(^4S^o)5p\ ^5P \longrightarrow 2s^2 2p^3(^4S^o)3s\ ^5S^o$ at 777.5, 394.8 and 369.5 nm
- $2s^2 2p^3(^4S^o)3p\ ^3P$ and $2s^2 2p^3(^4S^o)4p\ ^3P \longrightarrow 2s^2 2p^3(^4S^o)3s\ ^3S^o$ at 845.0 and 436.8 nm

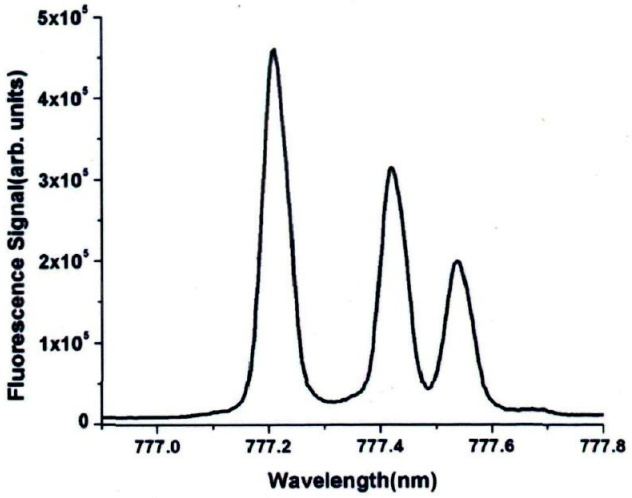

Figure 3.11: *Three lines of 777 nm are resolved by using 2400 g/mm grating spectrometer (10 torr O_2).*

- $2s^2 2p^3(^4S^o)4d\ ^5D^o$, $2s^2 2p^3(^4S^o)5d\ ^5D^o$, $2s^2 2p^3(^4S^o)6d\ ^5D^o$, $2s^2 2p^3(^4S^o)7d\ ^5D^o$ and $2s^2 2p^3(^4S^o)8d\ ^5D^o \longrightarrow 2s^2 2p^3(^4S^o)3p\ ^5P$ at 615.9, 533.2, 497.1, 477.5 and 465.7 nm
- $2s^2 2p^3(^4S^o)5s\ ^5S^o$, $2s^2 2p^3(^4S^o)6s\ ^5S^o$, $2s^2 2p^3(^4S^o)7s\ ^5S^o$ and $2s^2 2p^3(^4S^o)8s\ ^5S^o \longrightarrow 2s^2 2p^3(^4S^o)3p\ ^5P$ at 645.4, 543.5, 502.2 and 480.4 nm
- $2s^2 2p^3(^4S^o)4d\ ^3D^o$, $2s^2 2p^3(^4S^o)5d\ ^3D^o$, $2s^2 2p^3(^4S^o)6d\ ^3D^o$, $2s^2 2p^3(^4S^o)7d\ ^3D^o$ and $2s^2 2p^3(^4S^o)8d\ ^3D^o \longrightarrow 2s^2 2p^3(^4S^o)3p\ ^3P$ at 700.6, 596.2, 551.4, 527.7 and 513.3 nm
- $2s^2 2p^3(^4S^o)5s\ ^3S^o$, $2s^2 2p^3(^4S^o)6s\ ^3S^o$, $2s^2 2p^3(^4S^o)7s\ ^3S^o$ and $2s^2 2p^3(^4S^o)8s\ ^3S^o \longrightarrow 2s^2 2p^3(^4S^o)3p\ ^3P$ at 725.8, 604.9, 555.6 and 530.1 nm

The remaining ten transitions marked by a star or double star in table 3.2 have not been reported in the literature. Those ten new lines are listed below:

- $2s^2 2p^3(^4S^o)9s\ ^3P$ and $2s^2 2p^3(^4S^o)10s\ ^3P \longrightarrow 2s^2 2p^3(^4S^o)3p\ ^3P$ at 514.9 and 505.4 nm
- $2s^2 2p^3(^4S^o)9d\ ^3D^o \longrightarrow 2s^2 2p^3(^4S^o)3p\ ^3P$ at 503.9 nm

- $2s^22p^3(^4S^o)9s\ ^5S^o$, $2s^22p^3(^4S^o)10s\ ^5S^o$, $2s^22p^3(^4S^o)11s\ ^5S^o$ and $2s^22p^3(^4S^o)12s\ ^5P \longrightarrow 2s^22p^3(^4S^o)3p\ ^5P$ at 467.6, 459.1, 453.4 and 449.1 nm
- $2s^22p^3(^4S^o)9d\ ^5P$, $2s^22p^3(^4S^o)10d\ ^5P$ and $2s^22p^3(^4S^o)11d\ ^5P \longrightarrow 2s^22p^3(^4S^o)3p\ ^5P$ at 458.0, 452.5, and 448.5 nm

By means of the Rydberg formula (in the following section), we have verified that these transitions can be assigned to the unreported Rydberg transitions. Referring to these transitions, three new Rydberg states, $2s^22p^3(^4S^o)11s\ ^5S^o$, $2s^22p^3(^4S^o)12s\ ^5S^o$ and $2s^22p^3(^4S^o)10d\ ^5D^o$ which have not been reported previously, are observed in this experiment and shown in table 3.2, with the symbol of double star. The oxygen molecule undergoes neutral dissociations in the intense laser field. Most likely, the product pair consists of a ground state oxygen atom $O(^3P)$ and an excited oxygen atom of $O(n,l)$, where n and l are the principle and angular quantum numbers, respectively. A variety of products found in the spectrum indicate that many dissociation channels exist simultaneously. This indicates also that various SESs of O_2 have been created in the intense laser field.

We measure the pressure dependence of fluorescence intensity. Figure 3.12 shows the integrated fluorescence signal around 777 nm lines versus pressure. The pressure dependence below 10 Torr is linear and the slope is nearly one, which means that collisional effects are negligible. The linear pressure dependence shows that the emitters are the products of unimolecular dissociation. This is the same for all of the lines observed (see figure 3.13 for detail). Hence all of the experiments with oxygen have been done at 10 torr. The discussion is very similar to hydrogen molecules therefore the readers are referred to the fourth paragraph of the previous section 3.1 for more detailed discussion.

3.2.2 Intensity dependent fluorescence signal of O_2

To understand the dissociation process of the O_2 molecule, we measured the fluorescence intensity of the O atoms as a function of the laser intensity. Three slopes are obtained as 8.9, 11.1, and 11.3 in a log−log plot for the wavelengths of 615.9, 777.5, and 845.0 nm, respectively (Figure 3.14). In the view of multiphoton excitation theory, this observation implies that the rate−determining process may absorb at least ten photons (1.55 eV each photon at 800 nm) on average. In other words, the O_2 molecule can be excited to a highly excited state, whose energy (>15.5 eV) is beyond the first ionization potential of 12.06 eV [2]. The highly excited state, or the superexcited state, then undergoes dissociation leading to the product of O atoms we observed.

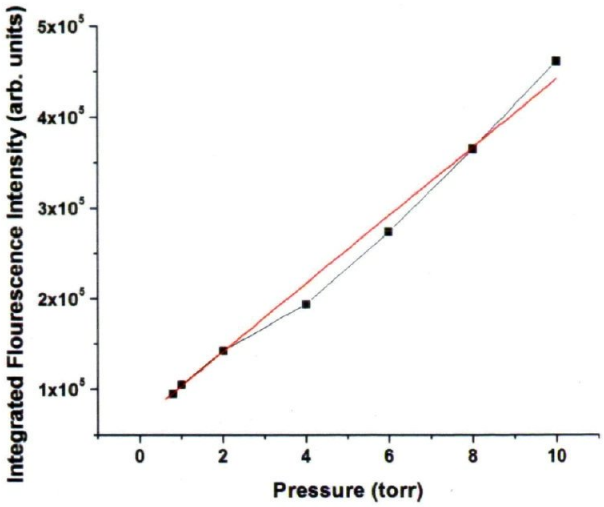

Figure 3.12: *Fluorescence signals around 777 nm versus pressure*

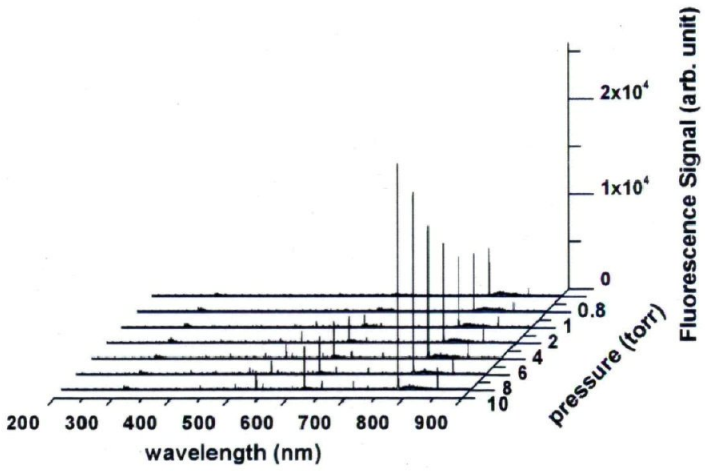

Figure 3.13: *Oxygen full spectra versus pressure.*

We theoretically investigated the multiphoton excitation dynamics of O_2 molecule in strong laser fields. Multiphoton excitations are caused by absorbing a certain number of photons. The slope in the log−log plot suggests the number of the photons involved in the excitation process. The calculation method has been described in detail in [67]. Only a brief introduction is given here. Our colleague made a quantum chemical calculation with the complete active space self−consistent−field (CASSCF) method

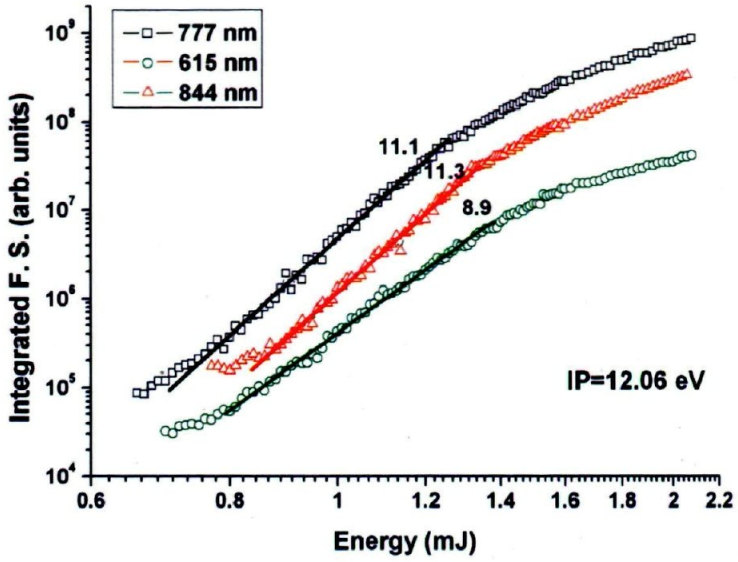

Figure 3.14: *Fluorescence intensity dependence on the laser intensity. The fluorescence is collected and integrated around 615.9, 777.5 and 845.0 nm, respectively.*

with the aug−cc−pVTZ basis set to obtain the excitation energy and transition dipole moment matrix elements between the eigenstates. For O_2 molecule, we take 96 valence states into the calculations. The first excitation energy is about 1.0 eV, and the highest eigenstate included has the energy of ~21 eV above the ground state. Figure 3.15 shows the calculated transition probabilities of the vertical excitation as functions of laser intensity for the 96 states. Most of the curves of power dependence have slopes between 9 and 11, which are in good agreement with the experimental results. It indicates that the O_2 molecule dissociates into O excited atomic products via its highly excited states. It should be noted here that only the molecules in SESs states can dissociate, because the threshold production of fragments (O(ground state) + O (Rydberg state)) is at least 15 eV. SESs of molecules are created in the excitation process. These superexcited molecules decay into the various channels "spontaneously".

3.2.3 Semiempirical method

Dissociation takes place in the SESs of oxygen molecule. To understand the dissociation mechanism, the PECs of the SESs should be understood at first. However, there is lack of quantum−mechanically calculated results for SESs so far, even for diatomic molecules like O_2. In this section, we first make an empirical PEC for the SESs. In light of these empirical (Morse type) PECs, we further interpret the dissociation processes.

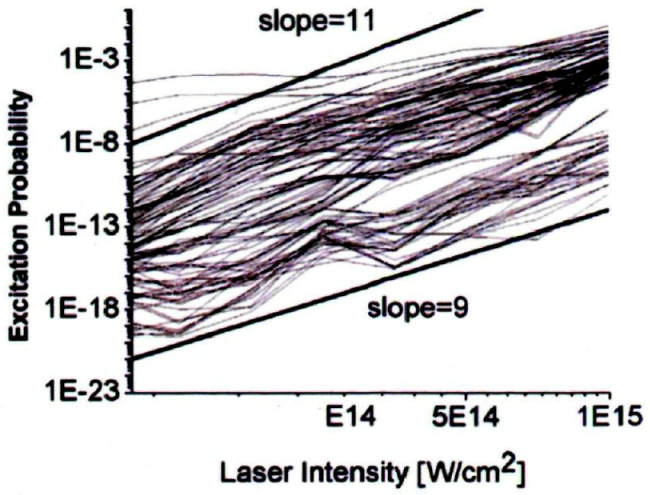

Figure 3.15: *Excitation probabilities to various excited states of O_2 as functions of laser intensity. Here, the laser pulse duration time is 42 fs, and the central frequency of the laser pulse is 800 nm.*

Following Hatano [29], we interpret the SESs as those appropriately excited Rydberg states. We shall start by proposing a spectroscopic nomenclature of such states. Quantitative justification of such interpretation through PEC calculation and comparison with experimental results will follow. The SES of a molecule O_2 is expressed as a symbol O_2^{**} followed by a more specific molecular notation ($(O_2^+$, spectral term of the ion to which the Rydberg states converges) $nl\lambda$, spectral terms of the molecule). For example, $O_2^{**}((O_2^+\ a^4\Pi_u)4s\sigma_g, {}^3\Pi_u)$ denotes a specific SES of oxygen molecule. In this case, the double asterisk means a superexcited state which possesses energy higher than the first IP. The SES is the Rydberg state converging to the excited state ($a^4\Pi_u$) of O_2^+ ion. The principle quantum number n, the angular quantum number l, and its projection onto the molecular axis λ of the molecule in the Rydberg series, are indicated by the symbols 4, s, and σ, respectively. Finally, the Rydberg state has a spectral term of ${}^3\Pi_u$). Unlike hydrogen molecules, all of the SESs in oxygen molecules that we found are bonding curves. Among the empirical functions, the Morse function is the most explicit one. The Morse function denotes the potential energy $V(r)$ of the molecule as a function of the bond distance r:

$$V_e = D_e(e^{-2a(r-r_e)} - 2e^{-a(r-r_e)}) \tag{3.1}$$

where D_e is the depth of the potential well and r_e is equilibrium bond distance. The symbol a is the Morse parameter. The vibrational frequency ω_e and the equilibrium bond distance r_e of the Rydberg states are adapted from those of the O_2 ions to which they converge. It is based on the ionic core approximation, which treats the Rydberg

molecules as ions. The depth of the potential well, D_e, consists of two parts, the zero point energy E_0 and the dissociation energy D_0. D_0 is the difference between the energy of the Rydberg O_2 molecule E_r and that of the products of $O + O^*$ (in Rydberg states) E_p, i.e. $D_0 = E_p - E_r$. The data of E_p are adapted from the NIST table [2]. E_r is obtained by the formula $E_r = IP - R/(n-\delta)^2$, where δ is the quantum defect and R is the Rydberg constant. To our knowledge, the correlation between the quantum numbers of high−Rydberg molecules and those of these Rydberg fragments is an unsolved problem. We thus assume that the principle quantum number (n) and the angular quantum number (l) do not change in the dissociation processes to correlate a specific PEC with its dissociation products. Our assumption is supported by the following well−known point: "If the core ion is formed in a sufficiently high excited state, it can dissociate with no help from the high−Rydberg electron. The fragments can separate to a large distance and still remain completely within the high−Rydberg orbital" [68]. Therefore, the possible products in the dissociation are shown on the right−hand side of the curves in Figure 3.16 to Figure 3.20. For example, in Figure 3.16 , $O_2^{**}((O_2^+\ A^2\Pi_u)4s\sigma_g,^3\Pi_u)$ can dissociate into two atoms, a ground state O atom (^3P) and a Rydberg atom $O(4s,^3S^o)$. With Equation (3.1), we have built the Morse type PECs for the SESs of oxygen molecules. The PECs are shown as the curves in Figure 3.16 to Figure 3.20. Each figure depicts two series of Rydberg states with different principle quantum numbers n. It can be seen in the figures that there are two types of curves, featured by different equilibrium distances and different depths of the potential well. The first type of PECs has short equilibrium bond distances about 1.30 Å, which is comparable to that of the ground state, 1.21 Å. The corresponding SESs converge to the $A(^2\Pi_u)$, $b(^2\Sigma_g^-)$ and $B(^2\Sigma_g^-)$ states of O_2^+ ion. The removed valence electron in the excitation is a non bonding electron of the molecules. Such excitation does not weaken the chemical bond, so that the potential well is deep. Usually, a vertical excitation from the ground state of O_2 to the kind of SES will create a low vibrationally excited molecule but will not lead to dissociation. For the second type of PECs, the equilibrium bond distances could be as long as about 1.7 Å. Doubly excited electrons make the $O-O$ bond weaker. These SESs correspond to Rydberg states converging to the ionic states of $O_2^+ d(^4\Sigma_g^+)$, or $O_2^+ f(^4\Pi_g)$. The potential wells of the PECs are shallow, so that the states are less stable.

Here we discuss some possible dissociation processes of the typical dissociation channels. As shown in Figure 3.16 to Figure 3.20, the SESs are created through the vertical excitation of the first type of Rydberg states. The SESs are low vibrationally excited, which do not lead to dissociation directly. However, via curve crossing, these SESs can transit to the second type of PECs of SESs: $O_2^{**}((O_2^+ d^4\Sigma_g^+)np\sigma_u,^3\Sigma_u^+)$, $O_2^{**}((O_2^+ f^4\Pi_u)np\sigma_u,^3\Pi_u)$, $O_2^{**}((O_2^+ f^4\Pi_u)np\sigma_u,^3\Pi_u)$, $O_2^{**}((O_2^+ d^4\Sigma_g^+)np\sigma_u,^3\Sigma_u^+)$, $O_2^{**}((O_2^+ f^4\Pi_u)np\sigma_u,^3\Pi_u)$ and $O_2^{**}((O_2^+ d^4\Sigma_g^+)np\sigma_u,^3\Sigma_u^+)$ series [64, 69, 70]. This tran-

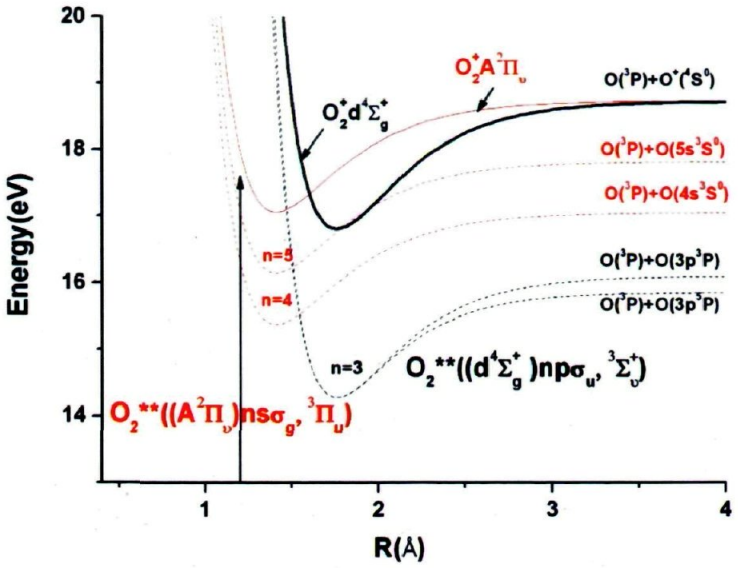

Figure 3.16: *PECs of the SESs series of* $O_2^{**}((O_2^+A^2\Pi_u)ns\sigma_g, {}^3\Pi_u)$ *and* $O_2^{**}((O_2^+d^4\Sigma_g^+)3p\sigma_u, {}^3\Pi_u^+)$. *The solid and dash lines show ionic states and SESs, respectively.*

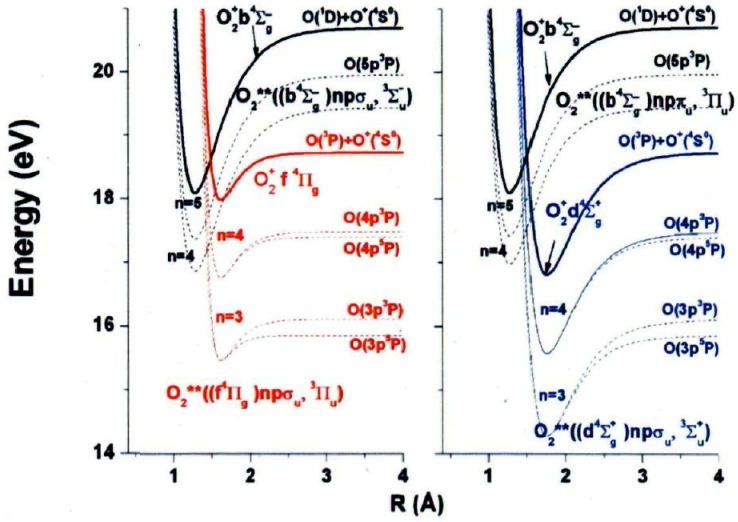

Figure 3.17: *PECs of the SESs series of* $O_2^{**}((O_2^+b^4\Sigma_g^-)np\sigma_u, {}^3\Sigma_u^-)$,$O_2^{**}((O_2^+f^4\Pi_u)np\sigma_u, {}^3\Pi_u)$ *and* $O_2^{**}((O_2^+b^4\Sigma_g^-)np\pi_u, {}^3\Pi_u)$ $O_2^{**}((O_2^+d^4\Sigma_g^+)np\sigma_u, {}^3\sigma_u^+)$. *The solid and dash lines show ionic states and SESs, respectively.*

sition usually produces highly vibrational excitation in these SESs. The vibrationally hot molecules thus would undergo dissociation. In other words, predissociation of the O_2 molecule takes place via these superexcited states. The variety of the fluorescence emissions in the experiment indicates that many predissociation channels occur. In

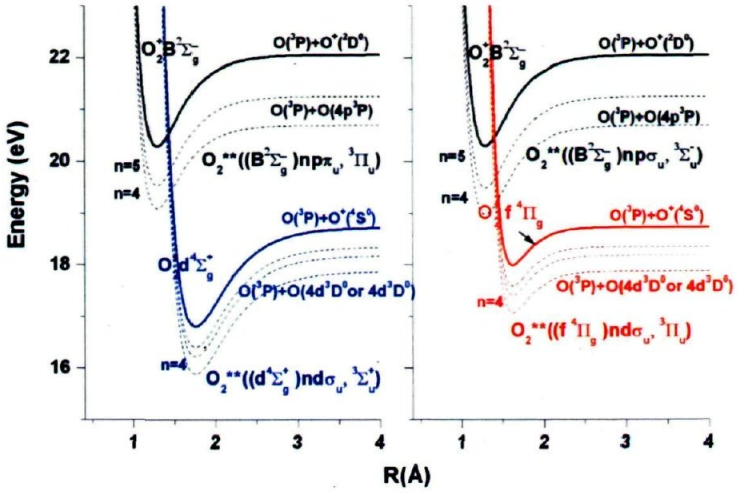

Figure 3.20: *PECs of the SESs series of* $O_2^{**}((O_2^+B^2\Sigma_g^-)np\pi_u,^3\Pi_u)$,$O_2^{**}((O_2^+d^4\Sigma_g^+)nd\sigma_u,$ $^3\Sigma_u^+)$ *and* $O_2^{**}((O_2^+B^2\Sigma_g^-)np\sigma_u,^3\Sigma_u^-)$ $O_2^{**}((O_2^+f^4\Pi_u)nd\sigma_u,^3\Pi_u)$ *The solid and dashed lines show ionic states and SESs, respectively.*

- **SESs of** $O_2^{**}((O_2^+A^2\Pi_u)ns\sigma_g,^3\Pi_u)$
  In the energy region of 15.3−17.1 eV, a Franck−Condon excitation may create the Rydberg states of n = 4, 5 of the $ns\sigma_g$ series converging to the $A^2\Pi_u$ state of O_+^2 ion. These SESs are stable and do not undergo dissociation directly. The stability energies of the states are 1.70 and 1.67 eV, respectively (Figure 3.16). However, it can be seen in Figure 3.16 that these Rydberg states can transit to the SES of $O_2^{**}((O_2^+d^4\Sigma_g^+)3p\sigma_u,^3\Sigma_u^+)$ via curve crossing. The transition results in a highly vibrational excitation in the latter state. The hot $O_2^{**}((O_2^+d^4\Sigma_g^+)3p\sigma_u,^3\Sigma_u^+)$ thus undergoes predissociation, leading to the products of O (^3P) + O(3p,^5P) or O (^3P) + O(3p,^3P). The production of O(3p,^5P) and O(3p,^3P) is verified by the emissions at 777.5 and 845.0 nm, which are assigned to the transitions of $O(3p,^5P\rightarrow 3s,^5S^o)$ and $O(3p,^3P\rightarrow 3s,^3S^o)$, respectively.

- **SESs of** $O_2^{**}((O_2^+b^4\Sigma_g^-)np\pi_u,^3\Pi_u)$ **and** $O_2^{**}((O_2^+b^4\Sigma_g^-)np\sigma_u,^3\Sigma_u^-)$
  At a higher excitation energy of 17.0 eV, Rydberg states of $O_2^{**}((O_2^+b^4\Sigma_g^-)np\pi_u,^3\Pi_u)$ and $O_2^{**}((O_2^+b^4\Sigma_g^-)np\sigma_u,^3\Sigma_u^-)$ can be produced by the vertical excitation directly (Figure 3.17). These Rydberg states of O_2 molecule cross to two other SESs of $O_2^{**}((O_2^+d^4\Sigma_g^+)3p\sigma_u,^3\Sigma_u^+)$ or $O_2^{**}((O_2^+f^4\Pi_g^+)3p\sigma_u,^3\Pi_u)$ individually. The transition via the curve crossing creates a highly vibrational excitation in the latter two states. The hot O_2 molecule thus undergoes dissociation. The products are O (^3P) + O (3p, ^5P)or O (^3P) + O (3p, ^3P). The observed emissions at 777.5 and 845.0 nm refer to the transitions of O(3p, $^5P\rightarrow$3s, $^5S^o$) and O(3p, $^3P\rightarrow$3s, $^3S^o$), respectively. At a higher excitation of 17.5 eV, $O_2^{**}((O_2^+b^4\Sigma_g^-)5p\sigma_u,^3\Sigma_u^-)$ and

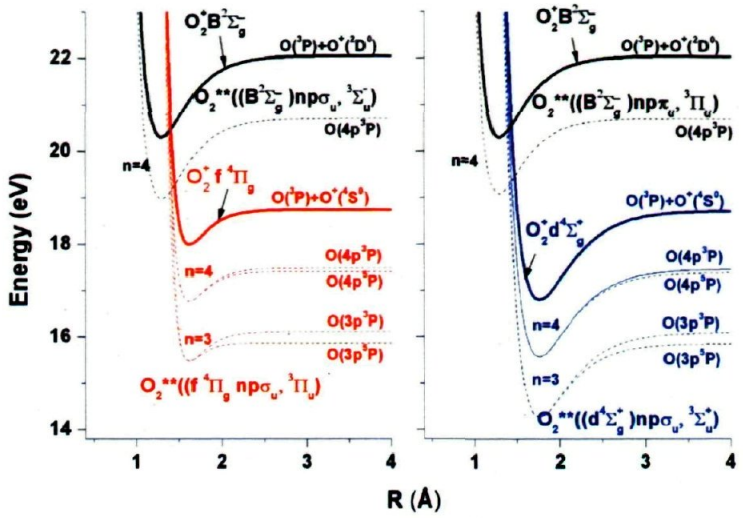

Figure 3.18: *PECs of the SESs series of* $O_2^{**}((O_2^+B^2\Sigma_g^-)np\sigma_u,{}^3\Sigma_u^-)$,$O_2^{**}((O_2^+f^4\Pi_u)np\sigma_u$, ${}^3\Pi_u)$ *and* $O_2^{**}((O_2^+B^2\Sigma_g^-)np\pi_u,{}^3\Pi_u)$ $O_2^{**}((O_2^+d^4\Sigma_g^+)np\sigma_u,{}^3\Sigma_u^+)$. *The solid and dashed lines show ionic states and SESs, respectively.*

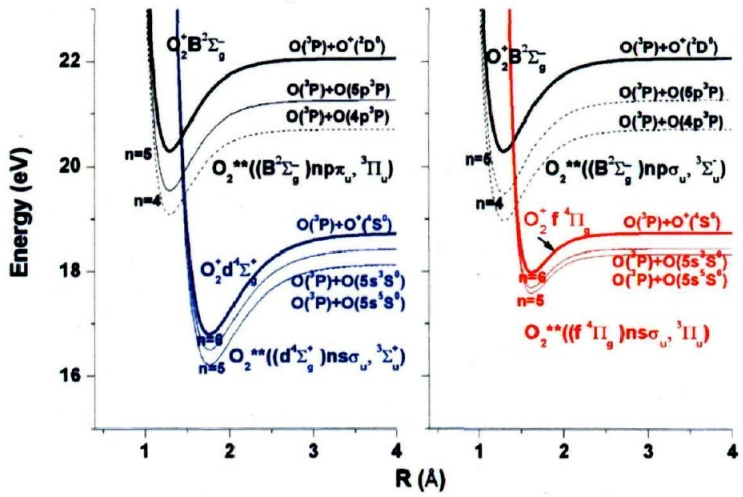

Figure 3.19: *PECs of the SESs series of* $O_2^{**}((O_2^+B^2\Sigma_g^-)np\pi_u,{}^3\Pi_u)$,$O_2^{**}((O_2^+d^4\Sigma_g^+)ns\sigma_u$, ${}^3\Sigma_u^+)$ *and* $O_2^{**}((O_2^+B^2\Sigma_g^-)np\sigma_u,{}^3\Sigma_u^-)$ $O_2^{**}((O_2^+f^4\Pi_u)ns\sigma_u,{}^3\Pi_u)$. *The solid and dashed lines show ionic states and SESs, respectively.*

light of the Morse PECs shown in Figures 3.16 to Figure 3.20, we are able to understand all these predissociation processes. Table 3.2 summarizes the excitation energy, the optically excited state, the dissociative state, the possible products and the product emissions of each dissociation process as follow:

$O_2^{**}((O_2^+ b^4\Sigma_g^-)5p\pi_u, {}^3\Pi_u)$ states may be created in the laser excitation (Figure 3.17). These SESs cross with the $O_2^{**}((O_2^+ f^4\Pi_g)4p\sigma_u, {}^3\Pi_u)$ and $O_2^{**}((O_2^+ d^4\Sigma_g^+)4p\sigma_u, {}^3\Sigma_u^+)$ states, respectively. The latter two states further dissociate, leading to the products of O (^3P) + O(4p, ^5P) or O (^3P) + O(4p,^3P), which emit the fluorescent lights at 394.8 nm or 436.8 nm,respectively.

- **SESs of $O_2^{**}((O_2^+ B^2\Sigma_g^-)np\pi_u, {}^3\Pi_u)$ and $O_2^{**}((O_2^+ B^2\Sigma_g^-)np\sigma_u, {}^3\Sigma_u^-)$**
  At a higher excitation energy of 19.0 eV, Rydberg states of $O_2^{**}((O_2^+ B^2\Sigma_g^-)4p\pi_u, {}^3\Pi_u)$ and $O_2^{**}((O_2^+ B^2\Sigma_g^-)4p\sigma_u, {}^3\Sigma_u^-)$ can be produced by the optical excitation (Figures 3.18 ,3.19 and 3.20). The SESs cross to the $O_2^{**}((O_2^+ B^2\Sigma_g^-)3p\sigma_u, {}^3\Sigma_u^-)$ or $O_2^{**}((O_2^+ B^2\Sigma_g^-)3p\sigma_u, {}^3\Sigma_u^-)$ states, producing the fragments of O (3p, ^3P) and O (3p, ^5P) (Figure 3.18). Meanwhile, the SESs cross to the $O_2^{**}((O_2^+ d^4\Sigma_g^+)5s\sigma_u, {}^3\Sigma_u^+)$ and $O_2^{**}((O_2^+ f^4\Pi_g)5s\sigma_u, {}^3\Pi_u)$ also, producing O (5s, $^5S^o$) or(5s, $^3S^o$) (Figure 3.19). The observed emissions at 645.4 and 725.8 nm refer to the transitions of O (5s, $^5S^o \rightarrow$ 3p, ^5P) and O(5s, $^3S^o \rightarrow$ 3p, ^3P), respectively. And the SESs will also cross to the $O_2^{**}((O_2^+ d^4\Sigma_g^+)4d\sigma_u, {}^3\Sigma_u^+)$ and $O_2^{**}((O_2^+ f^4\Pi_g)4d\sigma_u, {}^3\Pi_u)$, leading to the products of O (4d, $^5D^o$) and O (4d,$^3D^o$) (Figure 3.20). The observed emission at 615.9 nm and 700.6 nm refers to the transitions of O (4d, $^5D^o \rightarrow$ 3p, ^5P) and O (4d,$^3D^o \rightarrow$ 3p, ^3Po), respectively. Such observations verify the predissociation mechanism.

3.2.4 Lifetime measurement of SESs of O_2

The predissociation process consists of two steps. The first step can be represented by a wave packet moving on the first type of PEC before the curve crossing (Figure 3.16). In the second step, the wave packet transits across the crossing point, resulting in a highly vibrational excitation in the second type of PEC. The wave packet moves on the latter PEC further, leading to the production of two oxygen atoms. Quasi classical trajectory (QCT) calculations are carried out for the first step. A Gaussian wave packet in Wigner representation starts to move on the PEC with an average zero initial velocity [60]. According to Franck–Condon principle, the initial geometry is adapted as that of the ground state of O_2 molecule, which has a short bond distance of 1.21 Å. The wave packet is then accelerated by the repulsive force on the left wall of the PEC. Trajectories reflecting the moving time of the wave packet on the state of $O_2^{**}((O_2^+ A^2\Pi_u)ns\sigma_g, {}^3\Pi_u)$ are calculated. Figure 3.21 shows the calculated probability of the trajectories of the SES moving toward and reaching the crossing point as a function of time. The width of the curve indicates that the average moving time to the crossing point is about 100 fs. Otherwise, if it were a direct dissociation, the dissociation period would be as long as about 600 fs as predicted in a similar calculation. Autoionization process of SESs

for O_2 molecule is not considered in this work. Their rate are often estimated to be $10^{10}n^{-3}$ to $10^{12}n^{-3}$ s^{-1} (n means principal quantum number). For a Rydberg molecule of n=4, the autoionization lifetime is thus subnanoseconds [68], much longer than the neutral dissociation time of SES.

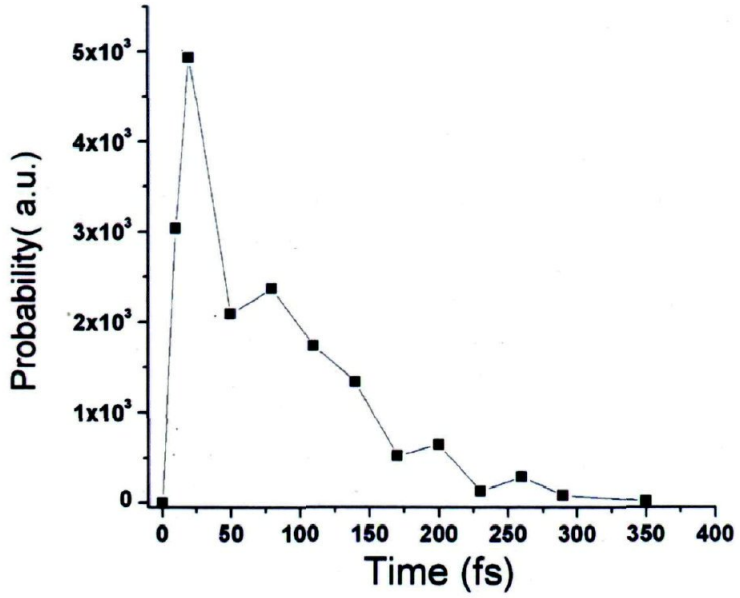

Figure 3.21: *Probability of the trajectories for* $O_2^{**}((O_2^+ b^4\Sigma_g^-)4p\pi_u, {}^3\Pi_u)$ *moving to the crossing point as a function of time.*

The crossing time of the initially excited SESs to the final dissociating PEC is inspected by an experiment using femtosecond lasers. On the basis of the above analysis, if during the crossing period, the initially excited SES population is reduced by a weak probe ultrashort laser pulse, the resultant fluorescence would be reduced. It is predicted that the fluorescence reduction time would be on the order of 100 fs (see Figure 3.21), corresponding to the transit time between the initial SES and the final dissociating SES as obtained in the previous paragraph. Once the crossing to the second type of SES is over, the weak probe pulse would not be able to de−excite the dissociating SES or Rydberg state. To monitor the dissociation process of the SESs, two sequential ultrafast laser pulses at different wavelengths have been employed. The time interval between the two laser pulses is varied in the experiment. The first (pump) laser pulse initiates the multiphoton excitation, creating a SES of the first type of PEC. The second (probe) laser pulse depopulates the SES either by further excitation or by stimulated emission. The depopulation of the superexcited states results in a decrease of product yields which causes a depletion of fluorescence emission. The fluorescence intensity has been measured as a function of the delay time between the pump and the probe

laser pulses. Figure 3.22 shows the fluorescence signals at 777.5 nm as a function of the delay time, respectively. It can be seen clearly that an obvious depletion of the fluorescence signal appears when the pump and probe pulses overlap each other. The maximum of the depletion is at the zero delay time. The rise time of the depletion is about 50 fs, which is the order of the laser pulse width. The decay lasts for 150 fs. The experimentally recorded curves shown in Figure 3.22 are analogous to the QCT calculated one shown in Figure 3.21. The results support that it is the predissociation process. Similar depletion curves of fluorescence depletion were also observed for the other wavelengths with roughly the same temporal width (see Figure 3.23). To broaden our knowledge about the SESs, we have tried to study the intensity dependence of depletion by changing the energy of probe pulses (Figure 3.24). The obvious conclusion is that depletion due to the probe pulse happens by a nonlinear process through the absorbtion of more than one photon of the probe pulse. The dip disappears at low intensities of probe pulse.

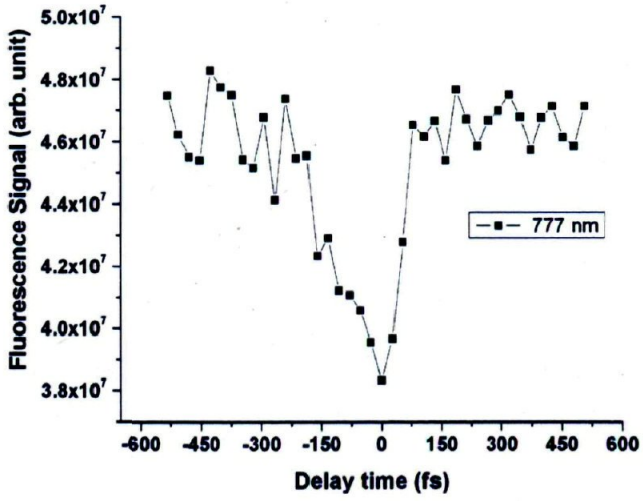

Figure 3.22: *Integrated fluorescence signal of* $2s^2 2p^3(^4S^o)3p,^5P \rightarrow 2s^2 2p^3(^4S^o)3s,^5S^o$ *at 777.5 nm versus the delay time between the pump and probe pulses. Negative delay time means the probe pulses are before the pump pulses.*

3.3 Nitric oxide NO

Up to now, we have studied neutral dissociation of homonuclear molecules (H_2 and O_2). In this section we investigate neutral dissociation of an heteronuclear molecule

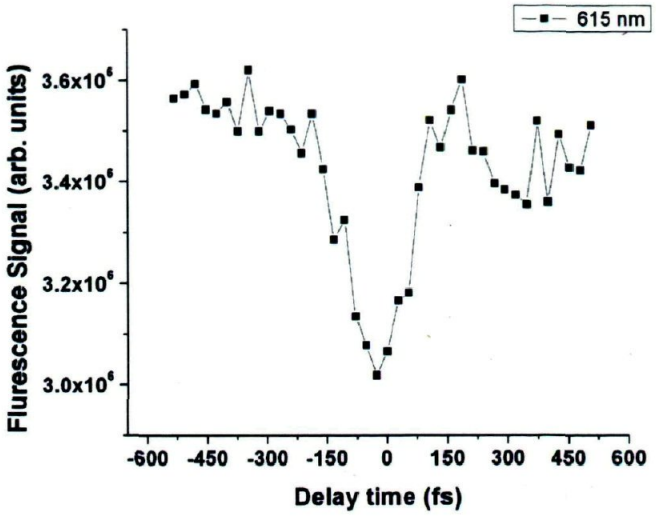

Figure 3.23: *Integrated fluorescence signal of* $2s^2 2p^3(^4S^o)4d, ^5P \rightarrow 2s^2 2p^3(^4S^o)3p, ^5S^o$ *at 615nm nm versus the delay time between the pump and probe pulses. Negative delay time means the probe pulses are behind the pump pulses.*

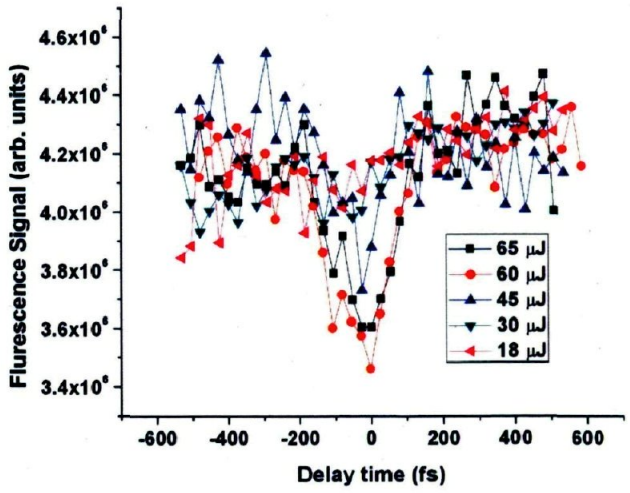

Figure 3.24: *Integrated fluorescence signal of* $2s^2 2p^3(^4S^o)3p, ^5P \rightarrow 2s^2 2p^3(^4S^o)3s, ^5S^o$ *at 777.5 nm versus the delay time between the pump and probe pulses for different probe energy. Negative delay time means the probe pulses are behind the pump pulses.*

(NO) in a strong laser field. The superexcited states of NO are produced by the excitation with ultrashort intense laser pulses. Fluorescent emission after the laser pulse is

detected. From the recorded spectral lines we found dissociation products of N and O atoms. The dissociation can be interpreted by our calculated PECs with a spectator model (the same model described SESs of hydrogen molecules). Garcia et al. measured the near−infrared dispersed fluorescence of neutral atomic fragments using narrow band synchrotron radiation photons of the energy 17.2 − 25.8 eV [71]. Thirteen atomic O or N species dissociated from the SES of NO were recorded. In order to interpret the dissociation mechanism, they tried to calculate the ab initio PECs for the SESs. At least 29 excitation processes for a certain symmetry of a NO molecule were calculated. However, the PECs and their crossings were too complicated in the high energy region. The dissociation mechanism remained obscure.

In this section, we report our experimental and theoretical study on the dissociation of NO. We obtain the PECs for the SESs of NO by another approach different from Garcia et al. [71]. Based on the PECs, we propose direct and predissociation mechanism to interpret the dissociation processes of SESs leading to excited N and O atoms respectively. The emissions of products thus could be well explained. These theoretical results can provide a better insight into the essence of SESs than before. Through the above studies, the concept of the SES of NO molecule and the mechanism of the dissociation are better clarified. Considering the Rydberg character of the SESs, we properly build the PECs for the SESs using the calculated PECs of NO^+ which the Rydberg states converge to.

The SESs of the molecule NO are produced by the intense Ti:sapphire laser pulses. Products of the neutral dissociation are detected by fragmentation spectroscopy. Figure 3.25 shows the wide range fluorescence spectrum recorded between the wavelengths of 200 and 900 nm. The spectral lines in the spectrum are attributed to the transitions of the oxygen or nitrogen atoms, which are the dissociation products of superexcited NO^{**}. The spectral lines in the emission spectrum are assigned as the transitions of excited oxygen atoms or nitrogen atoms. Moreover some transition from molecular band are observed. They are mainly from $\beta(B^2\Pi \rightarrow X^2\Pi)$ and $\gamma(A^2\Sigma^+ \rightarrow X^2\Pi)$ transitions. Eight transitions of O^* (Figure 3.26) and twenty transitions of N^* (Figure 3.27) in the fluorescence spectrum have been assigned. The observed transitions lines and their assignments are listed in Table 3.3. The minimum energy required to excite one of the excited fragments in both of the cases (O:10.74 eV Figure 3.26, N:11.75 eV Figure 3.27) is more than ionization energy of NO molecules (9.26 eV [72]). This indicate clearly that neutral dissociation process happens through absorption of many photons whose total energy is higher than first ionization potential.

We measured the pressure dependence of fluorescence intensity. Figure 3.28 shows the full spectra of NO in a strong laser field versus pressure. The pressure dependence

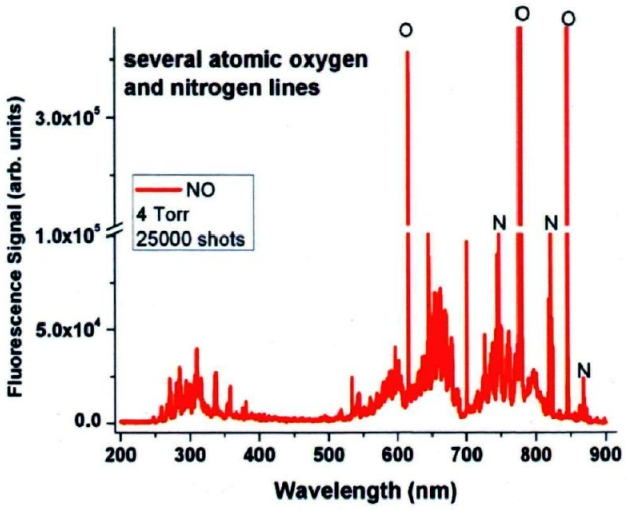

Figure 3.25: *The dispersed fluorescence spectrum for fragments of superexcited NO. The details of the atom lines such as configurations and spectroscopic terms of the excitation are listed in Table 3.3 at the end of this chapter*

below 4 torr is linear, which means the collision effect is negligible. The linear pressure dependence shows that the emitters are the products of direct laser excitation, but not those of collision effects. This is the same for all of the lines observed (see Figure 3.28 for detail). The discussion is very similar to hydrogen and oxygen molecules therefore I refer to previous section for more detail discussion. All of the experiments with NO, have been done at 4 torr pressure.

We measured the fluorescence intensity of some strong lines of the O or N atoms as a function of the laser intensity. Five slopes are obtained as 5.7, 8.9, 9.0, 9.1 and 7.6 in a log−log plot for the wavelengths of 615.6, 744.2, 777.4, 844.6 and 868.3 nm, respectively (see Figure 3.29). The strong laser intensity dependence indicates that a multiphoton excitation absorbing 6 to 9 ($\sim 9.3 - 13.95$ eV) photons takes place. The NO molecule can be excited to a highly excited state, whose energy is beyond the first ionization potential of nitric oxide molecule (9.264 eV [72]). The highly excited state, or the superexcited state, then undergoes dissociation leading to the product of N^* and O^* atoms which we observed. To interpret the dissociation process we use ionic core model, which has been successfully applied to explain the dissociation of H_2 and O_2 molecules in previous sections. Most superexcited states are Rydberg states consisting of an excited ion core and a Rydberg electron. In the ionic core model, the Rydberg electron can be treated as a spectator, not participating in the dissociation directly. The whole dissociation process involves two steps, dissociation

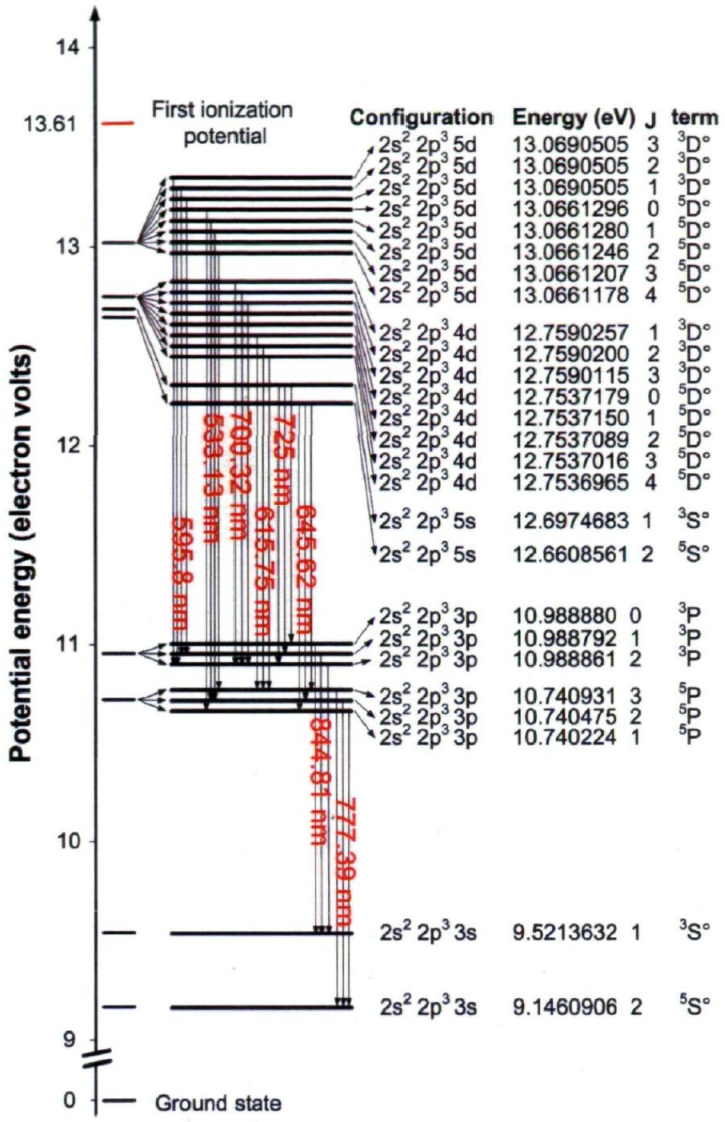

Figure 3.26: *The observed atomic lines in Figure 3.25 attributed to eight transitions from excited atomic oxygen[2]*

of the ion core into two fragments and recombination of the ionic fragment with the Rydberg electron. The principle quantum number n and angular quantum number l are supposed to be unchanged during the dissociation. To understand the dissociative process, it is necessary to know the related potential energy curve. However, accurate calculation for the high−lying states of molecules is extremely difficult. To obtain the PESs of high−lying Rydberg states, we first investigate the PESs of the excited states of NO^+, to which the Rydberg states converge. Two ionic states leading to the products of $O^+ + N$ and $N^+ + O$, respectively are calculated. The calculations are performed with the MOLPRO software package at CASSCF/avqz level [62]. In the

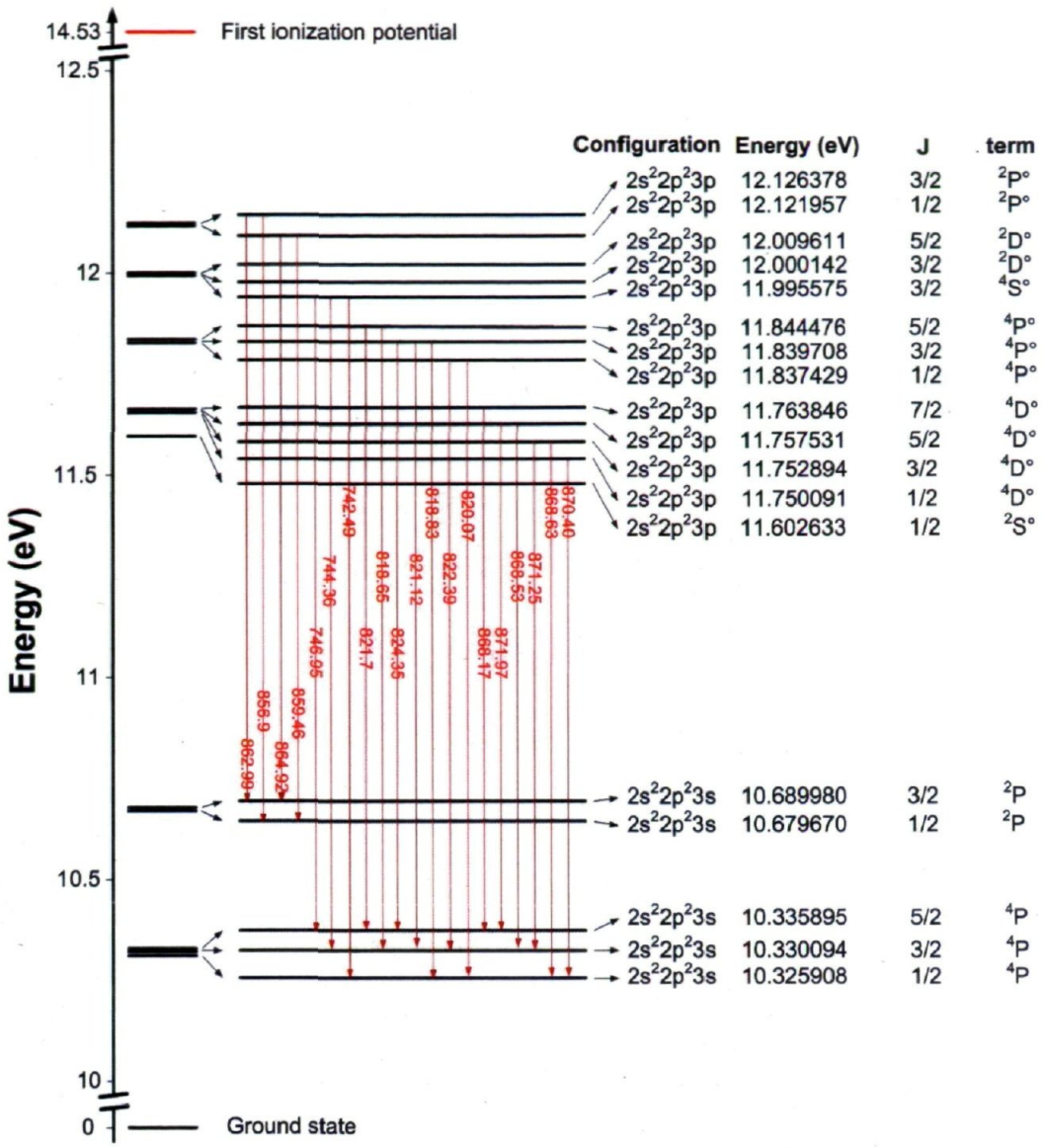

Figure 3.27: *The observed atomic lines in Figure 3.25 attributed to twenty transitions of atomic nitrogen [2]*

energy diagram (Figure 3.30), the dashed lines represent the ionic states at different inter−nuclear distances. The solid curves are the related Rydberg states, which are obtained by shifting down the ionic curve. The energy limit on the long−distance side is adjusted by the experimental data [2]. With these Rydberg PESs of NO, we are able to trace the dissociation pathway of the superexcited NO molecules, and to provide the possible dissociation mechanisms of superexcited NO^{**} molecules. In the strong laser fields, NO molecules may absorb many photons immediately accompanying with a vertical excitation. The equilibrium distance of the ground state of NO is 1.15 Å.

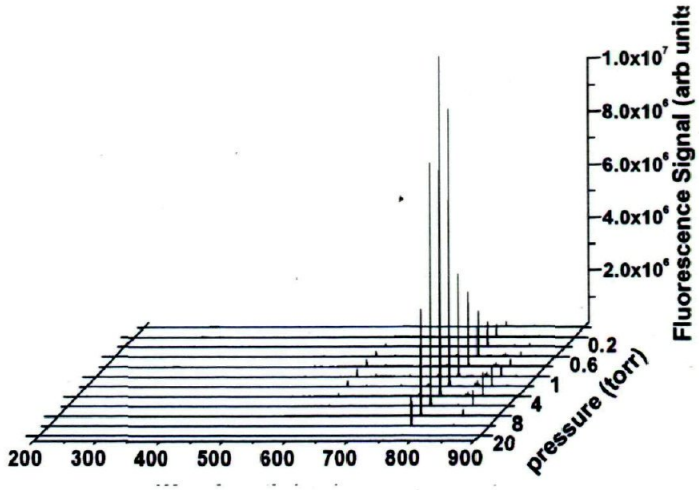

Figure 3.28: *Nitric oxide full spectra versus pressure of nitric oxide molecules.*

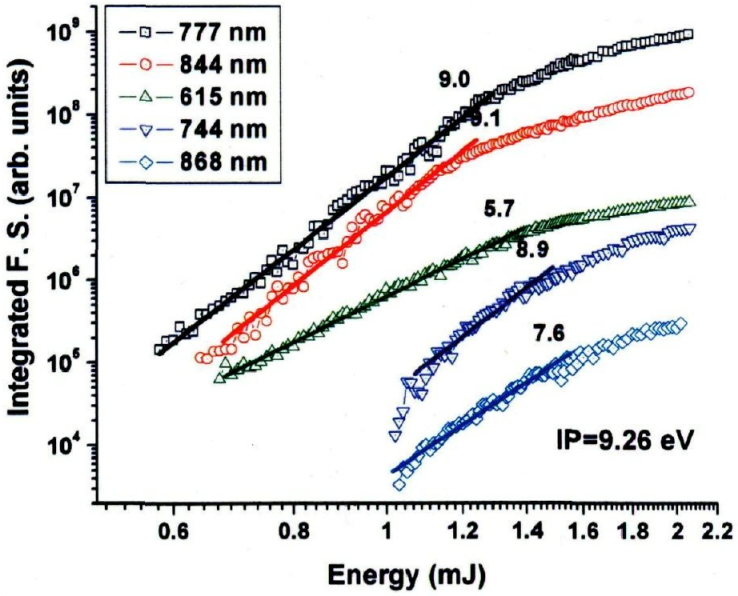

Figure 3.29: *Fluorescence intensity dependence on the laser intensity The fluorescence is collected and integrated around 615.6, 744.2, 777.4, 844.6 and 868.3 nm, respectively.*

A Franck−Condon transition can create superexcited NO^{**} molecule as indicated by the arrow in the energy diagram. After the laser excitation, the wave packet produced moves on the Rydberg PECs (shown by blue color in Fig. 3.30). Then the moving wave packet splits into two parts in the curve crossing region around 2.0 Å. Each part of the wave packet leads to a pair of dissociation products. A direct dissociation pathway shown by blue color in Fig. 3.30 produces the fragments of $O(^3P) + N^+$ ($2s^2 2p^2 3p, {}^4S^o$ or ${}^4P^o$ or ${}^4D^o$), which emit at the wavelengths of 746.9, 818−824, and

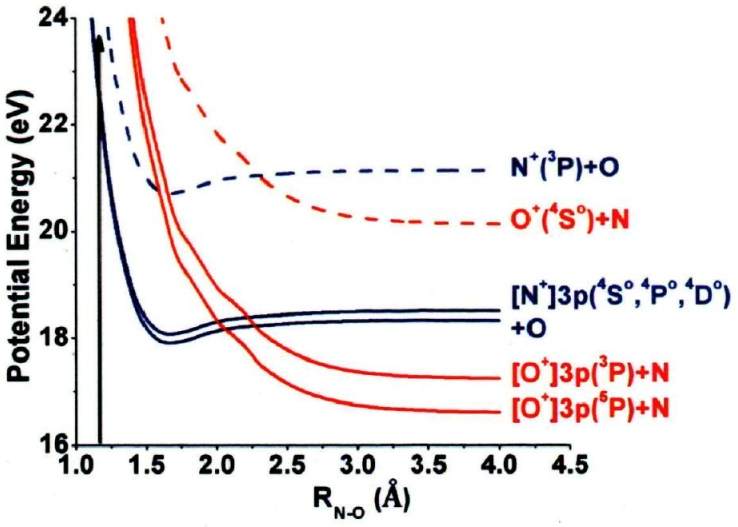

Figure 3.30: *Potential energy curves (PECs). The dashed lines are the ionic PECs to which the Rydberg−type SESs converge; the solid lines are PECs of the related SESs. The blue lines are the PECs that produced wave−packet moves on them. The red lines are PECs that wave−packet crosses to them from blue lines.*

868.3 nm, respectively. Another part of the wave packet crosses to the PESs shown in Fig. 3.30 by red color in the diagram. The curve crossing results in a predissociation, producing the products of $N(^4S^o) + O^*(2s^2 2p^3 3p, ^5P$ or $^3P)$, the products fluorescing at the wavelengths of 777.4 and 844.6 nm respectively.

To prove that those fluorescing fragments came from the SESs we have studied the lifetime of the SESs resulting in the fragment emitting the 777 nm lines by a pump and probe experiment (Figure 3.31). It is in the order of several tens of femtoseconds (160fs).

3.4 Conclusion

Our studies range from the simplest molecule (hydrogen, H_2) to the heteronuclear molecule of nitric oxides (NO). We can claim that neutral dissociation happened through all of them. Also, linear pressure dependent fluorescence signal was a proof that the process is the results of direct laser excitation. Based on our knowledge from single ionizing photon interaction with molecules we proposed multiphoton super−excitation responsible for neutral dissociation of the molecules. Spectra and intensity dependent

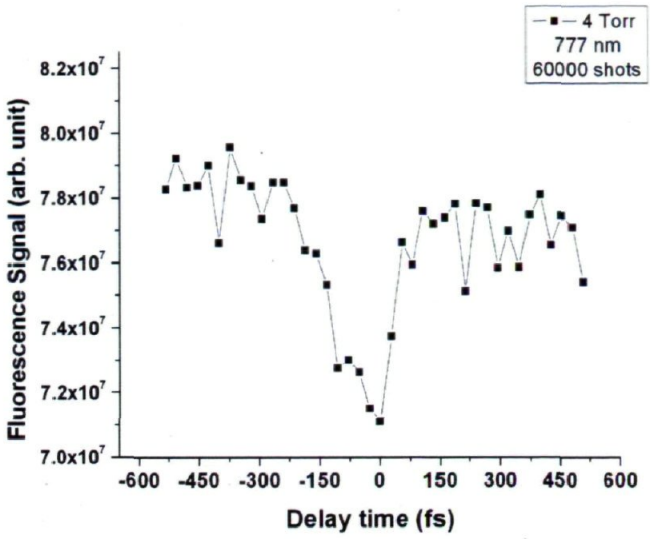

Figure 3.31: *Integrated fluorescence signal around 777 nm versus the delay time between the pump and probe pulses. Negative delay time means the probe pulses are behind the pump pulses.*

data show and strengthen our claim of multiphoton superexcitation in a strong laser filed. Lifetime measurement of SESs is a cast−iron evidence. Therefore, at the end of this chapter we would say that molecules in a strong laser field dissociate neutrally through SESs.

excitation energy (eV)	SESs OES	SESs DES	dissociation products	assignment of transition	emission wavelengths(nm) observation	emission wavelengths(nm) ref. [2]
15.3-17.1	$O_2^{**}((O_2^+ A^2\Pi_u)ns\sigma_g,^3\Pi_u)$ n=4,5	$O_2^{**}((O_2^+ d^4\Sigma_g^+)3p\sigma_u,^3\Pi_u^+)$	$O(3p,^5P)$	$2s^22p^3(^4S^o)3p,^5P \rightarrow 2s^22p^3(^4S^o)3s,^5S^o$	777.5	777.54
			$O(3p,^3P)$	$2s^22p^3(^4S^o)3p,^3P \rightarrow 2s^22p^3(^4S^o)3s,^3S^o$	845.0	844.68
17.0-18.0	$O_2^{**}((O_2^+ b^4\Sigma_g^-)np\pi_u,^3\Pi_u)$ n=4,5	$O_2^{**}((O_2^+ d^4\Sigma_g^+)3p\sigma_u,^3\Sigma_u^+)$	$O(3p,^5P)$	$2s^22p^3(^4S^o)3p,^3P \rightarrow 2s^22p^3(^4S^o)3s,^5S^o$	777.5	777.54
			$O(3p,^3P)$	$2s^22p^3(^4S^o)3p,^3P \rightarrow 2s^22p^3(^4S^o)3s,^3S^o$	845.0	844.68
		$O_2^{**}((O_2^+ d^4\Sigma_g^+)4p\sigma_u,^3\Sigma_u^+)$	$O(4p,^5P)$	$2s^22p^3(^4S^o)3p,^3P \rightarrow 2s^22p^3(^4S^o)3s,^3S^o$	394.8	394.75
			$O(4p,^3P)$	$2s^22p^3(^4S^o)4p,^3P \rightarrow 2s^22p^3(^4S^o)3s,^3S^o$	436.8	436.83
		$O_2^{**}((O_2^+ d^4\Sigma_g^+)5p\sigma_u,^3\Sigma_u^+)$	$O(5p,^3P)$	$2s^22p^3(^4S^o)5p,^3P \rightarrow 2s^22p^3(^4S^o)3s,^3S^o$	369.4	369.34
17.0-18.0	$O_2^{**}((O_2^+ b^4\Sigma_g^-)np\sigma_u,^3\Sigma_u^-)$ n=4,5	$O_2^{**}((O_2^+ f^4\Pi_g)3p\sigma_u,^3\Pi_u)$	$O(3p,^5P)$	$2s^22p^3(^4S^o)3p,^5P \rightarrow 2s^22p^3(^4S^o)3s,^5S^o$	777.5	777.54
			$O(3p,^3P)$	$2s^22p^3(^4S^o)3p,^3P \rightarrow 2s^22p^3(^4S^o)3s,^3S^o$	845.0	844.68
		$O_2^{**}((O_2^+ f^4\Pi_g)4p\sigma_u,^3\Pi_u)$	$O(4p,^5P)$	$2s^22p^3(^4S^o)3p,^5P \rightarrow 2s^22p^3(^4S^o)3s,^5S^o$	436.8	436.83
			$O(4p,^3P)$	$2s^22p^3(^4S^o)4p,^3P \rightarrow 2s^22p^3(^4S^o)3s,^3S^o$	394.8	394.75
		$O_2^{**}((O_2^+ f^4\Pi_g)5p\sigma_u,^3\Pi_u)$	$O(5p,^3P)$	$2s^22p^3(^4S^o)4p,^3P \rightarrow 2s^22p^3(^4S^o)3s,^3S^o$	369.4	369.34
19.0-21.0	$O_2^{**}((O_2^+ B^4\Sigma_g^-)np\sigma_u,^3\Sigma_u^-)$ n=4,5	$O_2^{**}((O_2^+ f^4\Pi_g)3p\sigma_u,^3\Pi_u)$	$O(3p,^5P)$	$2s^22p^3(^4S^o)3p,^5P \rightarrow 2s^22p^3(^4S^o)3s,^5S^o$	777.5	777.54
			$O(3p,^3P)$	$2s^22p^3(^4S^o)3p,^3P \rightarrow 2s^22p^3(^4S^o)3s,^3S^o$	845.0	844.68
		$O_2^{**}((O_2^+ f^4\Pi_g)4p\sigma_u,^3\Pi_u)$	$O(4p,^5P)$	$2s^22p^3(^4S^o)4p,^5P \rightarrow 2s^22p^3(^4S^o)3s,^5S^o$	394.8	394.75
			$O(4p,^3P)$	$2s^22p^3(^4S^o)4p,^3P \rightarrow 2s^22p^3(^4S^o)3s,^3S^o$	436.8	436.83
		$O_2^{**}((O_2^+ f^4\Pi_g)5p\sigma_u,^3\Pi_u)$	$O(5p,^3P)$	$2s^22p^3(^4S^o)4p,^3P \rightarrow 2s^22p^3(^4S^o)3s,^3S^o$	369.4	369.34
		$O_2^{**}((O_2^+ f^4\Pi_g)5s\sigma_u,^3\Pi_u)$	$O(5s,^5S^o)$	$2s^22p^3(^4S^o)5s,^5S^o \rightarrow 2s^22p^3(^4S^o)3p,^5P$	645.4	645.44
			$O(5s,^3S^o)$	$2s^22p^3(^4S^o)5s,^3S^o \rightarrow 2s^22p^3(^4S^o)3p,^3P$	725.8	725.45
		$O_2^{**}((O_2^+ f^4\Pi_g)6s\sigma_u,^3\Pi_u)$	$O(6s,^5S^o)$	$2s^22p^3(^4S^o)6s,^5S^o \rightarrow 2s^22p^3(^4S^o)3p,^5P$	543.5	543.69
			$O(6s,^3S^o)$	$2s^22p^3(^4S^o)6s,^3S^o \rightarrow 2s^22p^3(^4S^o)3p,^3P$	604.9	604.65
		$O_2^{**}((O_2^+ f^4\Pi_g)7s\sigma_u,^3\Pi_u)$	$O(7s,^5S^o)$	$2s^22p^3(^4S^o)7s,^5S^o \rightarrow 2s^22p^3(^4S^o)3p,^5P$	502.2	501.88
			$O(7s,^3S^o)$	$2s^22p^3(^4S^o)7s,^3S^o \rightarrow 2s^22p^3(^4S^o)3p,^3P$	556.6	555.5
		$O_2^{**}((O_2^+ f^4\Pi_g)8s\sigma_u,^3\Pi_u)$	$O(8s,^5S^o)$	$2s^22p^3(^4S^o)8s,^5S^o \rightarrow 2s^22p^3(^4S^o)3p,^5P$	480.4	480.3
			$O(8s,^3S^o)$	$2s^22p^3(^4S^o)8s,^3S^o \rightarrow 2s^22p^3(^4S^o)3p,^3P$	530.1	529.91
		$O_2^{**}((O_2^+ f^4\Pi_g)9s\sigma_u,^3\Pi_u)$	$O(9s,^5S^o)$	$2s^22p^3(^4S^o)9s,^5S^o \rightarrow 2s^22p^3(^4S^o)3p,^5P^\star$	467.6	
		$O_2^{**}((O_2^+ f^4\Pi_g)9s\sigma_u,^3\Pi_u)$	$O(9s,^3S^o)$	$2s^22p^3(^4S^o)9s,^3S^o \rightarrow 2s^22p^3(^4S^o)3p,^3P^\star$	514.9	
		$O_2^{**}((O_2^+ f^4\Pi_g)10s\sigma_u,^3\Pi_u)$	$O(10s,^5S^o)$	$2s^22p^3(^4S^o)10s,^5S^o \rightarrow 2s^22p^3(^4S^o)3p,^5P^\star$	459.1	645.44
			$O(10s,^3S^o)$	$2s^22p^3(^4S^o)10s,^3S^o \rightarrow 2s^22p^3(^4S^o)3p,^3P^\star$	505.4	
		$O_2^{**}((O_2^+ f^4\Pi_g)11s\sigma_u,^3\Pi_u)$	$O(11s,^5S^o)$	$2s^22p^3(^4S^o)11s,^5S^o \rightarrow 2s^22p^3(^4S^o)3p,^5P^{\star\star}$	453.4	
		$O_2^{**}((O_2^+ f^4\Pi_g)12s\sigma_u,^3\Pi_u)$	$O(12s,^5S^o)$	$2s^22p^3(^4S^o)12s,^3S^o \rightarrow 2s^22p^3(^4S^o)3p,^5P^{\star\star}$	449.1	
		$O_2^{**}((O_2^+ f^4\Pi_g)4d\sigma_u,^3\Pi_u)$	$O(4d,^5D^o)$	$2s^22p^3(^4S^o)4d,^5D^o \rightarrow 2s^22p^3(^4S^o)3p,^5P$	615.9	615.82
			$O(4d,^3D^o)$	$2s^22p^3(^4S^o)4d,^3D^o \rightarrow 2s^22p^3(^4S^o)3p,^3P$	700.6	700.22
		$O_2^{**}((O_2^+ f^4\Pi_g)5d\sigma_u,^3\Pi_u)$	$O(5d,^5D^o)$	$2s^22p^3(^4S^o)5d,^5D^o \rightarrow 2s^22p^3(^4S^o)3p,^5P$	533.2	532.97
			$O(5d,^3D^o)$	$2s^22p^3(^4S^o)5d,^3D^o \rightarrow 2s^22p^3(^4S^o)3p,^3P$	596.2	595.86
		$O_2^{**}((O_2^+ f^4\Pi_g)6d\sigma_u,^3\Pi_u)$	$O(6d,^5D^o)$	$2s^22p^3(^4S^o)6d,^5D^o \rightarrow 2s^22p^3(^4S^o)3p,^5P$	491.7	496.88
			$O(6d,^3D^o)$	$2s^22p^3(^4S^o)6d,^3D^o \rightarrow 2s^22p^3(^4S^o)3p,^3P$	551.4	551.28
		$O_2^{**}((O_2^+ f^4\Pi_g)7d\sigma_u,^3\Pi_u)$	$O(7d,^3D^o)$	$2s^22p^3(^4S^o)7d,^5D^o \rightarrow 2s^22p^3(^4S^o)3p,^5P$	477.5	477.38
			$O(7d,^3D^o)$	$2s^22p^3(^4S^o)7d,^3D^o \rightarrow 2s^22p^3(^4S^o)3p,^3P$	527.7	527.6

Continue on next page →

→Continued

excitation energy (eV)	SESs OES	SESs DES	dissociation products	assignment of transition	emission wavelengths(nm) observation	emission wavelengths(nm) ref. [2]
		$O_2^{**}((O_2^+ f^4\Pi_g)8d\sigma_u,^3\Pi_u)$	$O(8d,^5S^o)$	$2s^22p^3(^4S^o)8d,^5D^o \rightarrow 2s^22p^3(^4S^o)3p,^5P$	465.7	465.54
			$O(8d,^3D^o)$	$2s^22p^3(^4S^o)8d,^3D^o \rightarrow 2s^22p^3(^4S^o)3p,^3P$	513.3	513.27
		$O_2^{**}((O_2^+ f^4\Pi_g)9d\sigma_u,^3\Pi_u)$	$O(9d,^5D^o)$	$2s^22p^3(^4S^o)9d,^3D^o \rightarrow 2s^22p^3(^4S^o)3p,^5P^\star$	458.0	
			$O(9d,^3D^o)$	$2s^22p^3(^4S^o)9d,^3D^o \rightarrow 2s^22p^3(^4S^o)3p,^3P^\star$	503.9	
		$O_2^{**}((O_2^+ f^4\Pi_g)10d\sigma_u,^3\Pi_u)$	$O(10d,^5D^o)$	$2s^22p^3(^4S^o)10d,^5D^o \rightarrow 2s^22p^3(^4S^o)3p,^5P^\star$	452.5	
		$O_2^{**}((O_2^+ f^4\Pi_g)11d\sigma_u,^3\Pi_u)$	$O(11d,^5D^o)$	$2s^22p^3(^4S^o)11d,^5D^o \rightarrow 2s^22p^3(^4S^o)3p,^5P^{\star\star}$	448.5	
19.0-21.0	$O_2^{**}((O_2^+ B^2\Sigma_g^-)np\pi_u,^3\Pi_u)$ n=4,5	$O_2^{**}((O_2^+ d^4\Sigma_g^+)3p\sigma_u,^3\Sigma_u^+)$	$O(3p,^5P)$	$2s^22p^3(^4S^o)3p,^5P \rightarrow 2s^22p^3(^4S^o)3s,^5S^o$	777.5	777.54
			$O(3p,^3P)$	$2s^22p^3(^4S^o)3s,^3P \rightarrow 2s^22p^3(^4S^o)3s,^3S^o$	845.0	844.68
		$O_2^{**}((O_2^+ d^4\Sigma_g^+)4p\sigma_u,^3\Sigma_u^+)$	$O(4p,^5P)$	$2s^22p^3(^4S^o)4p,^5P \rightarrow 2s^22p^3(^4S^o)3s,^5S^o$	394.8	394.75
			$O(4p,^3P)$	$2s^22p^3(^4S^o)4p,^3P \rightarrow 2s^22p^3(^4S^o)3s,^3S^o$	436.8	436.83
		$O_2^{**}((O_2^+ d^4\Sigma_g^+)5p\sigma_u,^3\Sigma_u^+)$	$O(5p,^3P)$	$2s^22p^3(^4S^o)4p,^3P \rightarrow 2s^22p^3(^4S^o)3s,^4S^o$	369.4	369.34
		$O_2^{**}((O_2^+ d^4\Sigma_g^+)5s\sigma_u,^3\Sigma_u^+)$	$O(5s,^5S^o)$	$2s^22p^3(^4S^o)5s,^5S^o \rightarrow 2s^22p^3(^4S^o)3p,^5P$	645.4	645.4
			$O(5s,^3S^o)$	$2s^22p^3(^4S^o)5s,^3S^o \rightarrow 2s^22p^3(^4S^o)3p,^3P$	725.8	725.45
		$O_2^{**}((O_2^+ d^4\Sigma_g^+)6s\sigma_u,^3\Sigma_u^+)$	$O(6s,^5S^o)$	$2s^22p^3(^4S^o)6s,^5S^o \rightarrow 2s^22p^3(^4S^o)3p,^5P$	543.5	543.69
			$O(6s,^3S^o)$	$2s^22p^3(^4S^o)6s,^3S^o \rightarrow 2s^22p^3(^4S^o)3p,^3P$	604.9	604.65
		$O_2^{**}((O_2^+ d^4\Sigma_g^+)7s\sigma_u,^3\Sigma_u^+)$	$O(7s,^5S^o)$	$2s^22p^3(^4S^o)7s,^5S^o \rightarrow 2s^22p^3(^4S^o)3p,^5P$	502.2	501.88
			$O(7s,^3S^o)$	$2s^22p^3(^4S^o)7s,^3S^o \rightarrow 2s^22p^3(^4S^o)3p,^3P$	555.6	555.5
		$O_2^{**}((O_2^+ d^4\Sigma_g^+)8s\sigma_u,^3\Sigma_u^+)$	$O(8s,^5S^o)$	$2s^22p^3(^4S^o)8s,^5S^o \rightarrow 2s^22p^3(^4S^o)3p,^5P$	480.4	480.3
			$O(8s,^3S^o)$	$2s^22p^3(^4S^o)8s,^3S^o \rightarrow 2s^22p^3(^4S^o)3p,^3P$	530.1	529.91
		$O_2^{**}((O_2^+ d^4\Sigma_g^+)9s\sigma_u,^3\Sigma_u^+)$	$O(9s,^5S^o)$	$2s^22p^3(^4S^o)9s,^5S^o \rightarrow 2s^22p^3(^4S^o)3p,^5P^\star$	467.6	
			$O(9s,^3S^o)$	$2s^22p^3(^4S^o)9s,^3S^o \rightarrow 2s^22p^3(^4S^o)3p,^3P^\star$	514.9	
		$O_2^{**}((O_2^+ d^4\Sigma_g^+)10s\sigma_u,^3\Sigma_u^+)$	$O(10s,^5S^o)$	$2s^22p^3(^4S^o)10s,^5S^o \rightarrow 2s^22p^3(^4S^o)3p,^5P^\star$	459.1	
			$O(10s,^3S^o)$	$2s^22p^3(^4S^o)10s,^3S^o \rightarrow 2s^22p^3(^4S^o)3p,^3P^\star$	505.4	
		$O_2^{**}((O_2^+ d^4\Sigma_g^+)11s\sigma_u,^3\Sigma_u^+)$	$O(11s,^5S^o)$	$2s^22p^3(^4S^o)11s,^5S^o \rightarrow 2s^22p^3(^4S^o)3p,^5P^{\star\star}$	453.4	
		$O_2^{**}((O_2^+ d^4\Sigma_g^+)12s\sigma_u,^3\Sigma_u^+)$	$O(12s,^5S^o)$	$2s^22p^3(^4S^o)12s,^5S^o \rightarrow 2s^22p^3(^4S^o)3p,^5P^{\star\star}$	449.1	
		$O_2^{**}((O_2^+ d^4\Sigma_g^+)4d\sigma_u,^3\Sigma_u^+)$	$O(4d,^5D^o)$	$2s^22p^3(^4S^o)4d,^5D^o \rightarrow 2s^22p^3(^4S^o)3p,^5P$	615.9	615.82
			$O(4d,^3D^o)$	$2s^22p^3(^4S^o)4d,^3D^o \rightarrow 2s^22p^3(^4S^o)3p,^3P$	700.6	700.22
		$O_2^{**}((O_2^+ d^4\Sigma_g^+)5d\sigma_u,^3\Sigma_u^+)$	$O(5d,^5D^o)$	$2s^22p^3(^4S^o)5d,^5D^o \rightarrow 2s^22p^3(^4S^o)3p,^5P$	533.2	532.97
			$O(5d,^3D^o)$	$2s^22p^3(^4S^o)5d,^3D^o \rightarrow 2s^22p^3(^4S^o)3p,^3P$	596.2	595.86
		$O_2^{**}((O_2^+ d^4\Sigma_g^+)6d\sigma_u,^3\Sigma_u^+)$	$O(6d,^5D^o)$	$2s^22p^3(^4S^o)6d,^5D^o \rightarrow 2s^22p^3(^4S^o)3p,^5P$	497.1	496.88
			$O(6d,^3D^o)$	$2s^22p^3(^4S^o)6d,^3D^o \rightarrow 2s^22p^3(^4S^o)3p,^3P$	551.4	551.28
		$O_2^{**}((O_2^+ d^4\Sigma_g^+)7d\sigma_u,^3\Sigma_u^+)$	$O(7d,^5D^o)$	$2s^22p^3(^4S^o)7d,^5D^o \rightarrow 2s^22p^3(^4S^o)3p,^5P$	477.5	477.38
			$O(7d,^3D^o)$	$2s^22p^3(^4S^o)7d,^3D^o \rightarrow 2s^22p^3(^4S^o)3p,^3P$	527.7	527.65
		$O_2^{**}((O_2^+ d^4\Sigma_g^+)8d\sigma_u,^3\Sigma_u^+)$	$O(8d,^5D^o)$	$2s^22p^3(^4S^o)8d,^5D^o \rightarrow 2s^22p^3(^4S^o)3p,^5P$	465.7	465.54
			$O(8d,^3D^o)$	$2s^22p^3(^4S^o)8d,^3D^o \rightarrow 2s^22p^3(^4S^o)3p,^3P$	513.3	513.27
		$O_2^{**}((O_2^+ d^4\Sigma_g^+)9d\sigma_u,^3\Sigma_u^+)$	$O(9d,^5D^o)$	$2s^22p^3(^4S^o)9d,^5D^o \rightarrow 2s^22p^3(^4S^o)3p,^5P^\star$	458.0	
			$O(9d,^3D^o)$	$2s^22p^3(^4S^o)9d,^3D^o \rightarrow 2s^22p^3(^4S^o)3p,^3P^\star$	503.9	
		$O_2^{**}((O_2^+ d^4\Sigma_g^+)10d\sigma_u,^3\Sigma_u^+)$	$O(10d,^5D^o)$	$2s^22p^3(^4S^o)10d,^5D^o \rightarrow 2s^22p^3(^4S^o)3p,^5P^\star$	452.5	
		$O_2^{**}((O_2^+ d^4\Sigma_g^+)11d\sigma_u,^3\Sigma_u^+)$	$O(11d,^5D^o)$	$2s^22p^3(^4S^o)11d,^5D^o \rightarrow 2s^22p^3(^4S^o)3p,^5P^{\star\star}$	448.5	

*Ten new Rydberg transitions are marked by a single star

**The transitions referred to three new Rydberg states are marked by double star

Table 3.2: *Excitation energy, optically excited state (OES), dissociative excited state (DES), dissociation products ($O^*+O(^3P)$) and vertical transition for each dissociation process of the observed SESs of the O_2 molecule*

Wevelength (nm)	Excited Fragments	Configuration [2]	terms [2]
532.9	O	$2s^2 2p^3(^4S^o)5d \rightarrow 2s^2 2p^3(^4S^o)3p$	$^5D^o \rightarrow ^5P$
595.8	O	$2s^2 2p^3(^4S^o)5d \rightarrow 2s^2 2p^3(^4S^o)3p$	$^3D^o \rightarrow ^3P$
615.6	O	$2s^2 2p^3(^4S^o)4d \rightarrow 2s^2 2p^3(^4S^o)3p$	$^5D^o \rightarrow ^5P$
645.4	O	$2s^2 2p^3(^4S^o)5s \rightarrow 2s^2 2p^3(^4S^o)3p$	$^5S^o \rightarrow ^5P$
700.2	O	$2s^2 2p^3(^4S^o)4d \rightarrow 2s^2 2p^3(^4S^o)3p$	$^3D^o \rightarrow ^3P$
725.4	O	$2s^2 2p^3(^4S^o)5s \rightarrow 2s^2 2p^3(^4S^o)3p$	$^3S^o \rightarrow ^3P$
777.9	O	$2s^2 2p^3(^4S^o)3p \rightarrow 2s^2 2p^3(^4S^o)3s$	$^5P \rightarrow ^5S^o$
844.6	O	$2s^2 2p^3(^4S^o)3p \rightarrow 2s^2 2p^3(^4S^o)3s$	$^3P \rightarrow ^3S^o$
862.99	N	$2s^2 2p^2(^3P)3p \rightarrow 2s^2 2p^2(^3P)3s$	$^2P^o \rightarrow ^2P$
856.9	N	$2s^2 2p^2(^3P)3p \rightarrow 2s^2 2p^2(^3P)3s$	$^2P^o \rightarrow ^2P$
864.92	N	$2s^2 2p^2(^3P)3p \rightarrow 2s^2 2p^2(^3P)3s$	$^2P^o \rightarrow ^2P$
859.46	N	$2s^2 2p^2(^3P)3p \rightarrow 2s^2 2p^2(^3P)3s$	$^2P^o \rightarrow ^2P$
746.95	N	$2s^2 2p^2(^3P)3p \rightarrow 2s^2 2p^2(^3P)3s$	$^4S^o \rightarrow ^4P$
744.36	N	$2s^2 2p^2(^3P)3p \rightarrow 2s^2 2p^2(^3P)3s$	$^4S^o \rightarrow ^4P$
742.49	N	$2s^2 2p^2(^3P)3p \rightarrow 2s^2 2p^2(^3P)3s$	$^4S^o \rightarrow ^4P$
821.7	N	$2s^2 2p^2(^3P)3p \rightarrow 2s^2 2p^2(^3P)3s$	$^4P^o \rightarrow ^4P$
818.65	N	$2s^2 2p^2(^3P)3p \rightarrow 2s^2 2p^2(^3P)3s$	$^4P^o \rightarrow ^4P$
824.35	N	$2s^2 2p^2(^3P)3p \rightarrow 2s^2 2p^2(^3P)3s$	$^4P^o \rightarrow ^4P$
821.12	N	$2s^2 2p^2(^3P)3p \rightarrow 2s^2 2p^2(^3P)3s$	$^4P^o \rightarrow ^4P$
818.83	N	$2s^2 2p^2(^3P)3p \rightarrow 2s^2 2p^2(^3P)3s$	$^4P^o \rightarrow ^4P$
822.39	N	$2s^2 2p^2(^3P)3p \rightarrow 2s^2 2p^2(^3P)3s$	$^4P^o \rightarrow ^4P$
820.07	N	$2s^2 2p^2(^3P)3p \rightarrow 2s^2 2p^2(^3P)3s$	$^4P^o \rightarrow ^4P$
868.17	N	$2s^2 2p^2(^3P)3p \rightarrow 2s^2 2p^2(^3P)3s$	$^4D^o \rightarrow ^4P$
871.97	N	$2s^2 2p^2(^3P)3p \rightarrow 2s^2 2p^2(^3P)3s$	$^4D^o \rightarrow ^4P$
868.53	N	$2s^2 2p^2(^3P)3p \rightarrow 2s^2 2p^2(^3P)3s$	$^4D^o \rightarrow ^4P$
871.25	N	$2s^2 2p^2(^3P)3p \rightarrow 2s^2 2p^2(^3P)3s$	$^4D^o \rightarrow ^4P$
868.63	N	$2s^2 2p^2(^3P)3p \rightarrow 2s^2 2p^2(^3P)3s$	$^4D^o \rightarrow ^4P$
874.40	N	$2s^2 2p^2(^3P)3p \rightarrow 2s^2 2p^2(^3P)3s$	$^4D^o \rightarrow ^4P$

Table 3.3: *Details of the observed atomic lines after the dissciation of NO[2].*

Chapter 4

Neutral dissociation of some hydrocarbons by super−excited states

In this chapter, we present the experimental results of neutral dissociation of some simple hydrocarbons in a strong laser field. For brief reviews see ref. [73, 74][1].All experiments were carried out by the candidate. Also this chapter is a completion of [38]. It will be emphasized that the fragmentation of hydrocarbon molecules in a strong laser field is a universal phenomenon. Due to the complexity of theoretical calculations, it is nearly impossible to analyze the data theoretically. We have investigated superexcitation in methane, acetylene, ethylene, propylene, 1−butene and $cis-2-$butene. The spectra of all the above mentioned hydrocarbon molecules are obtained and discussed. Various fragments with different excitation energy imply superexcitation unambiguously. The emission intensity of some of the strongest lines versus laser intensity in a log−log plot are obtained and interpreted. It strengthens our claim about superexcitation in hydrocarbon molecules. Finally, due to some experimental difficulties we have only measured the lifetime of super−excited states of methane molecules.

[1]This chapter is based upon the following paper:

- A. Azarm, H. L. Xu, Y. Kamali, J. Bernhardt, D. Song, A. Xia, Y. Teranishi, S. H. Lin, F. Kong, and S. L. Chin. Direct observation of super−excited states in methane created by a femtosecond intense laser field. Journal of Physics B: Atomic, Molecular and Optical Physics, 41(22):225601, 2008.

4.1 Spectra

For the simplest hydrocarbon molecule, methane CH_4, the fluorescence of the products is recorded by the technique of time−resolved spectroscopy. Figures 4.1 and 4.2 show the fluorescence spectra emitted from the excited products in the range from 200 to 700 nm. The emission bands in the spectra are assigned as the transitions of $CH(A^2\Delta \rightarrow X^2\Pi)$, $CH(B^2\Sigma^+ \rightarrow X^2\Pi)$ and $CH(C^2\Sigma^+ \rightarrow X^2\Pi)$ and the Balmer lines of hydrogen atom (first and second line). CH bands and their different vibrational excitations are discussed in ref. [38]. Moreover, the Balmer series was discussed in the previous chapter. The reason why we do not see clearly the Balmer line in Figure 4.1 could be explained as follow: In Figure 4.1 the gate width is set to integrate the fluorescence signal over the longest lifetime of the excited fragments ($CH(A^2\Delta \rightarrow X^2\Pi)$ a few hundred nanoseconds). On the other hand in Figure 4.2 the gate width is chosen to be equal to the lifetime of the Balmer line from excited hydrogen atom which is the shortest one (few nanoseconds). Therefore, in Figure 4.2 with the shorter gate width we did not collect all of the florescence signal of the fragments with the exception of the Balmer lines. That is why the Balmer lines in Figure 4.2 are clearer than the Balmer lines in Figure 4.1. This is shown in the inset of Figure 4.2 and 4.1.

In all of the experiments, we measured the lifetime of each detected species to define the proper gate width. This task was carried out in a sequence mode of the gating system. In the sequence mode we fixed the gate width and change the gate delay, therefore we obtained the time dependent florescence signal (see Figures 4.3 and 4.4). In addition, the pressure dependence of the fluorescence signal is obtained to find out the strongest signal and simultaneously avoid the collisional processes. The collisional processes could result in the quenching of florescence signal and/or population of some excited states (see previous chapter).

The ionization potential of the investigated hydrocarbons is listed in table 4.1. As it is shown in the methane spectra (Figure 4.2), the Balmer line H_β is detected as well. H_β line comes from the transition $4l \rightarrow 2l$. It means that the $4l$ level of atomic hydrogen was populated. We know from the previous chapter that the energy level of $H(4l)$ is at 12.74 eV above the ground state [2]. The dissociation process of methane was proposed by Kong et al. [38] to be $CH_4 + n\hbar\omega \rightarrow CH_4^{**} \rightarrow CH + H_2 + H(4l)$. It thus needs at least 12.74 eV energy. Together with the energy necessary to dissociate the molecule into the other fragments, we can see that the energy absorbed by the parent molecule namely, $n\hbar\omega$, is larger than the ionization potential of CH_4 which is 12.61 eV. This indicates that the molecule is excited into some super−excited state. The same argument applies to all the other hydrocarbons studied in this chapter. The

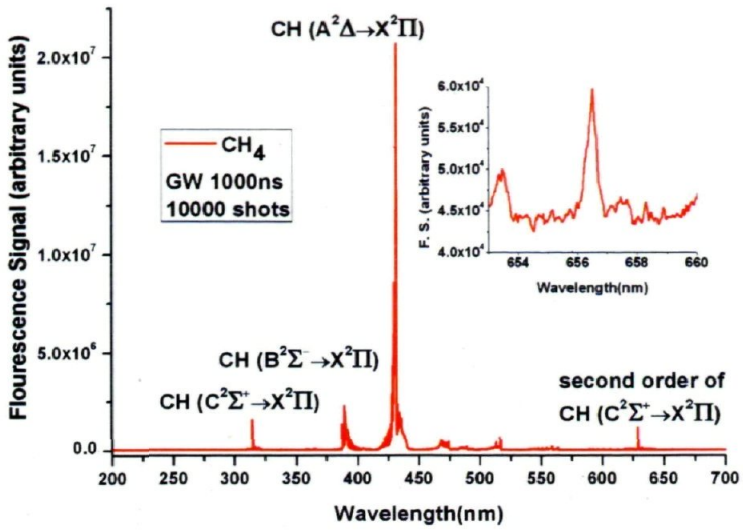

Figure 4.1: *Fluorescence spectra of CH_4 molecule in the strong laser field. Methane pressure was 20 torr, the gatewidth (GW) is equal to the longest lifetime of dissociated fragment and the inset shows the signal around the first Balmer line.*

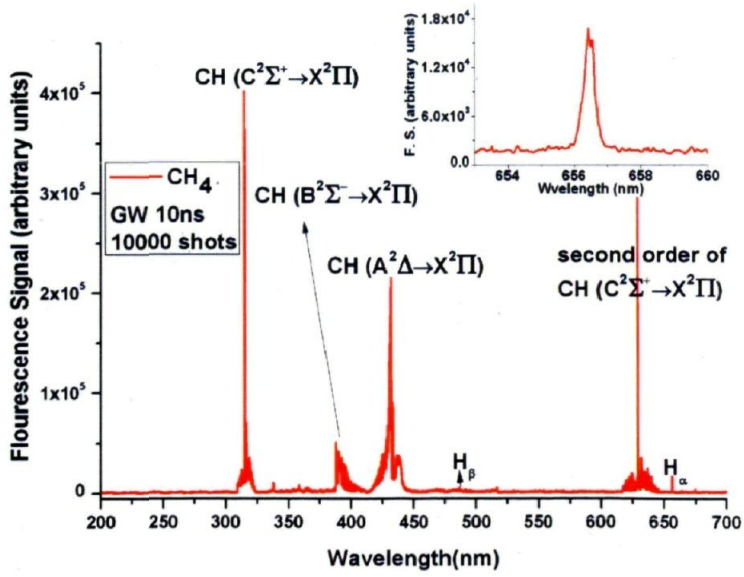

Figure 4.2: *Fluorescence spectra of CH_4 molecule in the strong laser field. Methane pressure was 20 torr, the gatewidth (GW) is equal to the shortest lifetime of dissociated fragment and the inset shows the signal around the first Balmer line.*

only difference is using the first Balmer line (H_α) instead of the second Balmer line (H_β). The observation of the first Balmer line H_α in the other hydrocarbon spectra (see Figures 4.5, 4.6, 4.7, 4.8 and 4.9) indicates that the $3l$ level of atomic hydrogen

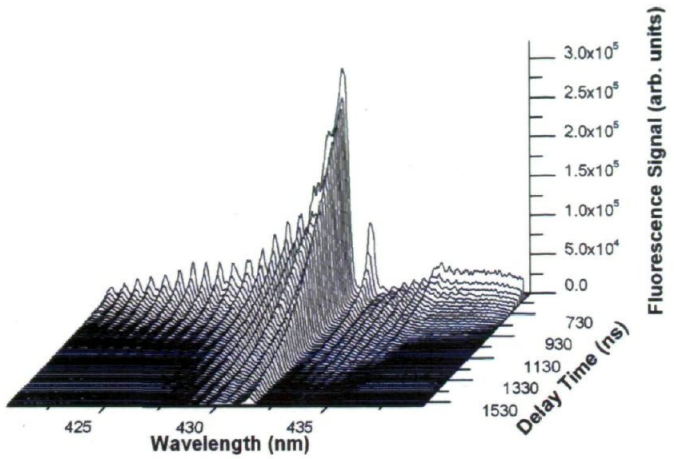

Figure 4.3: *Fluorescence signal of* $CH(A^2\Delta \rightarrow X^2\Pi)$ *transition in different time delay from methane at the pressure of 20 torr. Gatewidth for each gate delay time is fixed to 20 ns.*

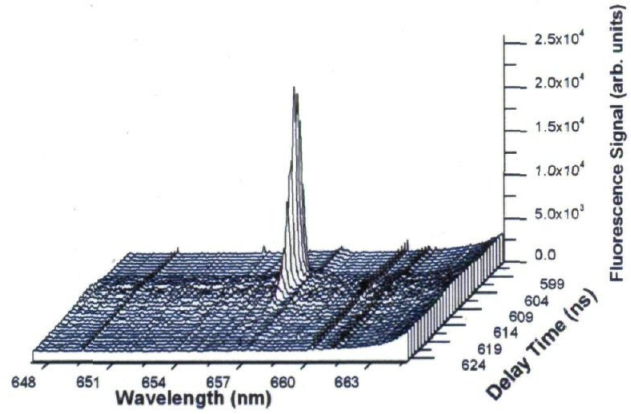

Figure 4.4: *Fluorescence signal of* H_α *transition in different delay time from methane in 20 torr. Gatewidth for each delay time is fixed to 1 ns.*

was populated. The energy level corresponding to $H(3l)$ is 12.08 eV [2]. Therefore the excitation energy in the dissociation process of C_2H_2 or C_2H_4 or C_3H_6 or $1-C_4H_8$ or $cis-2-C_4H_8$ $+n\hbar\omega \rightarrow$" *The other fragments in their ground states*" $+H(3l)$ needs an energy more than 12.08 eV which is greater than the ionization potential of each of them (acetylene 11.4 eV, ethylene 10.51 eV, propylene 9.73 eV, 1−butene 9.55 eV and $cis-2-$butene 9.11 eV). Again it indicates that these molecules are excited into the super−excited states. Therefore multiphoton superexcitation seems to be a general phenomenon even in the complex molecules.

methane CH_4	acetylene C_2H_2	ethylene C_2H_4	propylene C_3H_6	1−butene C_4H_8	cis−2−butene C_4H_8
12.61 [75]	11.4 [76]	10.51 [77]	9.73 [78]	9.55 [79]	9.11 [80]

Table 4.1: *Ionization potential of studied hydrocarbons in* eV

All the five hydrocarbon molecules (C_2H_2, C_2H_4, C_3H_6, $1-C_4H_8$ and $cis-2-C_4H_8$) dissociate under the irradiation of the intense laser at the same wavelength of 800 nm, regardless of their bond type, absorption wavelength, or molecular size. This indicates that neutral dissociation is one universal behavior of polyatomic molecules in intense laser fields. Figures 4.5, 4.6, 4.7, 4.8 and 4.9 show the spectra from acetylene, ethylene, propylene, 1−butene and $cis-2-$butene molecules in a strong laser field, respectively. The gate width is selected to be the longest lifetime of fragmented species (1000ns). The main feature of all of them is the swan bands which are absent in the spectra of methane. The swan system of C_2 ($A^3\Pi_g \rightarrow X'^3\Pi_u(\nu'' \rightarrow \nu')$) with different $\Delta\nu = \nu'' - \nu'$ from -2 to 2 is observed in all of the spectra. The observed swan system of C_2 is listed in Table 4.2.

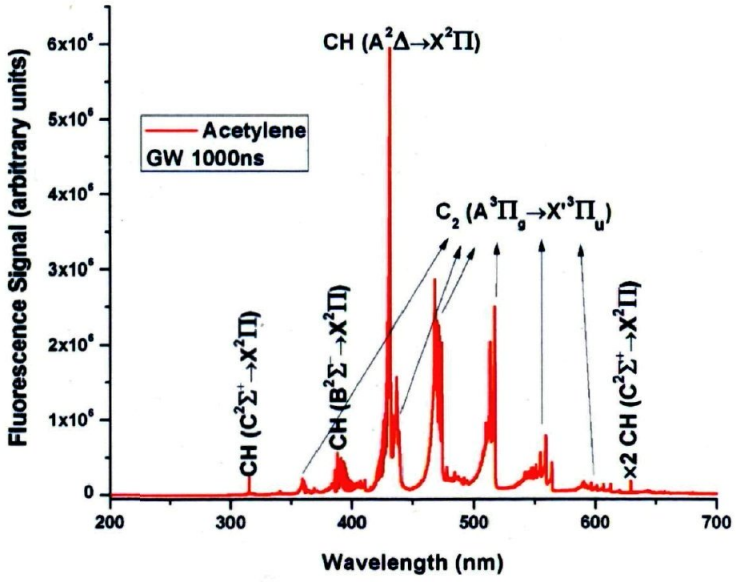

Figure 4.5: *Fluorescence spectra of C_2H_2 molecule in the strong laser field. Acetylene pressure was 0.8 torr.*

According to the assignment of the lines and bands observed in the spectra, the bright fragments are the electronically excited species. The appearance of the small products means that many bonds in each molecule have been cleaved. Such disintegra-

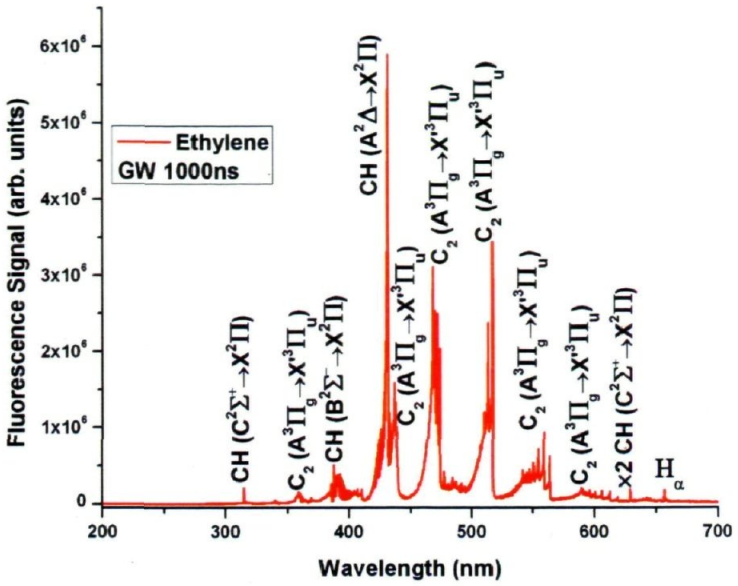

Figure 4.6: *Fluorescence spectra of C_2H_4 molecule in the strong laser field. Ethylene pressure was 0.8 torr.*

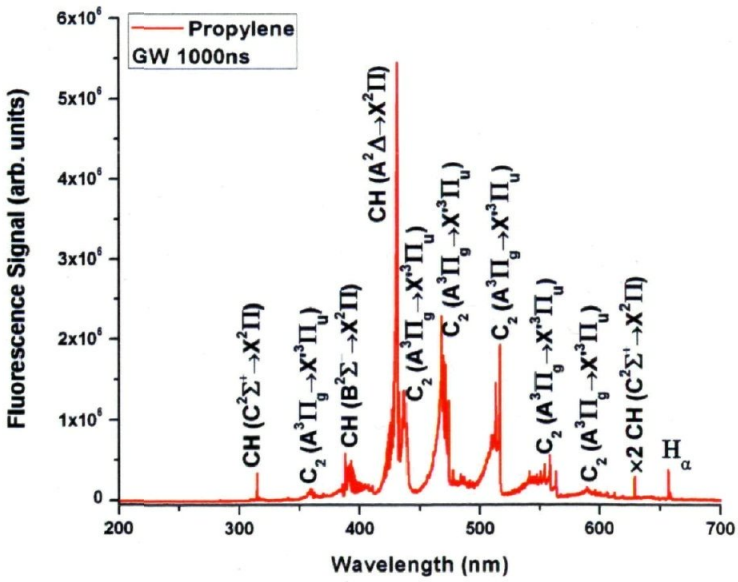

Figure 4.7: *Fluorescence spectra of C_3H_6 molecule in the strong laser field. Propylene pressure was 0.8 torr.*

tion of the molecule has been accomplished even with a single laser pulse. The excited fragmented products generated in the intense laser field are different from those in conventional synchrotron radiation dissociation. That is to say each excited fragment

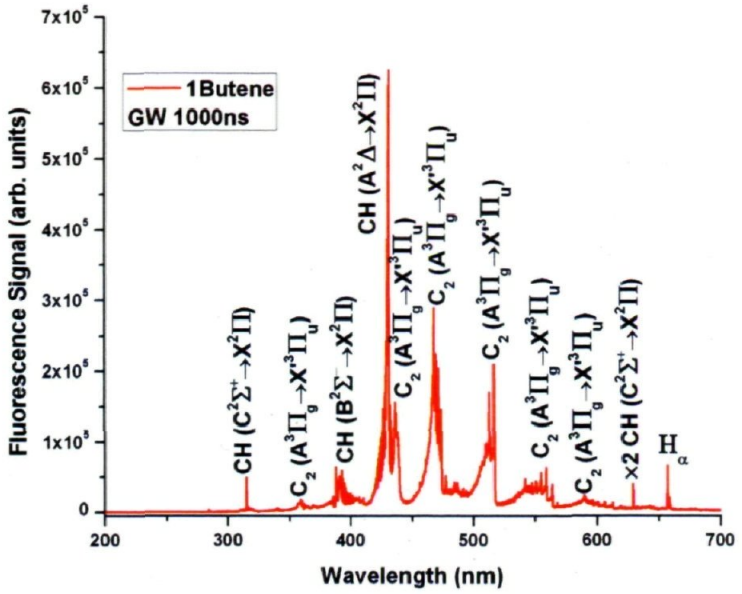

Figure 4.8: *Fluorescence spectra of C_4H_8 molecule in the strong laser field. 1−Butene pressure was 0.8 torr.*

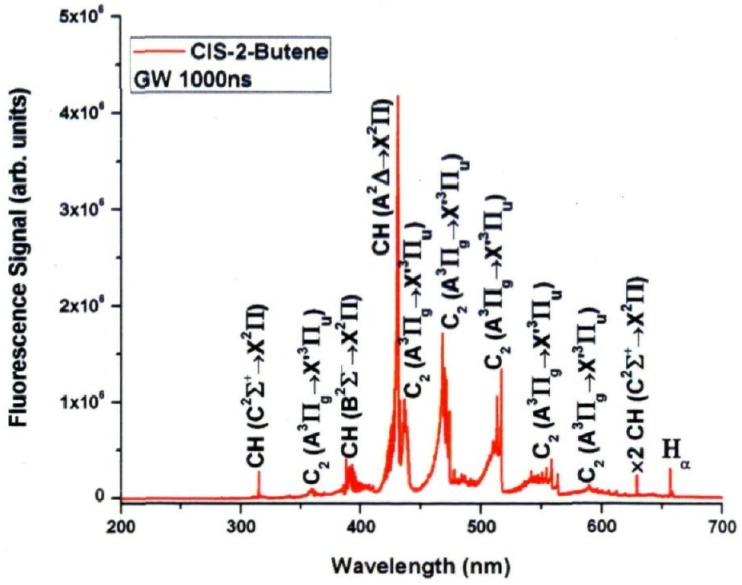

Figure 4.9: *Fluorescence spectra of C_4H_8 molecule in the strong laser field. $Cis-2-$ butene pressure was 0.8 torr.*

has its own appearance energy threshold. Therefore with lower energy SR's photon we cannot observe the fragment fluorescence signal. For example, with a photon energy of around 14.5 eV, the Balmer lines have not been observed in the dissociation of methane

$\Delta\nu$	ν'	ν''	Observed wavelength (nm)	from ref.[81]
-2	6	8	590.17	589.93
	4	6	596.14	595.86
	3	5	600.80	600.49
	2	4	606.13	605.97
	1	3	612.43	612.21
	0	2	619.36	619.12
-1	4	5	547.28	547.03
	3	4	550.46	550.19
	2	3	554.28	554.07
	1	2	558.74	558.55
	0	1	563.77	563.55
0	2	2	509.95	509.77
	1	1	513.20	512.93
	0	0	516.68	516.52
1	6	5	468.16	468.02
	4	3	468.66	468.48
	3	2	469.90	469.76
	2	1	471.74	471.52
	1	0	473.92	473.71
2	4	2	436.66	436.52

Table 4.2: *Swan system observed in hydrocarbon spectra* $A^3\Pi_g \rightarrow X'^3\Pi_u(\nu' \rightarrow \nu'')$

molecules [82]. Hence more study is necessary to find out the differences between the two cases.

4.2 Fluorescence signal versus intensity

In the multiphoton regime, molecules can be excited to the highly excited electronic states after absorbing many photons within a laser pulse. This is shown in Figure 4.10, 4.11, 4.12, 4.13, 4.14 and 4.15 for methane, acetylene, ethylene, propylene, 1−butene and $cis-2-$butene molecules respectively. In each set of data, the gas pressure was the same for each corresponding spectra. This pressure is written in the caption of each figure.

In the simplest hydrocarbon, methane CH_4, three of the fluorescence signals (from

the spectra in Figure 4.2) were selected. Transitions from $CH(A^2\Delta \rightarrow X^2\Pi)$, $CH(C^2\Sigma^+ \rightarrow X^2\Pi)$ and H_α at around 430, 315, and 656 nm versus intensity of the laser pulse are shown in a log−log plot in Figure 4.10. The horizontal axis is not the peak intensity of the laser field. It is the energy of the laser pulse which is proportional linearly to the intensity. Although we calculated the intensity based on gaussian pulse propagation (1−2 mJ corresponds to $1.4 \times 10^{14} - 2.9 \times 10^{14}$ Wcm^{-2}), we do not know exactly the pulse duration and focusing area. Therefore we use the energy of each pulse. In fact the physical quantity we derive from Figure 4.10 is independent of using intensity or energy in the x axis. The integrated fluorescence signal around 430, 315, and 656 nm ($CH(A^2\Delta \rightarrow X^2\Pi)$, $CH(C^2\Sigma^+ \rightarrow X^2\Pi)$ and H_α) versus energy of laser pulses shows initially a linear behavior at lower energy in the log−log scale (see Figure 4.10) and tends to saturate at higher energy. The slope of the linear part indicates the effective number of photons absorbed on the average in each process. In the previous study [38], the slope of $CH(A^2\Delta \rightarrow X^2\Pi)$ transition versus intensity was 10±1 which has a good agreement with the current value of 9. We interpret this slope as being the effective number of photons acquired by this species from the super−excited state. That is equivalent to saying that there is an effective 9−photon absorption. Nine photon absorption corresponds to the absorption of 13.95 eV (=number of photons×photon energy = 9×1.55 eV) which is higher than the ionization potential of methane molecules (12.61 eV see table 4.1). Figure 4.10 shows two different sets of slopes, one set for CH radicals (9 and 9.67 for transitions of $CH(A^2\Delta \rightarrow X^2\Pi)$ and $CH(C^2\Sigma^+ \rightarrow X^2\Pi)$ respectively (13.95−14.98 eV)) and another set for the Balmer line 8.44 (8.44×1.55 eV=13.08 eV). We do not know yet which reaction channel gives rise to these products. It could be that each product comes from a different channel. It could also be that all these products arise from the same channel. However, we can see in all these probable cases, the total energy absorbed giving rise to each or all the products is higher than the ionization potential of methane, confirming that some states above the ionization potential were populated, hence, super−excitation. Moreover, similar to the previous chapter, different slopes imply different sets of excitation to SESs. Therefore different SESs were populated in a strong laser field interaction with methane molecules.

Figure 4.11 shows the integrated florescence signal of $CH(A^2\Delta \rightarrow X^2\Pi)$, $C_2(A^3\Pi_g \rightarrow X'^3\Pi_u(\Delta\nu = \nu'' - \nu' = 1))$ and $C_2(A^3\Pi_g \rightarrow X'^3\Pi_u(\Delta\nu = \nu'' - \nu' = 0))$ at around 430, 470 and 515 nm from acetylene versus the energy of the laser pulses. Similar to methane molecule, the integrated florescence signal versus the energy of laser pulses in the log−log scale shows a linear behavior at lower energy region. The number of photons absorbed in each process or the line slopes of 9.15, 8.7 and 9.17 were measured for transition of $CH(A^2\Delta \rightarrow X^2\Pi)$, $C_2(A^3\Pi_g \rightarrow X'^3\Pi_u(\Delta\nu = \nu'' - \nu' = 1))$ and $C_2(A^3\Pi_g \rightarrow X'^3\Pi_u(\Delta\nu = \nu'' - \nu' = 0))$ at around 430, 470 and 515 nm. Indeed the total energy absorbed (effective number of photons participating in each process×photon

energy= $8.7-9.17\times 1.55$ eV) $12.4-13.9$ eV in this process is higher than the ionization energy of acetylene molecules 11.4 eV (see table 4.1). Unambiguously, multiphoton super excitation is confirmed in acetylene molecules exposed in a strong laser field.

In the rest of the hydrocarbon gases (ethylene C_2H_4, propylene C_3H_6, 1−butene $1-C_4H_8$ and $cis-2-$butene $cis-2-C_4H_8$), six fluorescence signals were chosen from transitions of $CH(A^2\Delta \rightarrow X^2\Pi)$, $CH(C^2\Sigma^+ \rightarrow X^2\Pi)$, $C_2(A^3\Pi_g \rightarrow X'^3\Pi_u(\Delta\nu = \nu'' - \nu' = 1))$, $C_2(A^3\Pi_g \rightarrow X'^3\Pi_u(\Delta\nu = \nu'' - \nu' = 0))$, $C_2(A^3\Pi_g \rightarrow X'^3\Pi_u(\Delta\nu = \nu'' - \nu' = -1))$ and H_α at around 430, 315, 470, 515, 555 and 657 nm, respectively. In all of them (Figures 4.12, 4.13, 4.14 and 4.15) all of the six integrated fluorescence signals versus energy of laser pulses show a linear behavior in the lower energy part of the log−log scale. The slopes of these lines is an indication of the effective number of photons absorbed in each process. In ethylene (Figure 4.12), the highest total energy absorbed 11.93 eV (=7.7 × 1.55 eV) is larger than the ionization potential of ethylene 10.51eV (see Table 4.1). In addition two distinct sets of slopes are recognized (see Figure 4.12). One set with slope of around 7 (from transition of $CH(A^2\Delta \rightarrow X^2\Pi)$, $CH(C^2\Sigma^+ \rightarrow X^2\Pi)$, $C_2(A^3\Pi_g \rightarrow X'^3\Pi_u(\Delta\nu = \nu'' - \nu' = 1))$ and $C_2(A^3\Pi_g \rightarrow X'^3\Pi_u(\Delta\nu = \nu'' - \nu' = 0))$ at around 430, 315, 470 and 515 nm respectively) and another with slope of around 5 (from transition of $C_2(A^3\Pi_g \rightarrow X'^3\Pi_u(\Delta\nu = \nu'' - \nu' = -1))$ and H_α at around 555 and 657 nm respectively). Considering that in one of the sets the total energy absorbed 8.74 to 9.02 eV (=(5.64 to 5.82)×1.55 eV) on the average is not more than the ionization potential of ethylene (10.51 eV). It does not support our hypothesis. In this case we have to consider non perturbative regime. Consequently, the slopes do not reperesent number of photons absorbed in the process.

In propylene (Figure 4.13), contrary to others, we can not find one of the slopes to support the claim that the fragments absorbed more energy than the ionization potential. The maximum slope in Figure 4.13 is 6.22; it is equal to the total energy of 9.64 eV which is less than ionization potential of propylene molecules 9.73 eV (see table 4.1). Finally two isomers of butene show that they also absorbed many photons in dissociation process by SESs. In Figure 4.14 the maximum slope is 7,59. It corresponds to 11.76 eV (ionization potential of 1−butene is 9.55 eV see table 4.1). Moreover, in Figure 4.15 the maximum slope is 6.8 for cis-2-butene. It corresponds to 9.3 eV (ionization potential of $cis-2-$butene is 9.11 eV, see table 4.1).

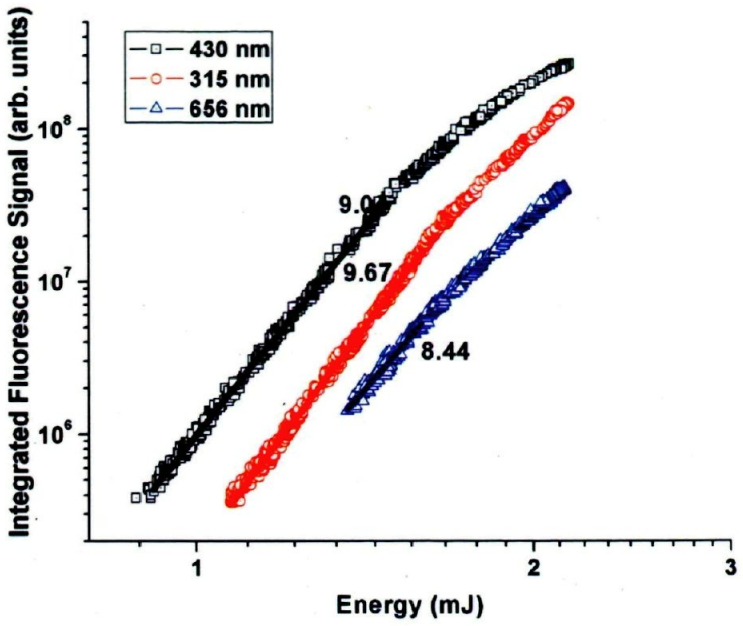

Figure 4.10: *Fluorescence signal versus laser energy which is proportional to intensity. The fluorescence is collected and integrated for transitions of* $CH(A^2\Delta \rightarrow X^2\Pi)$, $CH(C^2\Sigma^+ \rightarrow X^2\Pi)$ *and* H_α *at around 430, 315 and 656 nm, respectively, for methane. Methane pressure was 20 torr.*

4.3 Lifetime measurement of SESs

Currently, precise pathways and the final states in such super−excitation by fs lasers are still unknown because not much has been done in this direction yet. Even though we do not know exactly what these states are, it is expected that such SESs which are coupled to the continuum should have a very short lifetime. In previous SR studies, the lifetime of SESs ($\tau = \hbar/\Gamma$) can only be determined indirectly by measuring the line width (Γ) of the SESs. In theory, several methods have been used to calculate the line width of SESs [83]. Indirect experimental estimate of SESs lifetime was provided through the linewidth of SESs by measuring the ratio of kinetic energy spectra of different isotopes of hydrogen atoms [84]. However, a simple and direct measurement of the SES fs short lifetime is essential. This is done in the current work, using a pump probe technique.

We experimentally demonstrated for the first time that SESs of CH_4 excited by a fs Ti−sapphire laser indeed have a very short lifetime of about 160 fs. This observation establishes unequivocally the existence of SESs and could open up a new direction in more complex molecular superexcitation which could not be studied directly temporally

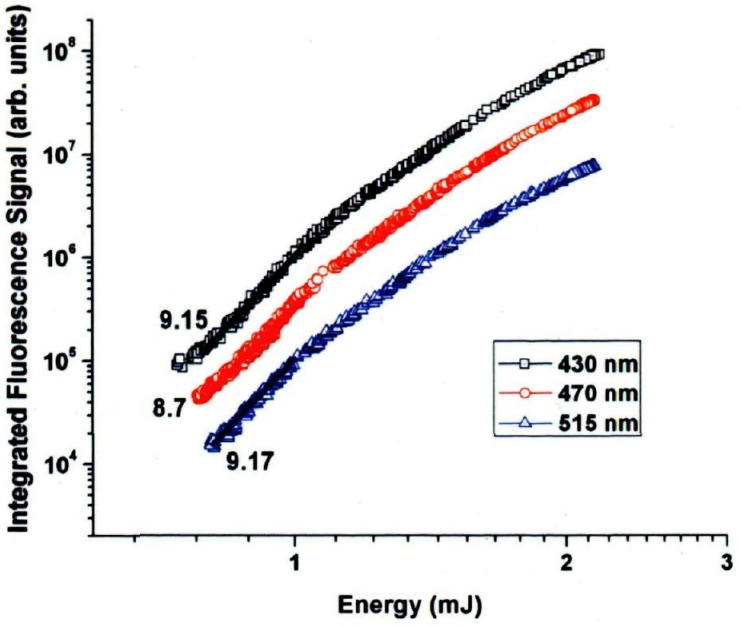

Figure 4.11: *Fluorescence signal versus laser energy which is proportional to intensity. The fluorescence is collected and integrated for transitions of* $CH(A^2\Delta \rightarrow X^2\Pi)$, $C_2(A^3\Pi_g \rightarrow X'^3\Pi_u(\Delta\nu = \nu'' - \nu' = 1))$ *and* $C_2(A^3\Pi_g \rightarrow X'^3\Pi_u(\Delta\nu = \nu'' - \nu' = 0))$ *at around 430, 470 and 515 nm ,respectively, for acetylene. Acetylene pressure was 0.8 torr.*

using synchrotron radiation. The main idea in this experiment is the following. We assume that the fs laser pulse excites the CH_4 into one of its SESs that decays quickly into the CH excited fragments which subsequently fluoresce. A delayed probe pulse at a different wavelength may destroy the SESs. Consequently, there will be a decrease in the CH fragments, hence a reduction in the CH fluorescence. This idea is shown schematically in Figure 4.16. The excited state inside the ionization continuum is just a representation of the SES which is not yet precisely defined. The current experiment monitors only the strongest $CH(A^2\Delta \rightarrow X^2\Pi)$ band.

In the recent work of Kato et al. [82], the SESs of the methane molecules were studied by synchrotron radiation from 12.65 to 41 eV in which five SESs had been found and discussed. One of them is populated by photons with an energy of around 14.5 eV resulting in $CH(A^2\Delta)$, $CH(B^2\Sigma^+)$ through neutral dissociation. It was noted that through this state excited hydrogen atoms cannot be generated because of the low energy of this state [82]. Although, in principle, fs laser excitation could be different from the VUV excitation, we observed the fluorescence emissions from $CH(A^2\Delta \rightarrow X^2\Pi)$, $CH(B^2\Sigma^+ \rightarrow X^2\Pi)$ and $CH(C^2\Sigma^+ \rightarrow X^2\Pi)$ and Balmer lines of Hydrogen atom (first and second line). This agrees with the $CH(A^2\Delta \rightarrow X^2\Pi)$, $CH(B^2\Sigma^+ \rightarrow X^2\Pi)$

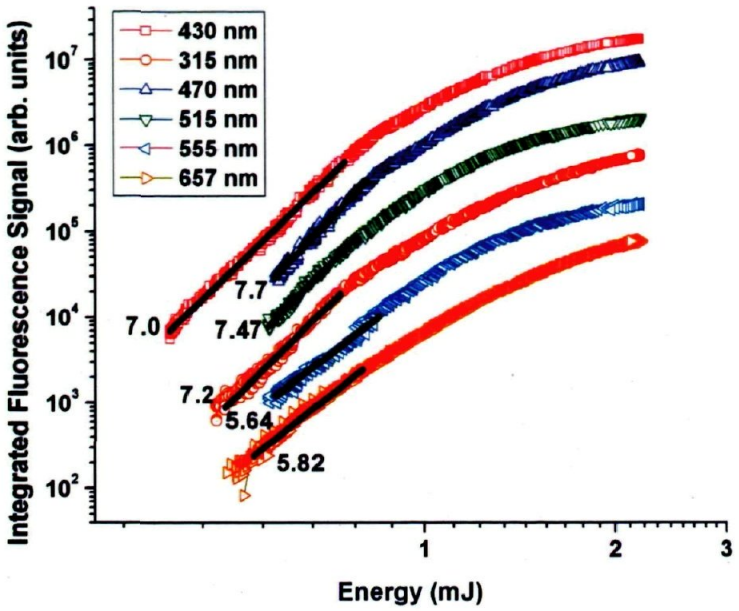

Figure 4.12: *Fluorescence signal versus laser energy which is proportional to intensity. The fluorescence is collected and integrated for transitions of* $CH(A^2\Delta \rightarrow X^2\Pi)$, $CH(C^2\Sigma^+ \rightarrow X^2\Pi)$, $C_2(A^3\Pi_g \rightarrow X'^3\Pi_u(\Delta\nu = \nu'' - \nu' = 1))$, $C_2(A^3\Pi_g \rightarrow X'^3\Pi_u(\Delta\nu = \nu'' - \nu' = 0))$, $C_2(A^3\Pi_g \rightarrow X'^3\Pi_u(\Delta\nu = \nu'' - \nu' = -1))$ *and* H_α *at around 430, 315, 470, 515, 555 and 656 nm ,respectively, for ethylene. Ethylene pressure was 0.8 torr.*

and $CH(C^2\Sigma^+ \rightarrow X^2\Pi)$ results observed by the synchrotron radiation excitation and contains richer information.

In the current experiment, the fluorescence signal of the $CH(A^2\Delta \rightarrow X^2\Pi)$ band at 431 nm was measured as a function of the delay time between the pump and probe pulses. The data were averaged over 100 laser shots and the fluorescence signals were integrated within the wavelength range from 428.5 to 433.5 nm, as well as within a time interval of 600 ns, in order to add up all the fluorescence in the temporal domain. Figure 4.17 shows the fluorescence signal as a function of the delay time. It can clearly be seen that when the delay time between the pump and probe is around zero, an obvious decrease in the fluorescence signal takes place. The fluorescence decrease occurs within a dip width of about 160 fs (FWHM). Since the maximum correlation time of the pump and probe pulses is less than the dip fs temporal width, we exclude the possibility of cross correlation of two pulses. It is noted that outside the dip the fluorescence signals keep almost constant; i.e. the probe pulse does no longer affect the dissociation. Our results clearly indicate that a dissociation channel of the CH excited fluorescing state has an intermediate state having a life time of about 160 fs that can be destroyed by the present probe pulse. Considering the effect of the pump and probe pulse durations

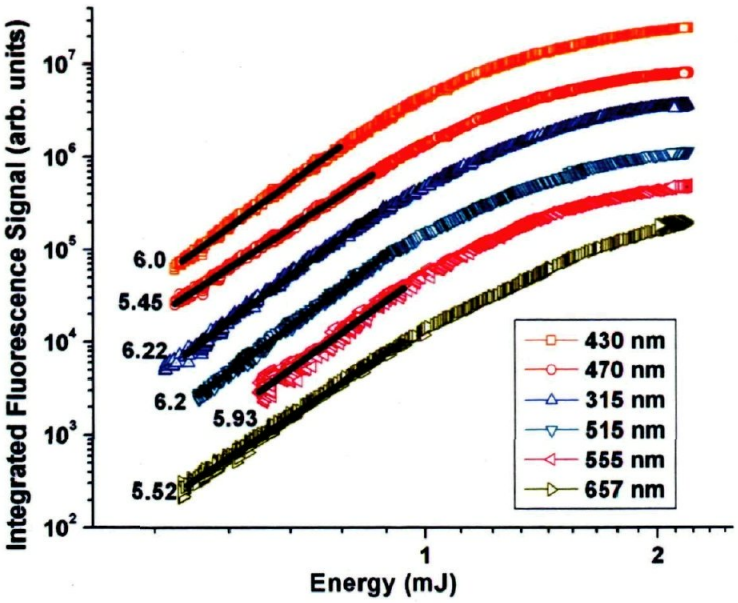

Figure 4.13: *Fluorescence signal versus laser energy which is proportional to intensity. The fluorescence is collected and integrated for transitions of* $CH(A^2\Delta \rightarrow X^2\Pi)$, $CH(C^2\Sigma^+ \rightarrow X^2\Pi)$, $C_2(A^3\Pi_g \rightarrow X'^3\Pi_u(\Delta\nu = \nu'' - \nu' = 1))$, $C_2(A^3\Pi_g \rightarrow X'^3\Pi_u(\Delta\nu = \nu'' - \nu' = 0))$, $C_2(A^3\Pi_g \rightarrow X'^3\Pi_u(\Delta\nu = \nu'' - \nu' = -1))$ *and* H_α *at around 430, 315, 470, 515, 555 and 656 nm ,respectively, for propylene. Propylene pressure was 0.8 torr.*

on the dip shape, the lifetime would be in the range of 50 to 160 fs.

The decrease in the fluorescence signal is slightly more than 5% of the value obtained when the probe beam does not temporally overlap the pump pulse. This may mean that the SES can be destroyed only with a small probability by the present probe pulse, or there are other channels having intermediate states that are not destroyed by the present probe. If an SES has a small destroying probability, it would mean that the state is really imbedded inside the ionization continuum. This is because the probe pulse would not be able to efficiently couple a state inside the continuum (SES) to another state in the continuum such as ionization, etc. Further information on the SES could be given by future detailed experiments with probe pulses having various intensities and frequencies.

We emphasize that the fluorescence depletion could not be explained by a simple ionization scheme where the neutral CH products are generated by the disintegration of the CH_4^+ ion or generated by electron ion recombination, since the lifetimes of these two processes are very long, in the nanosecond time scale. We would not have observed the depletion of the fluorescence only in a time zone of around 160 fs. Similarly, the

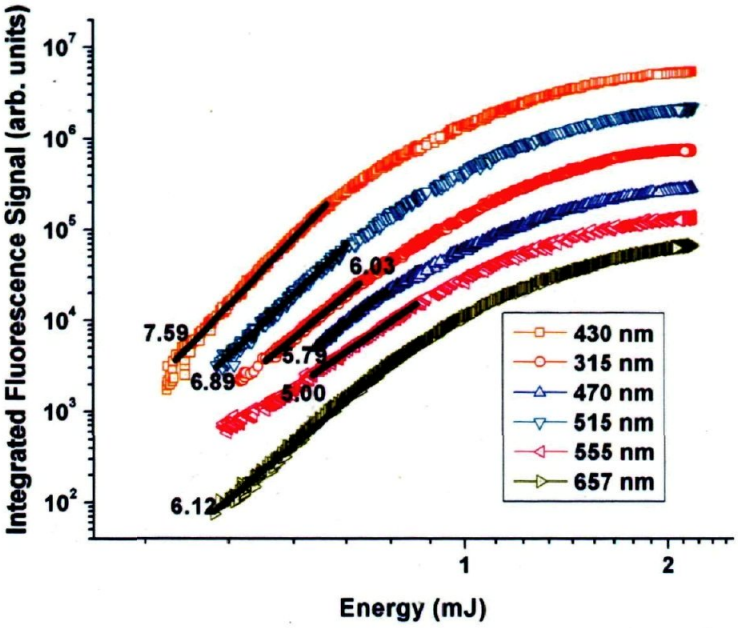

Figure 4.14: *Fluorescence signal versus laser energy which is proportional to intensity. The fluorescence is collected and integrated for transitions of* $CH(A^2\Delta \rightarrow X^2\Pi)$, $CH(C^2\Sigma^+ \rightarrow X^2\Pi)$, $C_2(A^3\Pi_g \rightarrow X'^3\Pi_u(\Delta\nu = \nu'' - \nu' = 1))$, $C_2(A^3\Pi_g \rightarrow X'^3\Pi_u(\Delta\nu = \nu'' - \nu' = 0))$, $C_2(A^3\Pi_g \rightarrow X'^3\Pi_u(\Delta\nu = \nu'' - \nu' = -1))$ *and* H_α *at around 430, 315, 470, 515, 555 and 656 nm ,respectively, for* 1−*butene. 1−Butene pressure was 0.8 torr.*

fluorescence depletion does not refer to the direct interaction between the probe laser pulse and CH_2 or $CH(A^2\Delta)$ species either, because the depletion takes place immediately after the first excitation without any time delay while the fluorescence lifetime of $CH(A^2\Delta)$ is normally in the nanosecond time scale.

4.4 Conclusion

In the current chapter our studies extended to some more complicated molecules. By observing many highly excited fragments with the spectroscopy method, we can claim that neutral dissociation happened through highly excited states (SESs) in all of the studied hydrocarbons. Intensity dependent data strengthen our claim of multiphoton superexcitation in a strong laser field. Hence, we could claim that neutral dissociation in a strong laser field by mutiphoton superexcitation is a universal pathway.

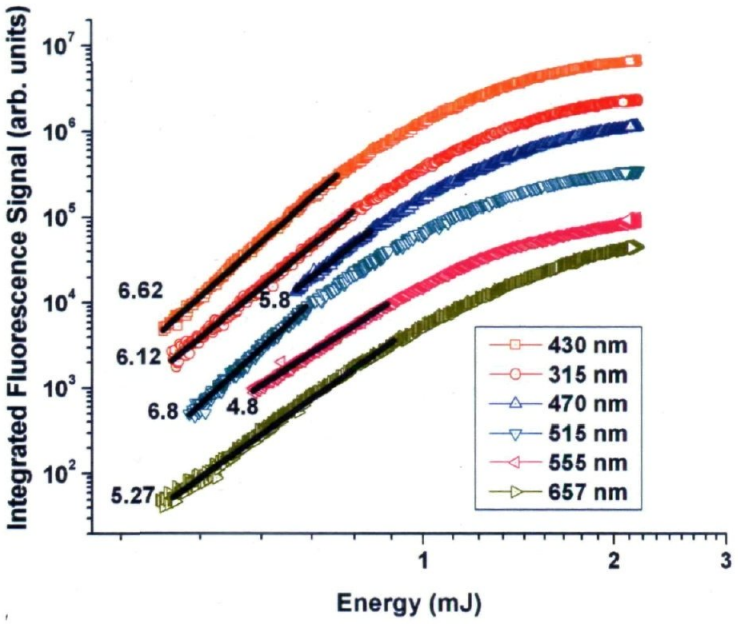

Figure 4.15: *Fluorescence signal versus laser energy which is proportional to intensity. The fluorescence is collected and integrated for transitions of* $CH(A^2\Delta \rightarrow X^2\Pi)$, $CH(C^2\Sigma^+ \rightarrow X^2\Pi)$, $C_2(A^3\Pi_g \rightarrow X'^3\Pi_u(\Delta\nu = \nu'' - \nu' = 1))$, $C_2(A^3\Pi_g \rightarrow X'^3\Pi_u(\Delta\nu = \nu'' - \nu' = 0))$, $C_2(A^3\Pi_g \rightarrow X'^3\Pi_u(\Delta\nu = \nu'' - \nu' = -1))$ *and* H_α *at around 430, 315, 470, 515, 555 and 656 nm ,respectively, for* $cis-2-$*butene.* $Cis-2-$*butene pressure was 0.8 torr.*

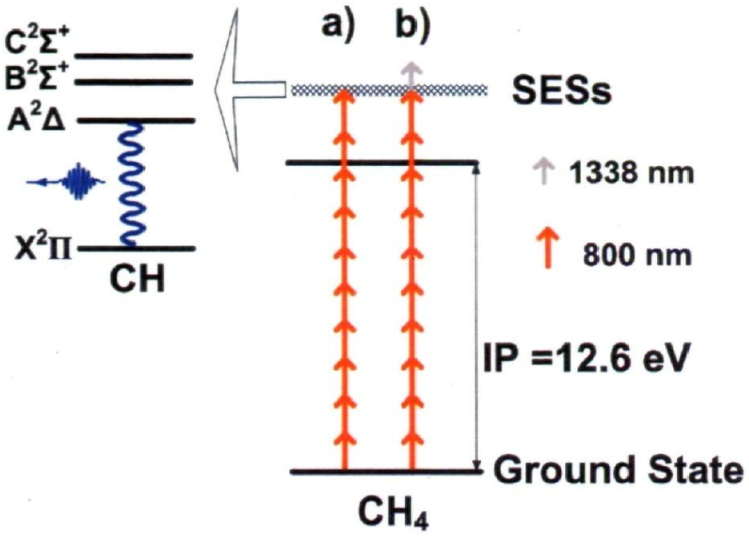

Figure 4.16: *Schematic diagram of the SESs excitation of CH_4: (a) the process is just with the pump pulse to excite the SESs (the regions except for the dip in Figure 4.17) and (b) the process of how the probe pulse depletes the SESs (the dip region in figure 4.17).*

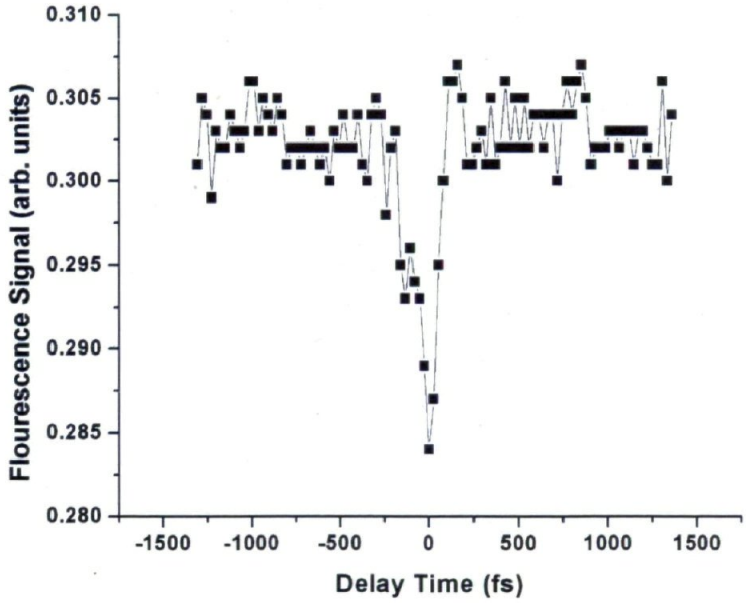

Figure 4.17: *Integrated fluorescence signal of $CH(A^2\Delta \rightarrow X^2\Pi)$ at around 431* nm *versus the delay time between the pump and probe pulses; negative delay time means the probe pulses are behind the pump pulses.*

Chapter 5

Summary and conclusion

In this chapter, first we summarize our results from previous chapters. Then, we conclude that neutral dissociation in a strong laser filed is a universal phenomena which we think is happening through excitation of superexcited states. Finally, based on our last studies, we propose to put more efforts to understand the mechanism or process responsible for the excitation of the superexcited state which could be population trapping (interference stabilization). Therefore it is worthwhile to study population trapping in the strong laser field interaction with molecules.

5.1 Summary

For the simplest molecule, hydrogen H_2, we found that it undergoes neutral dissociation in a strong laser field at intermediate intensities. The fluorescence spectra of the dissociation products are attributed to the Balmer series of the hydrogen atom (n→2), from n=3 up to n = 14. These excited products imply that parent molecules are excited to highly excited states, i.e. SESs, in intense laser fields. This point is supported by the laser intensity dependence of the fluorescence intensity of the hydrogen atom. After multiphoton excitation, superexcited H_2 molecules undergo spontaneous dissociation. To understand the dissociation mechanism of the SESs of H_2 molecules, empirical PECs for different SESs are built. Only repulsive PECs are used to interpret neutral dissociation. Using a pump−probe technique, the lifetime of transient SESs is measured to be around 180 fs.

For oxygen molecule O_2, we find that also it undergoes neutral dissociation in strong

laser fields at the intensity of 2×10^{14} W/cm^2. Thirty three emission lines have been recorded in the fluorescence spectroscopy. These emissions are caused by the excited oxygen atoms, which are the dissociation products of the oxygen molecules. Ten of them are the new Rydberg transitions, which have not been reported. Three new Rydberg states $2s^22p^3(^4S^o)11s\ ^5S^o$, $2s^22p^3(^4S^o)12s\ ^5S^o$ and $2s^22p^3(^4S^o)10d\ ^5D^o$ are identified for the first time. Laser power dependence of the fluorescence intensity shows that each oxygen molecule absorbs ten laser photons on an average. The total energy absorbed is about 15.5 eV which is higher than the first ionization potential (IP) of the molecule. This is an alternative method to prepare SESs as compared to the conventional method of SR excitation. After the multiphoton excitation, the superexcited O_2 molecules undergo spontaneous dissociation. To understand the dissociation mechanism of the SESs of O_2 molecules, Morse PECs for different SESs are built. Predissociation mechanism is suggested to explain the O−O bond cleavage. An ultrafast laser diagnostic experiment is performed for O_2 dissociation. A second laser pulse is employed to deplete the fluorescence intensity. The measured lifetime of 150 fs for the intermediate state is consistent with predissociation mechanism. QCT calculation shows that the predissociation process requires a short time of about 100 fs while direct dissociation needs a much longer time of 600 fs.

For nitric oxide molecules NO, we have found that it undergoes neutral dissociation in strong laser fields at the intensity of 2×10^{14} W/cm^2 as well. Twenty eight emitting lines have been recorded in the fluorescence spectroscopy. The emissions are assigned to the transition of excited N and O atoms. The emitters are the dissociation products of NO molecules. Intensity dependence of the strongest florescence signal confirms multiphoton superexcitation in nitric oxide molecules. After multiphoton excitation, the superexcited NO molecules undergo spontaneous dissociation. The upper limit life time of assigned SESs was measured to be about 160 fs. To understand the dissociation mechanism of the SESs of NO molecules, the ionic core model is used. The related PECs are built. Direct dissociation mechanism is suggested to explain the N−O bond cleavage leading to N^* and O^*. Pre−dissociation mechanism is suggested to explain the N−O bond cleavage leading to N^* and O^* fragments.

For the hydrocarbon molecules (CH_4, C_2H_2, C_2H_4, C_3H_6, $1-C_4H_8$ and $cis-2-C_4H_8$), we report a new type of photodissociation in the intense laser field. All the above mentioned hydrocarbons are exposed to the laser intensity of $2 \times 10^{14}\ Wcm^{-2}$. The transitions of $CH(A^2\Delta \rightarrow X^2\Pi)$,$CH(B^2\Sigma^+ \rightarrow X^2\Pi)$ and $CH(C^2\Sigma^+ \rightarrow X^2\Pi)$ plus Balmer lines of hydrogen atom and swan system of C_2 ($A^3\Pi_g \rightarrow X'^3\Pi_u(\nu'' \rightarrow \nu')$) with different $\Delta\nu = \nu'' - \nu'$ from -2 to 2 are observed in the fluorescence spectrum. Due to the lack of C_2 radical in CH_4, swan system was not observed in methane molecule. The dissociation is vigorous, producing highly vibrationally excited CH^* and C_2^* products,

as well as H^*. All of the hydrocarbons absorbed a number of photons with total energy more than the ionization potential. This is shown with comprehensive study of each band versus intensity of the laser field. Moreover, different channels were observed for multiphoton superexcitation. In addition, by using a pump−probe technique, we demonstrated direct evidence of SESs using, as an example, CH_4 in femtosecond intense laser fields. The decrease in the fluorescence signal of $CH(A^2\Delta \rightarrow X^2\Pi)$ has been observed and attributed to the depletion of the SESs of CH_4.

5.2 Conclusion

In conclusion, we found that many molecules (from the simplest molecule to complex hydrocarbons) undergo neutral dissociation in a strong laser field at intermediate intensities. We have enough evidence to claim that neutral dissociation is a universal phenomenon in strong laser field interaction with molecules. One of the evidences is the observation of many excited neutral fragments. The other is the intensity dependent experiment. And last but not least is an unambiguous depletion of the fluorescence signal from neutral excited fragments as a function of the delay time. Therefore, excitation of SESs during the interaction of an intense fs laser with a molecule is a universal reaction pathway that has not been considered so far by the intense laser science community. A new era is opened up to study SESs of molecules, in particular, their dynamics and characteristics induced by intense laser field.

5.3 Proposal

Based on our current understanding of SESs of molecules pumped by intense femtosecond laser pulses from this thesis and the results from single photon process of populating SESs [33], there are some similarities in between single and multiphoton superexcitation. However, there are some differences as well. The fundamental difference is the way SESs are populated. For example single photon process excites SESs through resonance processes. Apparently, the resonance process could not be responsible for multiphoton superexcitation. Hence multiphoton superexcitation process is still not clear. Therefore, we propose that using an intense femtosecond laser pulses, the excitation of SESs of molecules are mainly due to population trapping [85].

Interference stabilization of Rydberg states of an atom results in the trapping of population in some long lived Rydberg states. Interference stabilization (population

trapping) was first proposed by Fedorov and Movsesian in 1988 [86]. Essentially, when an atom is prepared in a highly excited state (e.g. a Rydberg state) and interacts with a short intense laser pulse, there is a probability that the atom resists being ionized and is trapped in a neighboring Rydberg state in the strong laser field. We would deduce that because any atom and molecule, including more complex molecules, possesses highly excited states and Rydberg states, the consequence of its interaction with a short intense laser pulse would result in some trapping (interference stabilization). In the other way we would claim that SESs are those Rydberg states converging to ionic state that could be excited by population trapping process.

Recently, we studied the fluorescence emitted from filaments in air using a pump and probe scheme with a femtosecond Ti−sapphire laser. The fluorescence intensities from the first negative band and the second positive band of nitrogen molecules show enhancement and change periodically as a function of the pump and probe time delay. We attribute this phenomenon to the universal yet probably forgotten phenomenon of population trapping of nitrogen molecules in highly excited states together with field induced alignment of nitrogen molecules followed by revivals of the rotational wave packets. Theoretical calculation of the alignment dynamics of nitrogen molecules is consistent with the experimental data. Population trapping of nitrogen molecules in highly excited states seems to be at the origin of the enhancement. We would like to underline the importance of the phenomenon of population trapping. Though proposed more than twenty years ago [86] and demonstrated [87, 88, 89] more than fifteen years ago, it received little attention in recent years. Our results show that trapping is an important phenomenon accompanying ionization during ultrafast strong laser field interaction with atoms and molecules. This phenomenon also shows up in the field of femtosecond laser filamentation in air, where the enhancement of nitrogen fluorescence by terahertz field is shown to be a new technique to remotely detect terahertz radiation, which otherwise would be absorbed by the humidity in air [90, 91].

As we know from the first chapter, superexcited states of a molecule are defined as those neutral states whose energy is higher than the first ionization potential [29]. Using synchrotron radiation, chemists have observed many such states in molecules through single photon excitation [29]. Superexcited molecules will decay through several channels, one of which being neutral dissociation resulting in the fluorescence of the dissociated particles [29]. Using intense femtosecond laser pulses, we have observed neutral dissociation of some molecules resulting in their characteristic fluorescence. We experimentally demonstrate that superexcitation is due to a highly nonlinear process. We analyze the data with semiempirical calculation in such a way that multiphoton resonant absorption into the superexcited states is responsible for this excitation.

Since the resonance process can not be responsible for population of SESs, we suggest to study interference stabilization and its connection to multiphoton superexcitation phenomena in details. Let us look closer. Such a resonant absorption in a high intensity laser field would only give rise to resonant ionization so that there is no more population left in the super−excited state. In the vertical multiphoton transition a resonance with a Rydberg state converging to an excited ionic state takes place. Because of the resonance with the Rydberg state, the excited electron would have a high probability to absorb one more photon to the continuum. It will then leave the parent ion with a kinetic energy leaving behind the ion in the excited state. No significant neutral Rydberg state would be left behind. However, if the intensity is strong enough satisfying the condition of trapping, a $\Lambda-$type transition would occur together with an interference stabilization. This trapping (stabilization) process would compete with the resonant ionization process. This is very similar to the trapping during a dynamic resonance with the Rydberg states in atoms and molecules described above. The fact that we have observed super−excitations in many molecular systems experimentally proves that such trapping would have been the excitation process of super−excited states using a short intense laser pulse. This idea can be further extended to the trapping onto a molecular neutral repulsive surface in the continuum at the initial internuclear distance through vertical transitions. From this position on the repulsive surface, the molecules will immediately undergo dissociation. This seems to be the case in H_2 whose neutral dissociation originates from some neutral excited dissociative surfaces.

We would propose that population trapping or interference stabilization in the multiphoton regime first proposed by Fedorov et al [86] seems to be a universal phenomenon in atoms and molecules interacting with an ultrafast intense laser pulse. Population trapping would also be responsible in the excitation of some super−excited states of molecules using intense short laser pulses. Finally, we propose deeper studies in interference stabilization to understand the mechanism of multiphoton superexcitation.

Bibliography

[1] T. E. Sharp. Potential-energy curves for molecular hydrogen and its ions. *Atomic Data and Nuclear Data Tables*, 2:119 – 169, 1970.

[2] Yu. Ralchenko, A. E. Kramida, J. Reader and NIST ASD Team (2011):. Nist atomic spectra database (ver. 4.1.0), [online]available:http://physics.nist.gov/asd3, 2011, August 23.

[3] Th. Maiman. Stimulated optical radiation in ruby. *Nature*, 187(4736):493–494, 1960.

[4] F. J. McClung and R. W. Hellwarth. Giant optical pulsations from ruby. *Journal of Applied Physics*, 33(3):828–829, 1962.

[5] I. S. Ruddock and D. J. Bradley. Bandwidth-limited subpicosecond pulse generation in mode-locked cw dye lasers. *Applied Physics Letters*, 29(5):296–297, 1976.

[6] H. W. Mocker and R. J. Collins. Mode competition and self-locking effects in a q-switched ruby laser. *Applied Physics Letters*, 7(10):270–273, 1965.

[7] P. M. Paul, E. S. Toma, P. Breger, G. Mullot, F. Auge, P. Balcou, H. G. Muller, and P. Agostini. Observation of a train of attosecond pulses from high harmonic generation. *Science*, 292(5522):1689–1692, JUN 1 2001.

[8] M. Hentschel, R. Kienberger, C. Spielmann, G. A. Reider, N. Milosevic, T. Brabec, P. Corkum, U. Heinzmann, M. Drescher, and F. Krausz. Attosecond metrology. *Nature*, 414(6863):509–513, NOV 29 2001.

[9] A. H. Zewail. Femtochemistry: Atomic-scale dynamics of the chemical bond. *The Journal of Physical Chemistry A*, 104(24):5660–5694, 2000.

[10] P. A. Franken, A. E. Hill, C. W. Peters, and G. Weinreich. Generation of optical harmonics. *Physical Review Letters*, 7:118–119, Aug 1961.

[11] P. Agostini, G. Barjot, J. Bonnal, G. Mainfray, C. Manus, and J. Morellec. Multiphoton ionization of hydrogen and rare gases. *Quantum Electronics, IEEE Journal of*, 4(10):667 – 669, oct 1968.

[12] G. S. Voronov and N. B. Delone. Ionization of the xenon atom by the electric field of ruby laser emission. *Jurnal of Experimental and Theoritical Physics Letters*, 1:66, 1965.

[13] S. L. Chin, F. Yergeau, and P. Lavigne. Tunnel ionisation of Xe in an ultra-intense CO_2 laser field (10^{14} Wcm^{-2}) with multiple charge creation. *Journal of Physics B: Atomic and Molecular Physics*, 18(8):L213, 1985.

[14] G. A. Mourou, T. Tajima, and S. V. Bulanov. Optics in the relativistic regime. *Reviews of Modern Physics*, 78:309–371, Apr 2006.

[15] D. Strickland and G. Mourou. Compression of amplified chirped optical pulses. *Optics Communications*, 55(6):447 – 449, 1985.

[16] R. G. Meyerand and A. F. Haught. Gas breakdown at optical frequencies. *Physical Review Letters*, 11:401–403, Nov 1963.

[17] L. V. Keldysh. Ionization in the field of a strong electromagnetic wave. *Soviet physics Journal of Experimental and Theoretical Physics*, 20:1307, 1965.

[18] P. Agostini, F. Fabre, G. Mainfray, G. Petite, and N. K. Rahman. Free-free transitions following six-photon ionization of xenon atoms. *Physical Review Letters*, 42:1127–1130, Apr 1979.

[19] A. McPherson, G. Gibson, H. Jara, U. Johann, T. S. Luk, I. A. McIntyre, K. Boyer, and C. K. Rhodes. Studies of multiphoton production of vacuum-ultraviolet radiation in the rare gases. *ournal of the Optical Society of America B*, 4(4):595–601, Apr 1987.

[20] M. Ferray, A. L'Huillier, X. F. Li, L. A. Lompre, G. Mainfray, and C. Manus. Multiple-harmonic conversion of 1064 nm radiation in rare gases. *Journal of Physics B: Atomic, Molecular and Optical Physics*, 21(3):L31, 1988.

[21] P. B. Corkum. Plasma perspective on strong field multiphoton ionization. *Physical Review Letters*, 71:1994–1997, Sep 1993.

[22] B. Walker, B. Sheehy, K. C. Kulander, and L. F. DiMauro. Elastic rescattering in the strong field tunneling limit. *Physical Review Letters*, 77:5031–5034, Dec 1996.

[23] S. Augst, D. D. Meyerhofer, D. Strickland, and S. L. Chin. Laser ionization of noble gases by coulomb-barrier suppression. *Journal of the Optical Society of America B*, 8(4):858–867, Apr 1991.

[24] H. Stapelfeldt and T. Seideman. Colloquium: Aligning molecules with strong laser pulses. *Reviews of Modern Physics*, 75:543–557, Apr 2003.

[25] M. Ivanov, T. Seideman, P. Corkum, F. Ilkov, and P. Dietrich. Explosive ionization of molecules in intense laser fields. *Physical Review A*, 54:1541–1550, Aug 1996.

[26] I. V. Litvinyuk, K. F. Lee, P. W. Dooley, D. M. Rayner, D. M. Villeneuve, and P. B. Corkum. Alignment-dependent strong field ionization of molecules. *Physical Review Letters*, 90:233003, Jun 2003.

[27] M. Lein, P. P. Corso, J. P. Marangos, and P. L. Knight. Orientation dependence of high-order harmonic generation in molecules. *Physical Review A*, 67:023819, Feb 2003.

[28] P. H. Bucksbaum, A. Zavriyev, H. G. Muller, and D. W. Schumacher. Softening of the H_2^+ molecular bond in intense laser fields. *Physical Review Letters*, 64:1883–1886, Apr 1990.

[29] Y. Hatano. Interaction of vacuum ultraviolet photons with molecules. formation and dissociation dynamics of molecular superexcited states. *Physics Reports*, 313(3):109 – 169, 1999.

[30] J. A. Berkowitz. *Atomic and Molecular Photoabsorption.* Academic Press, London, 2002.

[31] R. L. Platzman. Superexcited states of molecules. *Radiation Research*, 17(3):pp. 419–425, 1962.

[32] M. Inokuti. Scientific legacy of robert l. platzman. preliminary report. *Radiation Physics and Chemistry*, 60(4-5):283 – 290, 2001.

[33] Y. Hatano. Interaction of vacuum ultraviolet photons with molecules. formation and dissociation dynamics of molecular superexcited states. *Physics Reports*, 313(3):109 – 169, 1999.

[34] H. Nakamura. What are the basic mechanisms of electronic transitions in molecular dynamic processes? *International Reviews in Physical Chemistry*, 10(2):123–188, 1991.

[35] K. Kameta, N. Kouchi, M. Ukai, and Y. Hatano. Photoabsorption, photoionization, and neutral-dissociation cross sections of simple hydrocarbons in the vacuum ultraviolet range. *Journal of Electron Spectroscopy and Related Phenomena*, 123(2-3):225 – 238, 2002.

[36] G. E. Gadd, L. E. Jusinski, and T. G. Slanger. $N(^2D)$ production from predissociation of ns and nd Rydberg levels in NO. *The Journal of Chemical Physics*, 91(6):3378–3383, 1989.

[37] Helm H., Dyer M. J., Bissantz H., Huestis D. L. In Coherent Phenomena in Atoms and Molecules in Laser Fields, New York Plenum, 1992.

[38] F. Kong, Q. Luo, H. Xu, M. Sharifi, D. Song, and S. L. Chin. Explosive photodissociation of methane induced by ultrafast intense laser. *The Journal of Chemical Physics*, 125(13):133320, 2006.

[39] C. J. G. J. Uiterwaal, C. R. Gebhardt, H. Schröder, and K.-L. Kompa. Predicting intense-field photoionization of atoms and molecules from their linear photoabsorption spectra in the ionization continuum. *The European Physical Journal D - Atomic, Molecular, Optical and Plasma Physics*, 30:379–392, 2004.

[40] http://www.newport.com/Tsunami-Ultrafast-TiSapphire-Lasers/368126/1033/catalog.aspx.

[41] http://www.newport.com/Millennia-Prime-532-nm-CW-DPSS-Lasers/501529/1033/catalog.aspx.

[42] http://www.newport.com/Spitfire-Ace-Ultrafast-Amplifiers/988605/1033/catalog.aspx.

[43] http://www.newport.com/OPA-800C-Ultrafast-OPA/368110/1033/catalog.aspx.

[44] A. Weiner. *Ultrafast optics.* John Wiley and Sons, May 2009.

[45] C. Rullière. *Femtosecond Laser Pulses: Principles and Experiments.* Springer, October 2004.

[46] J.-C. Diels W. Rudolph. *Ultrashort Laser Pulse Phenomena.* Academic Press, September 2006.

[47] http://sales.hamamatsu.com/en/products/electron-tube-division/detectors/photomultiplier-tubes/part-r5916u-52.php.

[48] http://www.princetoninstruments.com/products/imcam/pimax/.

[49] H. L. Xu, A. Azarm, and S. L. Chin. Controlling fluorescence from n_2 inside femtosecond laser filaments in air by two-color laser pulses. *Applied Physics Letters*, 98(14):141111, 2011.

[50] F. Théberge, N. Aközbek, W. Liu, A. Becker, and S. L. Chin. Tunable ultrashort laser pulses generated through filamentation in gases. *Physical Review Letters*, 97(2):023904, Jul 2006.

[51] A. Azarm, D. Song, K. Liu, S. Hosseini, Y. Teranishi, S. H. Lin, A. Xia, F. Kong, and S. L. Chin. Neutral dissociation of hydrogen molecules in a strong laser field through superexcited states. *Journal of Physics B: Atomic, Molecular and Optical Physics*, 44(8):085601, 2011.

[52] D. Song, A. Azarm, Y. Kamali, K. Liu, A. Xia, Y. Teranishi, S. H. Lin, F. Kong, and S. L. Chin. Neutral dissociation of superexcited oxygen molecules in intense laser fields. *The Journal of Physical Chemistry A*, 114(9):3087–3095, 2010. PMID: 20043684.

[53] K. Liu, D. Song, A. Azarm, S. L. Chin, and F. Kong. Neutral dissociation of superexcited nitric oxide induced by intense laser fields. *Chinese Journal of Chemical Physics*, 23(3):252, 2010.

[54] M. Glass-Maujean, Ch. Jungen, H. Schmoranzer, A. Knie, I. Haar, R. Hentges, W. Kielich, K. Jänkälä, and A. Ehresmann. H_2 Superexcited States: Experimental and Theoretical Characterization of their Competing Decay-Channel Fluorescence, Dissociation, and Ionization. *Physical Review Letters*, 104(18):183002, May 2010.

[55] I. D. Williams, P. McKenna, B. Srigengan, I. M. G. Johnston, W. A. Bryan, J. H. Sanderson, A. El-Zein, T. R. J. Goodworth, W. R. Newell, P. F. Taday, and A. J. Langley. Fast-beam study of H_2^+ ions in an intense femtosecond laser field. *Journal of Physics B: Atomic, Molecular and Optical Physics*, 33(14):2743, 2000.

[56] G. N. Gibson, L. Fang, and B. Moser. Direct femtosecond laser excitation of the 2p state of H by a resonant seven-photon transition in H_2^+. *Physical Review A*, 74(4):041401, Oct 2006.

[57] B. Manschwetus, T. Nubbemeyer, K. Gorling, G. Steinmeyer, U. Eichmann, H. Rottke, and W. Sandner. Strong Laser Field Fragmentation of H_2: Coulomb Explosion without Double Ionization. *Physical Review Letters*, 102(11):113002, Mar 2009.

[58] http://physics.nist.gov/cgi-bin/cuu/Value?ryd|search_for=atomnuc!

[59] R. N. Coffee and G. N. Gibson. vuv fluorescence from selective high-order multiphoton excitation of N_2. *Physical Review A*, 69(5):053407, May 2004.

[60] S. Wang, X. Tang, L. Gao, M. E. Elshakre, and F. Kong. Dissociation of methane in intense laser fields. *The Journal of Physical Chemistry A*, 107(32):6123–6129, 2003.

[61] M. E. Elshakre, L. Gao, X. Tang, S. Wang, Y. Shu, and F. Kong. Dissociation of acetaldehyde in intense laser field: Coulomb explosion or field-assisted dissociation? *The Journal of Chemical Physics*, 119(11):5397–5405, 2003.

[62] H.-J. Werner, P. J. Knowles, G. Knizia, F. R. Manby, M. Schütz, et al. Molpro, version 2010.1, a package of ab initio programs, 2010. see http://www.molpro.net/.

[63] M. Ukai, N. Kouchi, K. Kameta, N. Terazawa, Y. Chikahiro, Y. Hatano, and K. Tanaka. Extreme ultraviolet photodissociation of O_2 via the free $(c^4\Sigma_u^-)3s\sigma_g$ state as probed by dispersed vacuum ultraviolet fluorescence. *Chemical Physics Letters*, 195(4):298 – 302, 1992.

[64] A. Karawajczyk, P. Erman, E. Rachlew-Källne, J. R. I. Riu, M. Stankiewicz, K. Yoshiki Franzén, and L. Veseth. Neutral fragmentation of superexcited oxygen molecules. *Physical Review A*, 61:032718, Feb 2000.

[65] T. Odagiri, H. Miyagi, M. Murata, H. Fukuzawa, M. Kurokawa, M. Kitajima, and N. Kouchi. 3d mapping of photoemission from a single oriented h_2o molecule. *Journal of Physics B: Atomic, Molecular and Optical Physics*, 42(5):055101, 2009.

[66] C. Y. R. Wu, E. Phillips, L. C. Lee, and D. L. Judge. O_2^+ $(A^4\Pi \rightarrow X^2\Pi_g)$ and O_2^+ $(b^4\Sigma_g^- \rightarrow a^4\Pi_u)$ emissions by photoionization of O_2. *The Journal of Chemical Physics*, 71(2):769–776, 1979.

[67] Y. Teranishi, M. Hayashi, F. Kong, S. L. Chin, S. D. Chao, H. Mineo, and S. H. Lin. Highly multiphoton molecular excitation by an intense laser pulse. *Molecular Physics*, 106(2-4):333–339, 2008.

[68] R. S. Freund. *Rydberg states of atoms and molecules.* Cambridge University Press:, 1983.

[69] J. T. Moseley, P. C. Cosby, J. B. Ozenne, and J. Durup. Predissociation lifetimes of the rotational and fine structure levels of $O_2^+(b^4\Sigma_g^-, v = 3, 4, 5)$. *The Journal of Chemical Physics*, 70(3):1474–1481, 1979.

[70] A. Ehresmann, H. Liebel, H. Schmoranzer, O. Wilhelmi, B. Zimmermann, and K.-H. Schartner. VUV-fluorescence spectroscopy of O_2 photodissociation into neutral excited fragments between 17 and 19 eV. *Journal of Physics B: Atomic, Molecular and Optical Physics*, 37(2):389, 2004.

[71] E. M. García, J. Á. Ruiz, P. Erman, A. Kivimäki, E. Rachlew-Källne, J. R. I. Riu, M. Stankiewicz, and L. Veseth. Neutral dissociation of superexcited states in nitric oxide. *Chemical Physics*, 293(1):65 – 73, 2003.

[72] G. Reiser, W. Habenicht, K. Müller-Dethlefs, and E. W. Schlag. The ionization energy of nitric oxide. *Chemical Physics Letters*, 152(2-3):119 – 123, 1988.

[73] A. Azarm, D. Song, S. Hosseini, K. Liu, Y. Teranishi, S. H. Lin, F. Kong, and S. L. Chin. 2011. in preparation.

[74] A. Azarm, H. L. Xu, Y. Kamali, J. Bernhardt, D. Song, A. Xia, Y. Teranishi, S. H. Lin, F. Kong, and S. L. Chin. Direct observation of super-excited states in methane created by a femtosecond intense laser field. *Journal of Physics B: Atomic, Molecular and Optical Physics*, 41(22):225601, 2008.

[75] J. Berkowitz, J. P. Greene, H. Cho, and B. Ruscić. The ionization potentials of ch_4 and cd_4. *The Journal of Chemical Physics*, 86(2):674–676, 1987.

[76] P. Plessis and P. Marmet. Electroionization study of acetylene and fragment ions. *International Journal of Mass Spectrometry and Ion Processes*, 70(1):23 – 44, 1986.

[77] K. Ohno, K. Okamura, H. Yamakado, S. Hoshino, T. Takami, and M. Yamauchi. Penning Ionization of HCHO, CH_2CH_2, and CH_2CHCHO by Collision with $He^*(2^3S)$ Metastable Atoms. *The Journal of Physical Chemistry*, 99(39):14247–14253, 1995.

[78] J. C. Traeger. A study of the allyl cation thermochemistry by photoionization mass spectrometry. *International Journal of Mass Spectrometry and Ion Processes*, 58(0):259 – 271, 1984.

[79] C. E. Van Der Meij, J. Van Eck, and A. Niehaus. The decomposition of $C_4H_8^+$ complexes at controlled internal energies . *Chemical Physics*, 130(1-3):325 – 334, 1989.

[80] J. C. Traeger. Heat of formation for the 1-methylallyl cation by photoionization mass spectrometry. *The Journal of Physical Chemistry*, 90(17):4114–4118, 1986.

[81] R. W. B. Pearse and A. G. Gaydon. *Identification of Molecular Spectra.* John Wiley and Sons, 1976.

[82] M. Kato, K. Kameta, T. Odagiri, N. Kouchi, and Y. Hatano. Single-hole one-electron superexcited states and doubly excited states of methane in the vacuum ultraviolet range as studied by dispersed fluorescence spectroscopy. *Journal of Physics B: Atomic, Molecular and Optical Physics*, 35(21):4383, 2002.

[83] L. S. Iwai and H. Nakamura. *Molecules In Laser Fields.* New York: Dekker, 1994.

[84] J. Geddes, K. F. Dunn, N. Kouchi, M. A. McDonald, V. Srigengan, and C. J. Latimer. Isotope effects in the autoionization of superexcited $^1\Sigma_u^+(Q_1)$ states in hydrogen. *Journal of Physics B: Atomic, Molecular and Optical Physics*, 27(14):2961, 1994.

[85] S.L. Chin, A. Azarm, H.L. Xu, T.J. Wang, M. Sharifi, A. Talebpour. *Progress in Ultrafast Intense Laser Sciences 8.* Springer, 2012.

[86] M. V. Fedorov and A. M. Movsesian. Field-induced effects of narrowing of photoelectron spectra and stabilisation of rydberg atoms. *Journal of Physics B: Atomic, Molecular and Optical Physics*, 21(7):L155, 1988.

[87] A. Talebpour, Y. Liang, and S. L. Chin. Population trapping in the co molecule. *Journal of Physics B: Atomic, Molecular and Optical Physics*, 29(15):3435, 1996.

[88] A. Talebpour, C.-Y. Chien, and S. L. Chin. Population trapping in rare gases. *Journal of Physics B: Atomic, Molecular and Optical Physics*, 29(23):5725, 1996.

[89] M. P. De Boer, J. H. Hoogenraad, R. B. Vrijen, L. D. Noordam, and H. G. Muller. Indications of high-intensity adiabatic stabilization in neon. *Physical Review Letters*, 71:3263–3266, Nov 1993.

[90] J. Liu, J. Dai, S. L. Chin, and X. C. Zhang. Broadband terahertz wave remote sensing using coherent manipulation of fluorescence from asymmetrically ionized gases. *Nature Photonics*, 4(9):627–631, 2010.

[91] T.-J. Wang, J.-F. Daigle, Y. Chen, C. Marceau, F. Théberge, M. Châteauneuf, J. Dubois, and S.L. Chin. High energy THz generation from meter-long two-color filaments in air. *Laser Physics Letters*, 7(7):517–521, 2010.

J'autorise le Professeur See Leang Chin à utiliser cette thèse en totalité ou en partie.